**Terms and Conditions of Use of Digitised Theses from Trinity College Library Dublin**

**Copyright statement**

All material supplied by Trinity College Library is protected by copyright (under the Copyright and Related Rights Act, 2000 as amended) and other relevant Intellectual Property Rights. By accessing and using a Digitised Thesis from Trinity College Library you acknowledge that all Intellectual Property Rights in any Works supplied are the sole and exclusive property of the copyright and/or other IPR holder. Specific copyright holders may not be explicitly identified. Use of materials from other sources within a thesis should not be construed as a claim over them.

A non-exclusive, non-transferable licence is hereby granted to those using or reproducing, in whole or in part, the material for valid purposes, providing the copyright owners are acknowledged using the normal conventions. Where specific permission to use material is required, this is identified and such permission must be sought from the copyright holder or agency cited.

**Liability statement**

By using a Digitised Thesis, I accept that Trinity College Dublin bears no legal responsibility for the accuracy, legality or comprehensiveness of materials contained within the thesis, and that Trinity College Dublin accepts no liability for indirect, consequential, or incidental, damages or losses arising from use of the thesis for whatever reason. Information located in a thesis may be subject to specific use constraints, details of which may not be explicitly described. It is the responsibility of potential and actual users to be aware of such constraints and to abide by them. By making use of material from a digitised thesis, you accept these copyright and disclaimer provisions. Where it is brought to the attention of Trinity College Library that there may be a breach of copyright or other restraint, it is the policy to withdraw or take down access to a thesis while the issue is being resolved.

**Access Agreement**

By using a Digitised Thesis from Trinity College Library you are bound by the following Terms & Conditions. Please read them carefully.

I have read and I understand the following statement: All material supplied via a Digitised Thesis from Trinity College Library is protected by copyright and other intellectual property rights, and duplication or sale of all or part of any of a thesis is not permitted, except that material may be duplicated by you for your research use or for educational purposes in electronic or print form providing the copyright owners are acknowledged using the normal conventions. You must obtain permission for any other use. Electronic or print copies may not be offered, whether for sale or otherwise to anyone. This copy has been supplied on the understanding that it is copyright material and that no quotation from the thesis may be published without proper acknowledgement.

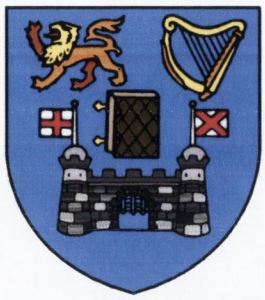

# Mechanical and morphological properties of carbon nanotubes polymeric composites

by

Umar Khan

A thesis submitted for the degree of
Doctor of Philosophy
in the University of Dublin

School of Physics
Trinity College Dublin

2009

## *Declaration*

I declare that the work in this thesis has not been previously submitted as an exercise for a degree to this or any other university. The work described herein is entirely my own, except for the assistance mentioned in the acknowledgements and the collaborative work mentioned in the list of publications. I agree that Trinity College Library may lend or copy this thesis on request.

**For my Family and Supervisor**

# Acknowledgements

First of all, I am extremely thankful to my supervisor, Prof Jonathan N Coleman, for giving me an opportunity to do this PhD, for his supervision, and financial and moral support. Without his supervision, assistance and teaching this thesis would have never been possible. I am equally thankful to Prof Werner Blau for all of his support.

I pay special gratitude to Dr Kevin Ryan for training me on various pieces of equipment and for spending a lot of time with me in Galway on the tensile tester. Thanks to Yenny Hernandez (senorita) for helping me out during my initial days in the group and also for her help with the electrical measurements.

It would be sinful if I don't pay gratitude to the team For WAR AGAINST ERROR. Many, many thanks to the very special Dr Denis McCarthy who was very helpful in proof reading my transfer report and thesis, also for his cup of coffee (first ever in Ireland). I pay special gratitude to young Karen Young for her very fast proof reading and her help in electrical measurements. Thanks to my nice office mate Niall McEvoy for his help in Raman spectroscopy and also in proof reading. I would also like pay thanks to Paula Russell-Hill (little miss bossy) for proof reading when it was needed most and all the help.Thanks to Dr Fiona Blighe for proof reading and general help.

Many thanks to MI guys; Trevor Woods, Dr Ramesh Babu, Dr Manuel Ruether and Dr Edward Moore for allowing me to use their various pieces of equipment and all of their help. I am grateful to Jeanette Cummins for all of her quick help over the time I spent here. Many thanks to Anna Drury for her help and for keeping a kind eye on all of my and everyone's activities in the Lab.

Thanks to Mr John Kelly and all administrative staff, especially Robert Gallagher. Thanks to all the workshop crew; Mick Reilly, Dave Grouse and Pat Murphy, for all their help in preparing the strip cutter and Teflon trays.

Thanks to French David Blond for discussing various scientific and non scientific issues with me. I am also grateful to Ian O'Connor for his SEM and over all help. I would like to pay thanks to the chosen one, Christopher Kufazvinei, for all of his help and preaching. Thanks to Darren lee for trying to resolve my Origin issues (which were never resolved though).

I am grateful to all of you guys, Dr Shane Bergin, Paula Russell-Hill (Miss Bossy), Dr Helen Cathcart Dr Martin Djiango, Dr Zhenyu Sun, Dr Sukanta, Philip Lyons, Marguerite Hughes, Mustafa Lotya, Denise Charles, Evelyn Doherty and the old group members Dr Valeria Nicolosi, Dr Rob Murphy, Dr James Doyle, Dr Rory Leahy, Dr Adam Strevens, Dr Sharon King, Dr Eimhin Ní Mhuircheartaigh and Dr Grace Jordan.

Before coming to Ireland I was naturally nervous but you guys provided me with a lot of support, help and gave me so much love that makes me feel like I am in family, for which I do not have words to describe my appreciation, so I would leave it like that.

I am very thankful to my family for supporting me throughout my PhD. Very special thanks to my wife Salma and two little daughters Nazish and Mehek whose patience and cooperation made it possible for me to be able to finish my thesis. Thanks to my father Shamsur Rehman, sister Shahida, brothers Iftikhar and Haroon for their unconditional support.

Abstract viii

Chapter 1 Introduction to composite material 1

1.1 Background and Motivation 1

1.2 Thesis Outline 3

1.3 References 4

Chapter 2 Introduction of materials and literature review 6

2.1 Introduction 6

2.2 From carbon to carbon nanotubes 6

2.2.1 Types of CNTs 9

2.2.2 Mechanical properties of Carbon nanotubes 11

2.2.3 Production of Carbon nanotubes 13

2.3 Polymer 17

2.3.1 Types of polymers 20

2.3.2 Mechanical properties of polymers 21

2.3.3 Effect of CNTs and additive .... indicator of mechanical Properties 23

2.4 Type of CNTs composites based on processing 25

2.4.1 Solution based 25

2.4.2 Melt processing 26

2.4.3 Novel method of composites fabrication 27

2.5 Models for fibre reinforced composites 29

2.5.1 Rule of Mixtures 29

2.5.2 Halpin and Tsai model 31

2.6 Requirement for effective reinforcement and role of funtionalised CNTs 32

2.7 Mechanical properties of CNTs composites 35

2.8 Conclusion 37

2.9 References 38

Chapter 3 Materials and characterisation techniques 44

3.1 Introduction 44

3.2 Carbon nanotubes 44

3.3 Polymer matrices 45

3.4 Solvents 47

3.5 Characterisation techniques 47

3.5.1 Thermo gravimetric analysis (TGA) 47

3.5.2 Differential Scanning calorimetry (DSC) 49

3.5.3 Dynamic mechanical thermal analysis (DMTA) 51

3.5.4 Tensile testing (TT) 53

3.6 References 56

Chapter 4 The effect of solvent choice on the mechanical properties of carbon nanotube-polymer composites 57

4.1 Introduction 57

4.2 Sample preparation 58

4.3 Characterisation techniques 59

4.4 Results and discussion 60

4.4.1 TGA analysis 60

4.4.2 DSC study 63

4.4.3 DMTA 71

4.4.4 Tensile testing 76

4.5 Conclusion 80

4.6 References 81

Chapter 5 Mechanical reinforcement of thermoplastic polyurethane by functionalised SWCNTs 83

5.1 Introduction 83

5.2 Sample preparation 85

5.3 Results and discussion 86

5.3.1 Thermo gravimetric analysis (TGA) analysis 86

5.3.2 DSC characterisation 87
5.3.3 Dynamic mechanical analysis 94
5.3.4 Cyclic mechanical testing 98
5.3.5 Mechanical 104
5.4 Conclusion 117
5.5 References 120
Chapter 6 Preparation of thermoplastic polyurethane composites with pristine and pristine + functionalised mix carbon nanotubes 123
6.1 Introduction 123
6.2 Sample preparation 124
6.3 Result and discussion 125
6.4 Conclusions 150
6.5 References 151
Chapter 7 Conclusions and future work 154
7.1 Conclusion 152
7.2 Future work 156
7.3 Publication list 158

# Abstract

Carbon nanotubes (CNT) are incorporated to the polymers to enhance their electrical and mechanical properties. All of the samples in this thesis were prepared from the liquid phase using the solution casting method. The change in morphological and mechanical properties of PVA based composites with the addition of double walled carbon nanotubes has been studied using differential scanning calorimetry (DSC), thermal gravimetric analysis (TGA), differential thermal gravimetric analysis (DTGA), dynamic thermal analysis (DMTA), and tensile testing. Three different solvents i.e. water, dimethylsulfoxide (DMSO), and N-methylpyrrolidone (NMP) have been used for solution based composite formation. It has been found that the composite properties are affected not only by the solvent boiling point but also by the polymer solubility and, more importantly, the affinity of the carbon nanotubes CNTs for the solvent. The data obtained for the NMP solutions is consistent with solvent trapping at the polymer-nanotube interface, whereas the DMSO study has shown that the solvent remains trapped more in the matrix than at the CNT-PVA interface. Almost no water was found in water based samples. Maximum reinforcement was found with the composites prepared using water as the solvent, those prepared with DMSO exhibited intermediate reinforcement, while NMP composites showed a reduction in mechanical properties compared with their respective polymer only samples.

To enhance the mechanical properties of water born thermoplastic polyurethane (TPU) single wall carbon nanotubes (SWCNT), very thin and thick multiwall carbon nanotubes (MWCNT) were added as fillers. The mechanical reinforcement imparted by the various CNTs was found to be in the order of their external diameters. The stiffness of the (low stress and stiffness) plateau (strain) region was enhanced significantly by the incorporation of 2.5 wt% MWCNTs. The stiffness was increased up to the level of the stiffness in the strain induce crystallisation/strain hardening region without a loss in ductility. It was found that at high mass fractions ($m_f$) CNTs form networks around the polymer particles. Thus at high $m_f$ CNT-CNT interaction is dominant rather than CNT-polymer interactions. In TPU work, a novel approach of mixed-CNTs was adopted to enhance the CNT dispersions. This increases the loading level and subsequently improves the mechanical properties. The mixed-CNT samples were prepared by mixing the polyethyleneglycol-SWCNTs with very thin and thick MWCNTs. At 7 wt% loading mix-CNT samples exhibited an increase of a factor of 8 in the Young's modulus.

The mechanical properties of TPU were enhanced by the incorporation of three different types of funtionalised SWCNTs, each of different solubility. To understand the reinforcement mechanism in depth, Scanning electron microscopy (SEM), DSC, DMTA and cyclic/mechanical testing were carried out. The DSC study revealed the enhancements of hard and soft segment HS and SS crystallinity with water soluble and THF soluble CNTs respectively. Results from the DMTA study were consistent with those obtained by DSC. The best increase in Young's modulus (x 23) was observed with polyethyleneglycol PEG-SWCNTs (20 wt%). The plateau region was also enhanced significantly with each increment of CNTs. To avoid formation of CNT networks around the polymer particles, the polymer was dissolved in THF. Octadecylamine functionalised single wall carbon nanotubes (ODA-SWCNT) were then incorporated into it. For ~0.12 wt% CNT loading, strength and toughness increased by a factor 2 and 4 respectively. In these composites the mechanical properties surprisingly did not decline, but saturated at high $m_f$. Studies revealed that ODA-SWCNTs interact with the hard segment and water soluble CNTs with the soft segment of TPU.

# Chapter 1

## Introduction to composite materials

### 1.1 Background and motivation

Generally speaking, composites are materials consisting of multiphase components of different physical or chemical characteristics *[1]*. The constituents in a composite are combined in such a way that the individual materials are clearly distinguishable. Usually composites are composed of a matrix e.g. polymers, metals, clay etc and one or more fillers e.g. glass fibres, carbon fibres, CNT *[2]*. Composites can be divided into many classes on the basis of matrix, filler *[3]*or preparation technique e.g. ceramics, polymeric, metallic, fibrous, particle filled, melt processed, laminated, solution based composites etc. These kinds of materials, in which a strong and stiff material (filler) are held by an substance (matrix), have been known to mankind since prehistoric times. Examples evident in nature include tree trunks, skeletal bones and also muscles which are reinforced by fibres/ligaments.

Although composites can be fabricated for a variety of purposes, it should be noted that, in this thesis, composites are described mainly in terms of structural materials.

The need for composite materials arises due to the fact that in many cases conventional materials do not have the required properties. The endeavour for such materials with improved properties led mankind to the invention of artificial composite materials. Such artificial composites can be traced back to 4000 BC, when straw and mud were mixed to form bricks for building construction *[4]*. In modern times, the mud-straw bricks of old have been replaced by steel reinforced concrete composites.

For many years the main structural materials were derived from natural sources like wood, metals, alloys and natural rubber etc. With the dawn of the industrial revolution it

was realized that, due to huge production demands, natural resources alone were not sufficient. Limitations on the availability of natural materials caused problems however, the difficult and time consuming processing conditions of these materials were even more problematic. This led scientists to seek out alternative synthetic materials. In the quest for such a synthetic material, Leo Baekeland prepared the first synthetic polymer in 1907 *[5]*. This opened the door for a whole new range of materials. Soon, with the invention of glass fibres, polymers started to be used as the matrix for modern composite materials. Various fillers ranging from nano-particles *[6]* to fibres *[7]* in combination with various matrices e.g. thermoplastics*[8]* and thermoset *[9]* have been used for composite preparations.

The aim of modern age composites is to make stiffer, stronger, tougher or conductive materials, whilst at the same time making these materials lighter. The beauty of polymeric composite materials is that, in most cases, these properties can be tuned simply by varying the proportions of ingredients within a particular composite system.

Modern composite materials are used in automobiles, civil and military aircraft and even very advanced high-tech space shuttles *[10]*. Various parts of these vessels are subjected to extreme physical and thermal stresses. Traditional strong or stiff materials simply cannot withstand these extreme stresses or sometimes the densities of theses materials are too high. Generally, many of their parts are fabricated with fibre reinforced polymeric composites whose properties are tailored to withstand these extreme stresses *[10]*. Another advantage of the polymeric composite is its design flexibility, the polymeric composite can be moulded to various complex designs which are normally very difficult or even impossible to fabricate in the case of traditional materials.

In 1991 Iijima a Japanese scientist discovered carbon nanotubes (CNTs) *[13]*. Since then there has been much research into their use as a filler in polymer matrices *[14]*. This interest in CNTs exists because they potentially have all of the properties required for a highly efficient filler i.e high stiffness, high strength, flexibility, chemical inertness, heat resistance, high electrical conductivity, thermal conductivity, high aspect ratio, high surface area and low density as well *[15-18]*.No conventional single filler has all of these properties simultaneously. There are certain issues involved with CNTs used a filler which will be discussed in coming chapter.

For a good composite there are certain conditions which have to be fulfilled. A high length to diameter ratio (aspect ratio) is very important, it will maximise stress transfer to the filler *[11]* and hence, mechanically reinforce composites. The filler must be dispersed evenly throughout the matrix *[12]* i.e. little or no aggregation of the fillers. Otherwise it will result in either poor stress transfer due to the fact that these aggregates are held by van der Waal's forces or inhomogeneous stress in various parts of the inhomogeneous composite and hence, poor quality composites will result. There should also be good interfacial bonding between the matrix and filler.

## 1.2 Thesis outline

The work done in this thesis predominantly describes the mechanical properties of solution based CNT composite systems. Various factors affecting these properties are also investigated. Carbon nanotubes tend to remain in bundles *[19]* and achieving good dispersions is often not possible with many preparation techniques. Thus, solution based composites preparation technique was selected because, very good dispersion of the CNTs is possible in common solvents and polymers *[19-24]*. Therefore potentially good quality CNTs composites film can be prepared with the solution based technique.

In this thesis various problems associated with the reinforcement of polymers by incorporation of the CNT were not only identified but tried to be resolved in the following work.

Chapter 1 gives an introduction to composite materials, motivations and an outline of the thesis.

Chapter 2 describes the background of CNTs and CNT polymeric composites. There is also an overview of previous work done in the field and mechanical reinforcement theory.

Chapter 3 describes the various materials and experimental techniques used for this PhD work.

Chapter 4 describes the morphological and mechanical properties of solution based dropcast free standing PVA-DWNT composites. Preparation with three different solvents of different B.P and the different affinity for PVA and CNT is described i.e. water, DMSO and NMP. The effect of solvent choice on the morphological properties and mechanical behaviour of DWCNT–PVA composites is also investigated. Effectively solvent PVA/matrix interaction and solvent CNT interaction are investigated within a particular composite system using various experimental techniques.

Chapter 5 describes the mechanical properties of various pristine CNTs-thermoplastic polyurethane/water composites. The chapter also describes the novel approach of the composites preparation using a mixture of pristine and functionalised CNTs with in the same matrix.

Chapter 6 reports the work done on the characterisation of composites prepared with functionalised CNTs and thermoplastic polyurethane.

Chapter 7 summaries the work done for the PhD and highlights the significant findings and future work.

## 1.3 References


[1] D. William, W. Callister., *Fundamentals of materials science and engineering, an introduction*, Wiley, New Yark **2003**.

[2] C. Harper, *Handbook of Plastics, Elastomer, And Comosites*, McGraw-Hill, Inc, New York **2002**.

[3] F. Hussain, M. Hojjati, M. Okamoto, R. E. Gorga, *Journal of Composite Materials* **2006**, *40*, 1511.

[4] J. N. Coleman, U. Khan, W. J. Blau, Y. K. Gun'ko, *Carbon* **2006**, *44*, 1624.

[5] F. M Blighe., in *School of Physics*, Trinity College Dublin University of Dublin, Dublin **2007**.

[6] U. Khan, K. Ryan, W. J. Blau, J. N. Coleman, *Composites Science and*

*Technology* **2007**, *67*, 3158.
[7] A. Kelly, W. R. Tyson, *Journal of the Mechanics and Physics of Solids* **1965**, *13*, 329.
[8] S. M. Liff, N. Kumar, G. H. McKinley, *Nat Mater* **2007**, *6*, 76.
[9] H. P. J. Zhu, F. Rodriguez-Macias, J. L. Margrave, V. N. Khabashesku, A. M. Imam, K. Lozano, E. V. Barrera, *Advanced Functional Materials* **2004**, *14*, 643.
[10] R Kevin. Uleck, P. J. B. J. C., R. B. M. Hilditch, in *Handbook of Materials Selection*, (Ed: K. Myer), **2007**, 1129.
[11] H. L. Cox, *British Journal of Applied Physics* **1952**, *3*, 72.
[12] M. Cadek, J. N. Coleman, V. Barron, K. Hedicke, W. J. Blau, *Applied Physics Letters* **2002**, *81*, 5123.
[13] S. Iijima, *Nature* **1991**, *354*, 56.
[14] J. N. Coleman, U. Khan, Y. K. Gun'ko, *Advanced Materials* **2006**, *18*, 689.
[15] J. W. Che, T. Cagin, W. A. Goddard, *Nanotechnology* **2000**, *11*, 65.
[16] S Berber, Y Kwon*, a. D. Tománek, *Physical Review Letters* **2000**, *84*, 4613.
[17] B. Q. Wei, R. Vajtai, P. M. Ajayan, *Applied Physics Letters* **2001**, *79*, 1172.
[18] B M Kim, A. M. S. Fuhrer, *Journal of Physics: Condensed Matter* **2004**, *16*, R553.
[19] S. Giordani, S. B. V., N. S. Lebedkin, W. J., B. J. N. Coleman, *physica status solidi (b)* **2006**, *243*, 3058.
[20] B. Zhao, H. Hu, A. Yu, D. Perea, R. C. Haddon, *J. Am. Chem. Soc.* **2005**, *127*, 8197.
[21] B. Zhao, H. H. R. , C. Haddon, *Advanced Functional Materials* **2004**, *14*, 71.
[22] S. Niyogi, M. A. Hamon, H. Hu, B. Zhao, P. Bhowmik, R. Sen, M. E. Itkis, R. C. Haddon, *Acc. Chem. Res.* **2002**, *35*, 1105.
[23] J. Amiran, V. Nicolosi, S. D. Bergin, U. Khan, P. E. Lyons, J. N. Coleman, *J. Phys. Chem. C* **2008**, *112*, 3519.
[24] S. K. Tetsuya Uchida, *Journal of Applied Polymer Science* **2005**, *98*, 985.

# Chapter 2

# Introduction of materials and literature review.

## 2.1 Introduction

This chapter will provide a general introduction to the materials used throughout this work. The different types and properties of carbon nanotubes (CNTs) will be discussed along with the various methods of CNT production. The chapter also introduces polymers and their classification. An overview of the mechanical properties of carbon nanotube polymer composites and the theory of mechanical reinforcement will be discussed.

## 2.2 From carbon to carbon nanotubes

The word carbon has been derived from Latin carbo meaning coal or charcoal. Carbon is known since the prehistoric era in the form of soot, and coal. For centuries carbon was considered to have two crystalline allotropic forms, diamond and graphite.
Diamond is the stiffest and strongest material known to man. The excellent mechanical properties of diamond are due to the C-C covalent bonding of its 3D structure (Fig. 2.1) where each carbon atom is $sp^3$ hybridised (Fig.2.1).

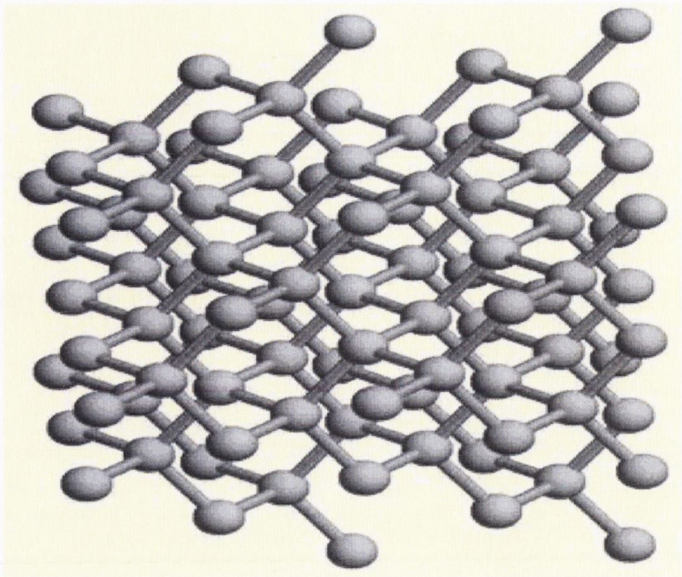

Fig. 2.1 3D bonding structure in diamond (www.chm.bris.ac.uk)

Shown in figure 2.2, graphite the other well known form of carbon, consists of sheets (graphene) of hexagonal networks of $sp^2$ hybridised carbon atoms. Unlike diamond, graphene sheets are held together by weak Van der Waals forces.

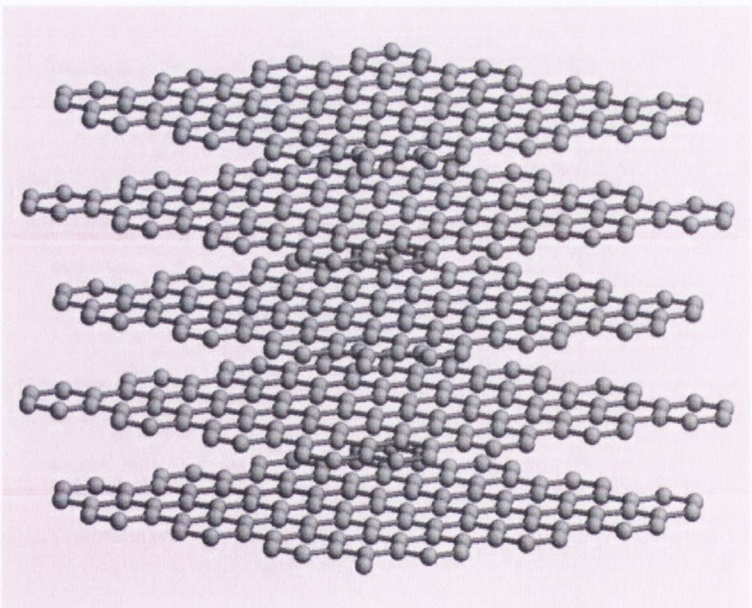

Fig.2.2 Structure of graphene sheets in graphite (www.chm.bris.ac.uk)

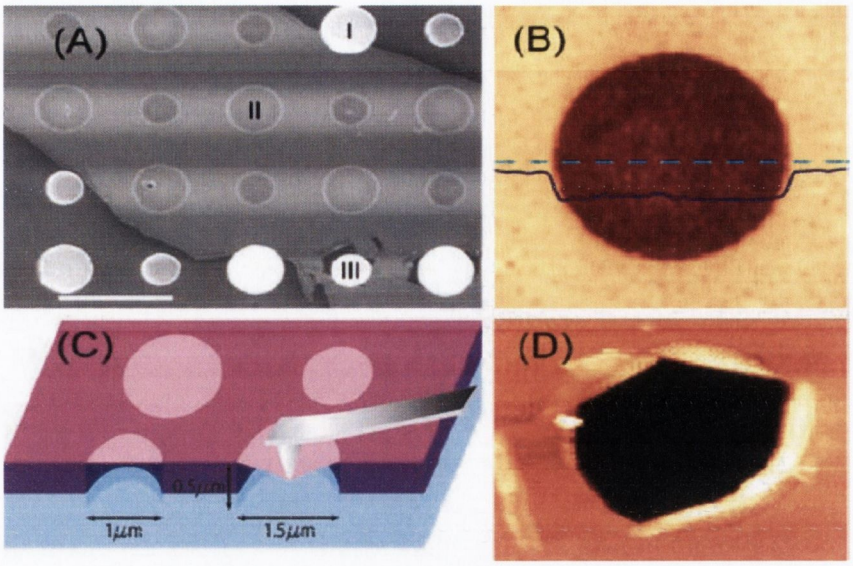


Fig. 2.3 Scanning electron micrograph of a large graphene flake spanning an array of circular holes 1 **μ**m and 1.5 **μ**m in diameter. Area I shows a hole partially covered by graphene, area II is fully covered, and area III is fractured from indentation. Scale bar, 3 **μ**m. (***B***) Noncontact mode AFM image of one membrane,1.5 **μ**m in diameter. The solid blue line is a height profile along the dashed line. The step height at the edge of the membrane is about 2.5 nm. (***C***) Schematic of nanoindentation on suspended graphene membrane. (***D***) AFM image of fractured surface *[1]*.

Graphene sheets exhibit very good mechanical properties. In 2007, Frank *et a.l* was able to measure the mechanical properties of graphene sheets which were a few atomic layers thick using AFM. They suspended stacks of graphene sheets (each less than 5 layers thick) over trenches of a silicon dioxide substrate. They extracted the Young's modulus of ~0.5TPa*[2]* . Using the same AFM technique in 2008, Lee and coworkers were able to measure the mechanical properties of a single atomic layered graphene sheet*[1]* . They used a silicone substrate with holes in it of diameters = 1.1μm and depth = 500 nm (Fig 2.3). They mechanically deposited the graphite flakes over the holes. They used the nano indentation method to measure the mechanical properties of graphene. Their work reveals that the mono atomic layer graphene has a Young's modulus of 1TPa and intrinsic strength of 130 GPa.

In 1985, Kroto *et al.* discovered another allotrope of carbon called the buckyball or $C_{60}$ *[3]*. This spherical molecule consists of 60 carbon atoms arranged in a sphere of 20

hexagons and 12 pentagons (Fig. 2.4). In 1995 their buckyball work was rewarded with a Nobel prize.

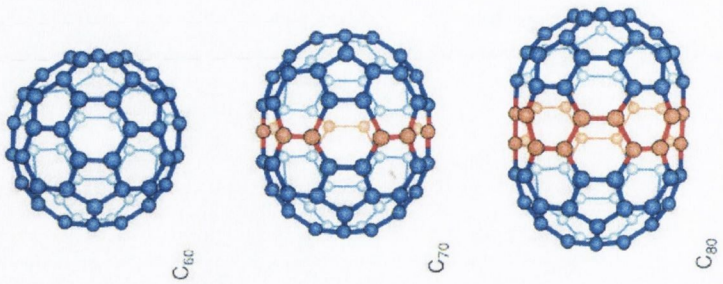


Fig. 2.4 C60, C70, C80 buckyball model

Research on buckyballs lead scientists to the discovery, that they consist of 60, 70 or, 80 molecules; many other sizes of buckyballs are also possible. In 1991, while studying the soot formed during electric discharge between the two graphite electrodes, Ijima observed rolled concentric multilayered graphene structures (Fig. 2.4) called multi walled carbon nanotubes (MWCNT) (Fig.2.5) *[4]*.

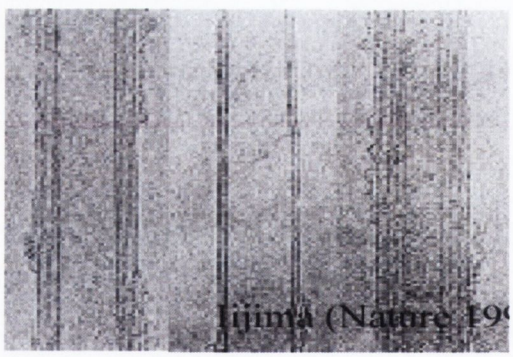

Fig. 2.5 Multi wall carbon nanotubes image *[4]*

## 2.2.1 Types of CNTs

Primarily there are two main types of carbon nanotubes. Single walled carbon nanotubes (SWCNT) (Fig. 2.6) and multi walled carbon nanotubes (MWCNT) (Fig. 2.7). A single walled carbon nanotube is a single rolled graphene sheet with a diameter of

the order of one nanometre and a length of up to centimetres. MWCNTs consist of two or more concentric rolled graphene sheets like a telescope (Fig. 2.7). Each sheet is separated by a distance of 0.35 nm*[4]* . Multi walled carbon nanotubes can have diameters from 2 nm-100 nm and lengths of up to micrometers*[5]* . Based on the rolling up pattern of graphene sheet there are three possible types of CNTs. Shown in figure 2.6 A,B,C are the armchair, zigzag and chiral CNTs respectively. Generally speaking, in the armchair structure the C-C bond (Fig. 2.6 A) is perpendicular to the tube axis while in zigzag structure the C-C bond (Fig. 2.6 b) is parallel to the tube axis. All other arrangements in which the C-C bond is at an angle to axis is called chiral.

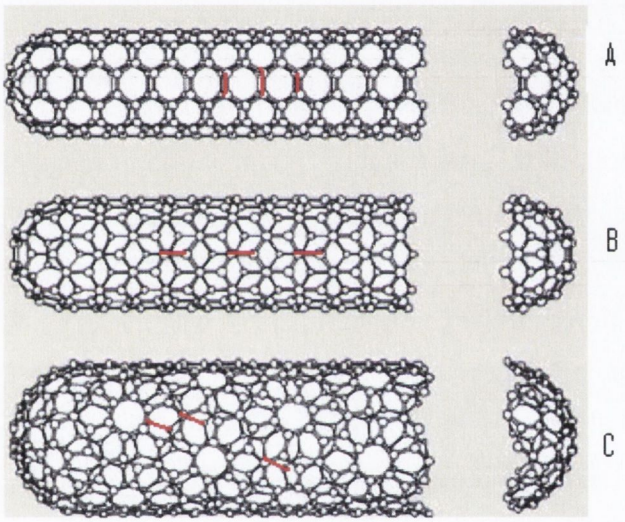


Fig. 2.6 SWCNT A) armchair,B) zigzag and C) chiral

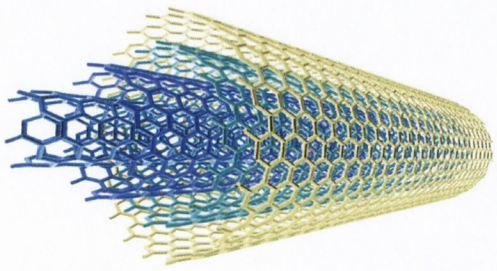

Fig. 2.7 Shows concentric multilayered MWCNT

### 2.2.2 Mechanical properties of carbon nanotubes

Soon after their discovery, it was expected that CNTs would exhibit superior mechanical properties because of their analogy to graphite. Graphite has an in plane modulus of about 1.06 TPa*[6]* . Work from Perepelkin on the C-C bond strength had suggested that graphite can have a tensile strength of 130 GPa*[7]* . In addition to this in 1961 Bacon fabricated graphite whiskers, which demonstrated strengths of 20 GPa*[8]*. Therefore on the basis of previous work it was expected that these miniatures should demonstrate superior properties.

Soon after CNTs were discovered, work started to measure their mechanical properties *[5]*. Perhaps the first attempt to measure the mechanical properties of CNT was made by Overny *et al.* His work was based on computer simulations. In his work he calculated the Young's modulus of SWCNTs to be 1500 GPa.*[9]* . Later work of other researcher also suggested that the Young's modulus was in range of 1TPa*[10]* . Using the amplitude of intrinsic thermal vibration of carbon nanotubes in their SEM study Tracey *et al.* calculated the modulus to be in the range of 0.41 to 4.15TPa*[11]* .

The first direct mechanical measurement was made by Wong *et al.* in 1997. In their work, they randomly deposited the arch multi wall carbon nanotubes on an $MoS_2$ substrate and pinned them with square $SiO_2$ pads. They measured the force verses displacements via atomic force microscopy (AFM) along the tube lengths at various positions. The work demonstrated that the nanotubes had an average Young's modulus of 1.28 TPa. The study also showed that the average bending strength was 14 GPa*[12]* . In another study by Salvetat *et al.* a solution of MWCNTs was dropped on an alumina ultrafiltration membrane with a pore size of 20 nm. Some of the CNTs arranged themselves across the pores. The CNTs were bent with an AFM tip. The modulus obtained was in the range of 650-1220 GPa and 10-15GPa for arc-discharge MWCNT and for catalytically grown MWCNT respectively*[13]* . In 2000 Yu and his co researchers attached both ends of a MWCNT to the cantilever of an AFM (Fig.2.8). Under the scanning electron microscope (SEM) they stretched the MWCNT and recorded the actual stress strain curves. Their work suggested a MWCNT can be strained up to 12% of its original length before failure. The work also revealed that failure occurs at the outer layer and the inner tube comes out in the form of a telescope. From the stress strain curves they obtained the values for the Young's

modulus in the range of 0.27 to 0.95 GPa. Young's modulus is the stress to strain ratio in elastic part of stress strain curve. The measured values for the ultimate strength were in the range of 11 to 63 GPa. Their work also showed that MWCNTs can have a toughness value of about 1240 J/g.*[15]* . Toughness is the total energy needed to break a sample and is measured by integrating the total area under the (stress strain) curve.

Some time later, the first attempts to measure the mechanical characteristics of SWCNT were made by Salvetat *et a.l* in 1999 *[16]*. They obtained a value of 1TPa for a small bundle of SWCNT *[16]*. They also measured the mechanical properties of large diameter ropes of SWCNTs. Their study demonstrated slippage between the nanotubes in the bundles. They recorded the values of modulus in the range of 0.32 to 1.47 GPa. The percent strain at break and toughness values were shown to be approximately 5.3% and 770 J/g respectively*[17]* . The same AFM technique and experimental procedure that was used for measuring the mechanical behavior of MWCNTs was adopted for tensile testing SWCNTs .

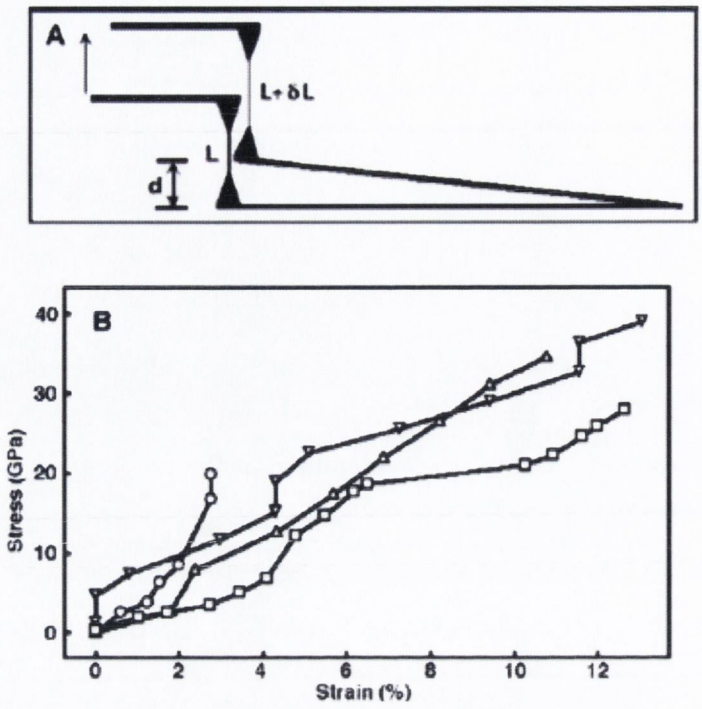


Fig. 2.8 (A) The experimental setup showing the attachment of MWCNT to the AFM tip to measure stress strain curve (B) stress strain curve of a MWCNT stretched using AFM *[15]*

### 2.2.3 Production of carbon nanotubes

There are three popular techniques in use nowadays for the production of carbon nanotubes, arc discharge, laser ablation and chemical vapor deposition.

**Arc discharge:**

The first yield of CNTs in milligrams was produced in 1992 by Ebbsen *et al* using the arc discharge method*[18]* . This technique pioneered CNTs synthesis. It was with this technique in 1991 that Ijimi discovered MWCNTs. In this technique, two graphite electrodes, are put in a chamber of inert atmosphere, usually helium gas at low pressure. A high direct current is applied across the graphite electrodes usually between 50 to 100A with a potential difference of about 20V. The current is kept constant by varying the distance between the two electrodes. In practice the distance is varied by moving the cathode while keeping the anode static. Under the influence of high current, carbon atoms

at the graphite surface are converted to plasma. This plasma condenses on the anode in form of a hard tube with a core of soot and multiwall carbon nanotubes. In 1993 Bethune *et al* produced single wall carbon nanotubes using the arc discharge method*[19]* . They bored holes in the anode and filled the holes with a Fe, Ni and Co mixture. This was followed by vaporizing the mixture by applying a current between the two electrodes in the range of 95 to 105 A. Using the arc plasma jet method in 1999 Morio *et al.* were able to achieve 50% yield of CNTs. Their highest production rate was 1.74g/h *[20].* In an endeavor to further increase production yields, Liu produced a 30% yield of SWCNTs at a rate of 2g/h using the arc discharge method in 2000*[21]* .

Remarkably Zhao and a co-researcher demonstrated the production of CNTs with a yield of 95%*[22]* . They were not only able to demonstrate high yield but simultaneously demonstrated a production rate of >45g/h *[22].* In their production setup, the arc was generated between the anode and the pure graphite cathode at a current of 60 A in a 400 Torr static helium atmosphere. The distance between the electrodes was maintained at ~2 mm by continuously feeding the cathode throughout the arc process. They observed cloth-like soot formation on the entire inner wall of the chamber. In general, an 80 mm anode rod can be consumed in 5 min forming 5.3 g of soot. Cadek *et al.* were able to produce a 48% yield of MWCNTs with the arc discharge method *[23]* (Fig. 2.9)

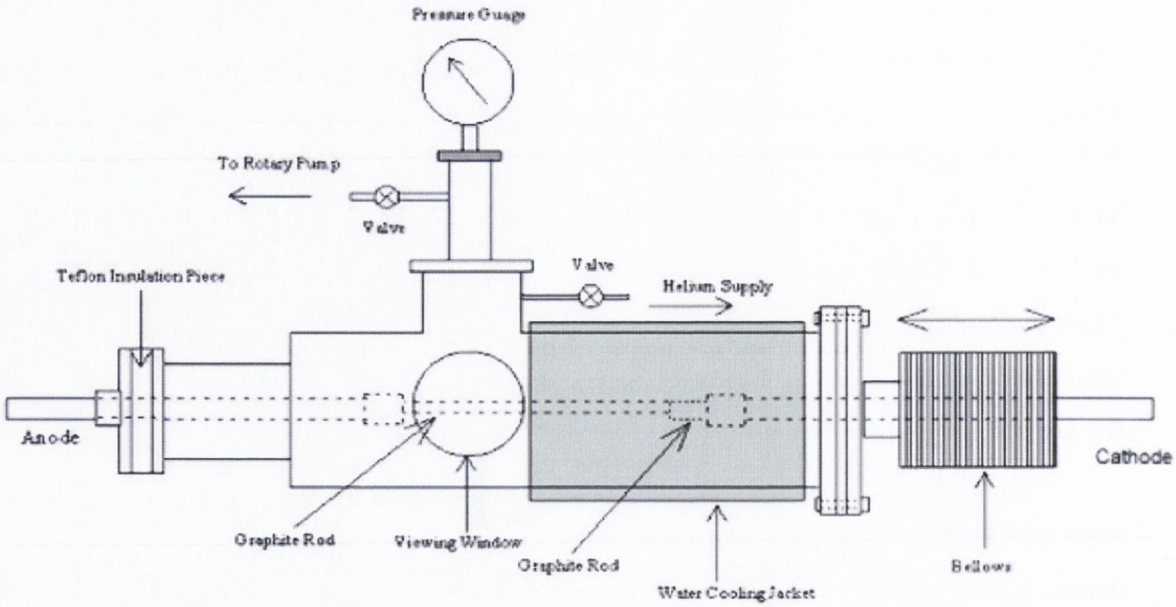


Fig. 2.9 Schematic diagram of Arch discharge for CNTs synthesis*[24]* .

Even though a good yield of CNTs can be produced through the arc discharge technique, there are a few outstanding issues. There are a lot of impurities present in the end product and hence the CNTs need purification. Another problem associated with this method is the short length of the CNTs produced, up to a maximum of 50 micro-meters *[25]*.

**Laser ablation:**

In this technique high purity graphite is mixed together with a catalyst e.g Ni, Co. This mixture is then targeted by high power laser beam, generating a very high temperature of about 1200 $^{o}$C . CNT growth is taken place in an inert gas atmosphere, usually argon. The nanotubes grow until too many catalyst atom aggregates on their ends*[26]*. The temperature and choice of catalyst can effect the quantity and quality of the tubes*[23]*. In 1996 for the first time Smalley and co-worker used this technique to produce high yield of SWCNTs in excess of a 70% yield*[27]*. Although a high yield can be produced with laser ablation this technique is not widely used because of the slow rate of production and high costs.

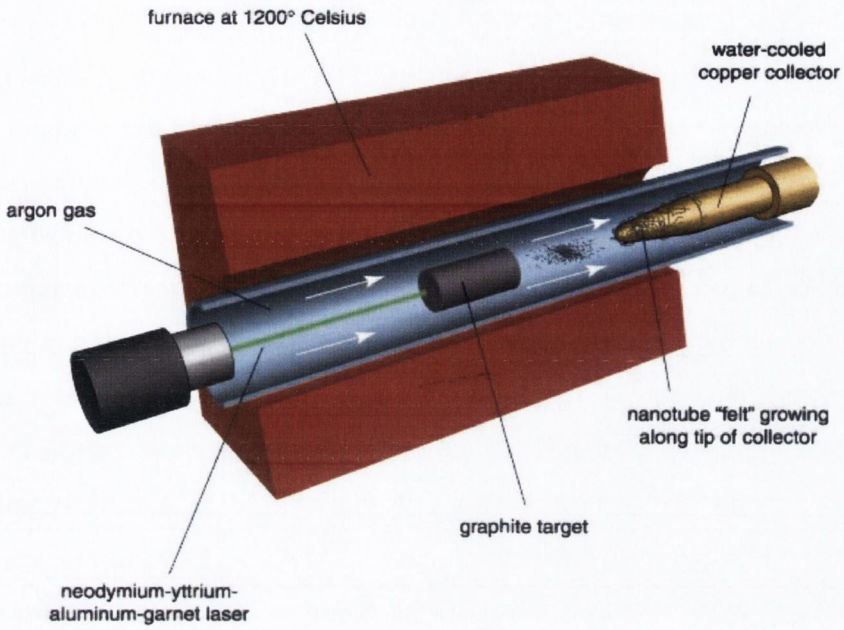


Fig. 2.10 Laser ablation experimental setup of CNTs synthesis *[28]*. Middle of images shows the source (graphite) of CNT, image also shows the collection of CNTs on copper collector at the (extreme right ).

**Chemical Vapour Deposition (CVD):**

The most common technique for the production of CNTs is chemical vapour deposition (CVD). Commonly CVD production setups consist of a high temperature furnace*[28]*. The temperature can be in the range of 500 to 1100 °C while atmospheric pressure is maintained. A hydrocarbon source like methane, acetylene, ethanol etc is introduced with a process gas e.g. hydrogen, ammonia, nitrogen. The hydrocarbon decomposes and grows over the nano catalyst usually Ni, Fe, Co in the form of CNTs. A catalyst can either be used on a substrate or can be introduced in the gaseous phase. CNT diameters and lengths can be controlled by changing the catalyst particle size or varying the experimental conditions. Biproducts in the CVD process can be amorphous carbon and graphite.

The CVD method has been known since 1959 from the work of Walker*[29]* . In 1959 for the first time CVD was used for the deposition of carbon. The experimental setup consisted of a 600mm long tube with an inner diameter of 25mm.The temperature was kept between 450 and 700 $C^{o}$ and hydrogen was used as the process gas. Carbon monoxide was

used as a carbon source. The first successful attempt to produce CNTs using the CVD method was adopted by Jose *et a.l* in 1993*[30]* . CNTs were grown by heating Fe/graphite at 700 $C^{o}$. Then a mixture of $N_2$/acetylene was introduced into the system at rate of 150 cc/minute at atmospheric pressure. Using plasma enhanced chemical vapour deposition, in 2000 Chris *et al.* was able to produce MWCNTs perpendicular to the substrate regardless of the tilting angle and surface of the substrate*[31]* . The experimental setup consisted of a 6 inch diameter stainless steel cylinder. The system was powered with a microwave power of 2.45 GHz, 5KW. The substrate was sputtered with Co catalyst prior to CVD. The chamber temperature was kept at 825 $C^{o}$ in a flowing hydrogen atmosphere at a pressure of 20 torr. One kW microwave plasma was then turned on. The hydrogen atmosphere was replaced by an ammonia/acetylene mixture. MWCNTs were observed growing perpendicular to the substrate 10 seconds after the introduction of the ammonia/acetylene mixture. Instead of using a petroleum based hydrocarbon, in 2007 researchers from Meijo university grew CNTs from camphor, purified from camphor tree extracts.*[32]* . They were able to grow 1.62 g of CNTs from 3 g of camphor in 1 hour. This corresponds to a camphor-to-CNT production efficiency ~50% with purity of over than 88%.

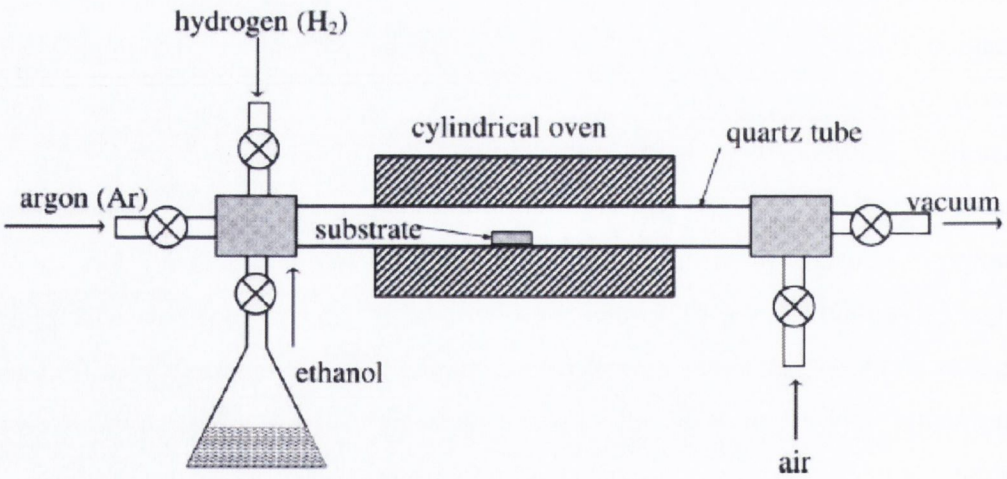


Fig. 2.11 CVD experimental set-up *[33]*

Compared to the arc discharge and laser ablation methods, the CVD technique is cost-effective, provides good yields and a good production rate of up to 50 kg per day *[25]*.

The issue with this method is that CNTs produced with CVD can have more defects than carbon nanotubes produced by either laser ablation or the arch discharge technique. Therefore the resultant CNTs from CVD exhibit reduced mechanical and electrical properties

## 2.3 Polymer

The word polymer is derived from the Greek word pelu meaning many and meros meaning part*[34]* . Polymers are long chain molecules usually with one or more repeating units of atoms. Polymers can consist of entangled disordered chains called *amorphous regions* or may be arranged in orderly repeated folded structures called *lamellae.* The ordered part of the polymer is referred to as crystalline Fig. 2.12.

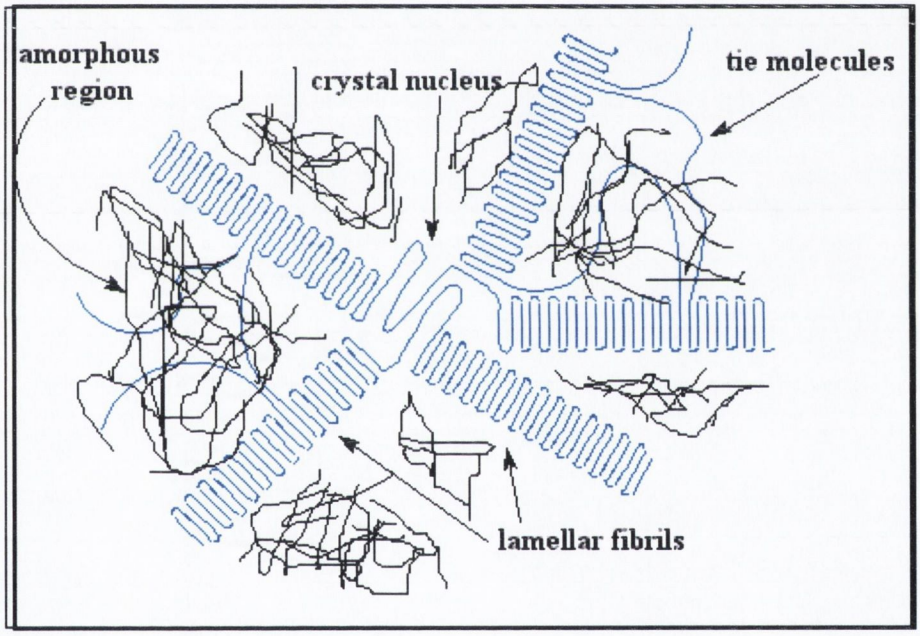


Fig.2.12 Illustrative model of semi crystalline polymer

Below a certain temperature amorphous polymers are hard and glassy or brittle because their chains remain coiled, tangled and motionless. But above a certain temperature the molecules become free to rotate and slip past each other due to the fact that molecules gain sufficient thermal energy to overcome the intermolecular interaction. The temperature is called glass transition temperature ($T_g$). Above the $T_g$ the polymer no longer remains

hardened, glassy or brittle but converts into a rubbery state. The glass transition temperature varies from polymer to polymer.

Usually the glass transition temperature is measured by differential scanning calorimetry (DSC) or dynamic mechanical thermal analysis (DMTA). In the case of DSC, because the heat capacity of a polymer increases at the $T_g$, this appears as a step in the DSC graph. The midpoint of the slope in step is usually taken as the $T_g$. While in DMTA analysis, when the ratio of loss and storage modulus is plotted as function of temperature, the highest peak in the plot is taken at $T_g$. Static $T_g$ is usually lower compared to the dynamic $T_g$ because $T_g$ is strain rate dependent*[35]*. Glass transition temperature of a polymer is decreased due to the trapped solvent in it (Fig.2.13).

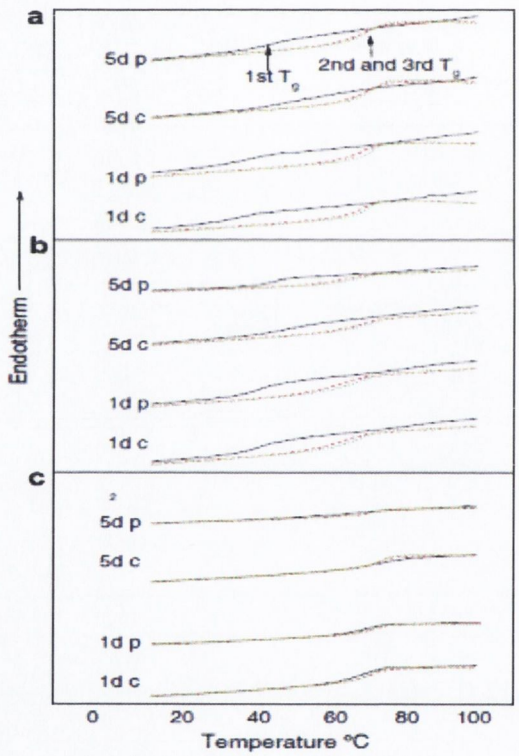


Fig.2.13 Three DSC heat run for SWCNT-PVA composites shows the effect of trapped solvent effect on Tg.

### 2.3.1 Types of polymers (on the basis of intermolecular interactions)

Polymers can be classified in many ways i.e., on the basis of their mechanical deformation, their thermal properties, polymerisation or number of repeating units. Below polymers have been classified into two basic types on the basis of intermolecular interactions among the polymer chains.

(1) Thermoplastics and

(2) Thermosets.

**Thermoplastic polymers**

The class of polymers in which long chain molecules are held by physical attractive forces (Fig.2.14)., and can be made soften from glassy/rigid state to a rubbery state, melt and be moulded under the influence of heat are referred to as thermoplastics. The temperature above which the polymer is converted to the rubbery state from glassy state is called as glass transition temperature ($T_g$). Many thermoplastics can be dissolved in organic solvents *[36-40]*. These polymers can be used as the matrix for the preparation of solution based and melt process CNT composites *[41,42]*. Thermoplastics can be rigid eg. Polyvinylchloride (PVC), flexible e.g. polyethylene (PE) or elastomeric e.g. thermoplastic polyurethane TPU.

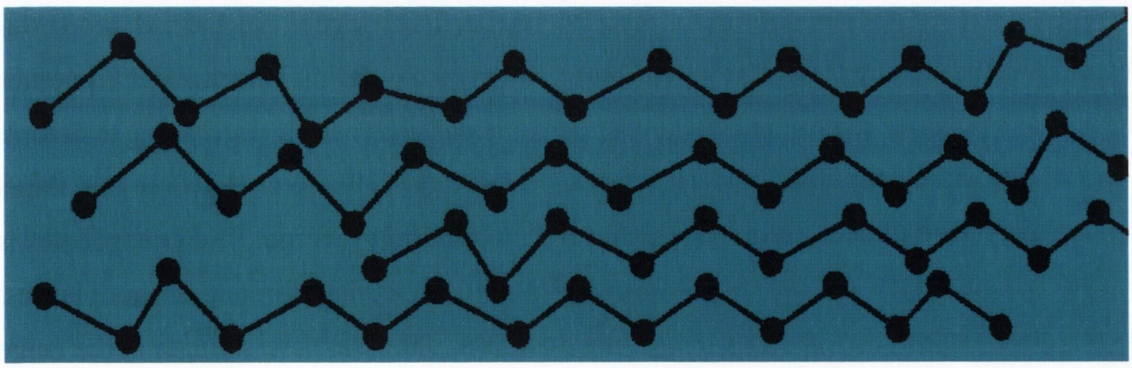

Fig 2.14 Thermoplastic molecular model shows polymer molecular chains without chemical crosslinking.

**Thermoset polymers:**

As the name implies, the polymer chains are permanently set in a particular form. The polymer chains are held together by chemical bonding hence forming a fixed network

(Fig.2.15). These molecules can not be heat moulded because of the molecules fixity. These polymers can not be dissolved in solvents due to the fixed and giant nature of their crosslinked structure. Thermoset polymers can be used as a matrix for solution based composites only by mixing CNTs with monomer or monomer solution. They are difficult to use as a matrix for the preparation of nanocomposites due the viscosity build-up during the polymerisation process which negatively affects dispersion of the CNTs.

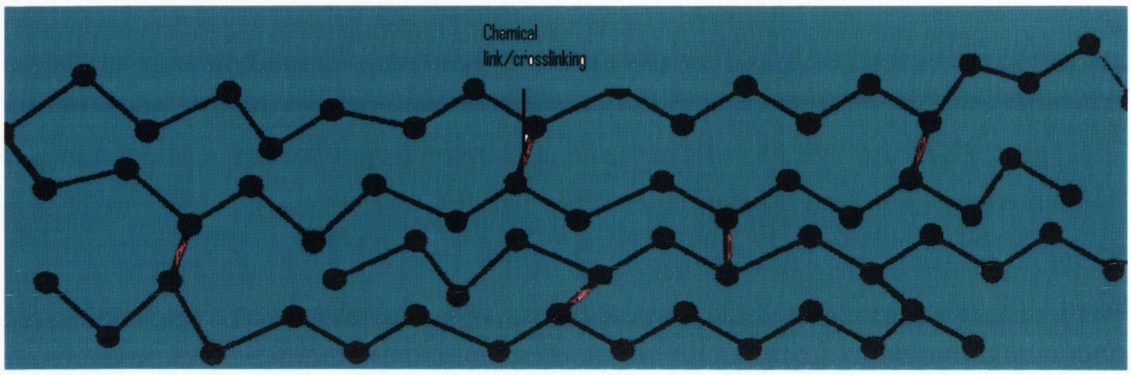


Fig. 2.15 Thermoset polymer molecular model shows polymer molecular chains chemically crosslinked together (presented by red line).

### 2.3.2 Mechanical properties of polymers

In general among plastics, thermoset plastics have higher mechanical properties than thermoplastic ones (Fig 2.16). Thermoset polymers have higher mechanical properties because the polymer chains are held by chemical bonding and need a larger force to deform the polymer. Examples of thermoset polymers are epoxy, kevlar etc. However this thesis deals mainly with thermoplastic polymers. Low mechanical properties in thermoplastics is due to its relatively weaker physical chain-chain interactions. Among thermoplastics, thermoplastic elastomers are very interesting materials. They can have strength in the range of rigid plastic and very high toughness in the range of kevlar and spider silk*[43-45]* .

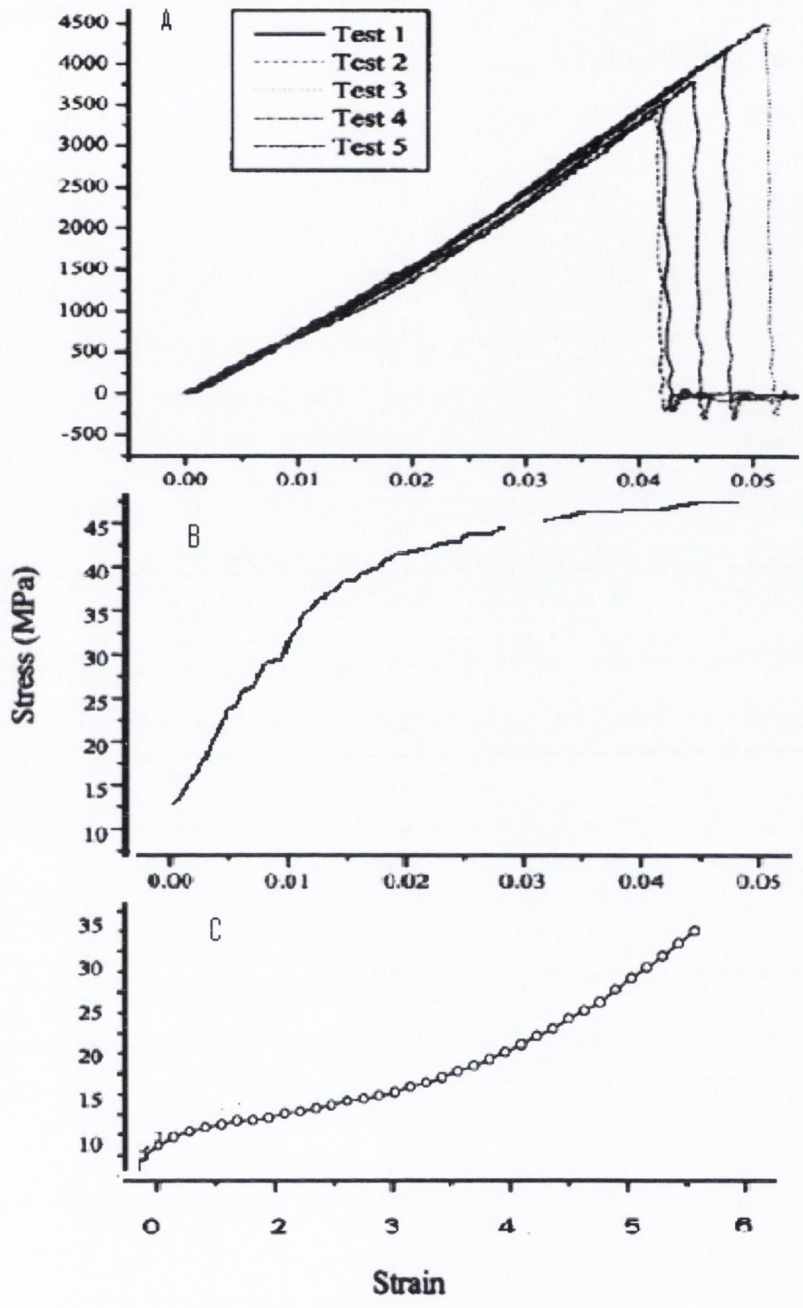


Fig 2.16 Typical stress strain curves for various polymers. A) Thermoset polymer (kevlar)*[46]* B) Thermoplastic polymer (PVA). C) Thermoplastic elastomer (TPU).

### 2.3.3 Effect of CNTs and solvent additives on thermal properties of polymer: indicator of mechanical properties

**Glass transition temperature**

Above $T_g$ polymer molecules can rotate and move freely*[35, 47]*. Thus any additive which will restrict molecular mobility will increase $T_g$ of the polymer. For a good reinforcement, the filler must have good interfacial bonding with the polymer*[5, 48]* . If the filler binds effectively to the polymer, it will restrict the polymer chains mobility, subsequently increasing $T_g$ of the polymer. Accordingly increases in $T_g$ reflects good interfacial boding and indicates the mechanical reinforcement by the filler. On the other hand, if a filler interrupts the inter-chain attractive forces and has no effective interfacial bonding with them, this could have a negative impact on the overall composite. Reduction in $T_g$ can also be due to the degradation of the polymer because low molecular weight polymers have lesser $T_g$ compared to the high molecular counterpart*[35]* . Degradation of a polymer also reduces the polymers mechanical properties*[49, 50]* . This means a reduction in $T_g$ with incorporation of filler can also be attributed to the degradation of polymer during processing. Again this will result in an overall reduction of mechanical properties of the composite. Composites prepared by solution processing can have some trapped residual solvent in them. Due to the plasticising effect, such solvents reduces the $T_g$ *[35]*, hence the mechanical properties of the polymer. The same reasons apply to the reduction in $T_g$ of polymer by a solvent apply to the filler. To understand the mechanical reinforcement of polymeric composites, $T_g$ measurement can be a good tool to understand the reinforcement in polymeric composites

Addition of CNTs to a polymer is usually associated with an increase in the $T_g$ due to restriction of the molecular mobility of the polymer chains. Ogasawara *et al.* showed that MWCNTs immobilize polymer chains and increases $T_g$*[51]* . Increases in $T_g$ have also been observed elsewhere*[52]*. As mentioned earlier any additive which facilitates chain mobility or degrade polymer decreases the $T_g$ of a polymer. Plasticizers are substances with small molecules*[53]* which are added to polymers to make them more flexible. The introduction of a plasticizer to a polymer reduces its strength and stiffness but increases its strain at break. Plasticizer also reduces the $T_g$ of the polymer*[53]* . Usually trapped solvent can have this effect and will be discussed in detail in chapter 3.

**Crystallinity**

An increase in the crystallinity of a polymer enhances its mechanical properties *[54, 55]*. Thus, introduction of filler into a polymer which increases crystallinity would mean an increase in mechanical properties of the polymer. The addition of CNTs not only influences the amorphous part of a polymer but can significantly alter the polymer crystallinity. It has been found that in many cases CNTs nucleate and increase crystallinity in polymeric composites*[52, 56] [54, 55]*.

The crystallinity of a polymer can be measured using a differential scanning calorimeter which will be discussed in detail in chapter 3. At $T_g$ the crystalline phase in the polymer does not change to a rubbery state because of its ordered structure. Ordered structures are more stable than amorphous ones and pass through thermal transitions at higher temperatures.

**Thermal stability**

In many cases composites are used in high temperature environments. Even though a filler imparts reinforcements to the matrix it can alter thermal stability of the polymer. Thus the filler effect of the thermal stability of the polymer must be known.

Other than affecting the $T_g$ and crystallinity (Fig.2.17) of a polymer, the addition of CNTs can significantly influence its thermal stability*[57-60]*. Polymer crystallinity can be measured using DSC which will be discused in chapter 3. In many cases the introduction of CNTs increases the thermal stability of the polymer at certain loading levels *[57-60]*. At very high loading, CNTs can have negative effect on polymer thermal stability*[58]* (Fig. 2.18).

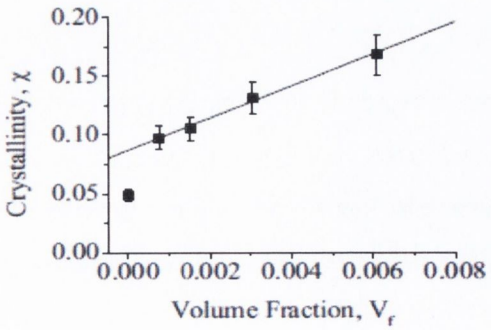


Fig.2.17 Increase in crystallinity of PVA with the introduction of CNTs*[36]*

The thermal stability of a polymer is usually measured by thermogravimetric analysis (TGA). The technique has described in Chapter 3 of the thesis.

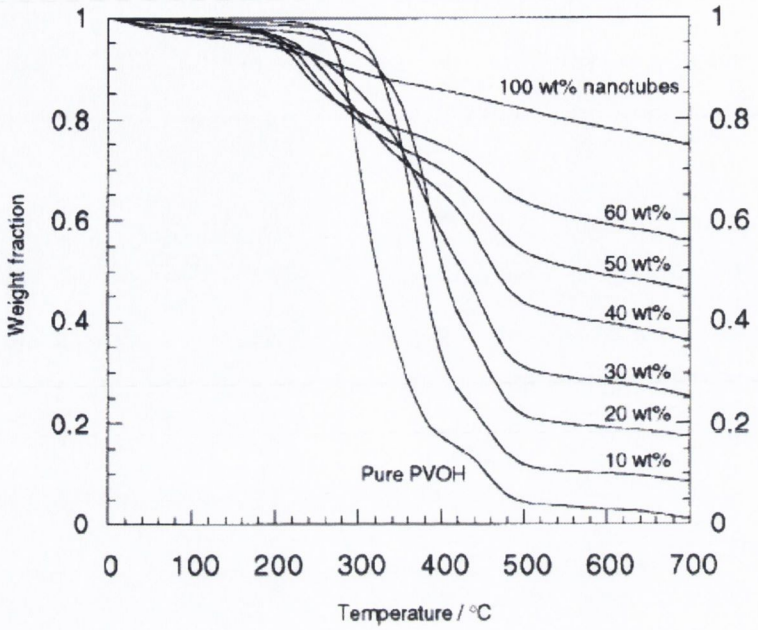


Fig.2.18 Effect of CNTs weight fraction (weight of CNTs /weight of CNTs+polymer ) on thermal degradation of PVA *[58]*

## 2.4 Type of CNT composites based on processing

Based on processing, CNT composites can be divided into three types,

(1) Solution based composites

(2) Melt processed composites and

3) Novel composites.

### 2.4.1 Solution based

The desire to disperse CNTs efficiently in polymer matrices for mechanical reinforcement makes solution based composites the most popular type of carbon nanotube polymer composite. It has been shown by various research groups that CNTs can also be dispersed very efficiently in organic solvents*[61-65]*. Various types of CNTs-polymer can

be dispersed/dissolved in many solvents *[36-40]*. A compatible CNT-polymer-solvent system can give rise to a homogenous and reinforced nanocomposite. In the solution based method, in general CNTs are dispersed in a solvent or in a polymer solution by energetic agitation *[66]*. This is followed by drying of the sample i.e, controled evaporation of solvent, leaving behind a CNTs composite.

In 1998 Jin*[42]* and co-researchers dispersed arc MWCNTs in chloroform by sonication for one hour. The matrix, polyhydroxyaminoether was introduced to the dispersion and was further sonicated for one hour. The composite solution was poured into a Teflon tray and dried in ambient conditions in a fume hood. The loading level of CNTs in the resultant composite was 50%*[42]* . In another study, Shaffer *et al.* dissolved polyvinylalcohol (PVA) in water. This was followed by mixing the PVA solution with a water MWCNTs dispersion. The dried composite was filled with up to 60 wt% CNTs*[58]* . In 2000 Qian used the same technique for the preparation of polymeric CNTs composites, using polystyrene as matrix and MWCNTs as a filler*[67]* . In subsequent years Safadi *et al.* and Valasco used the same method for the fabrication of CNTs composites*[52, 68]* . In 2004 Cadek prepared CNT/PVA/water composites using solution based techniques*[56]* . In 2006 Whitten *et al.* prepared SWCNT-DNA/distilled water composites with help of a dispersion agent*[69]* . In the following year Cong *et al.* prepared solution based composite using brominated poly(2,6-diphenyl-1,4-phenylene oxide) as matrix and chloroform as solvent. They used SWCNTs and MWCNTs as a filler to fabricate mechanically strong nanocomposite membranes for gas separating purposes*[70]* .

### 2.4.2 Melt processing

In spite the fact that CNTs disperse well in many solvents and polymer solutions, there are still many polymers which are insoluble in solvents. Many industrial manufacturing processes are based on melt processing of polymers. A combination of these factors attracted scientists to investigate the melt processing of CNT composites. The technique utilises the property of amorphous or semicrystalline polymers that allows them to soften and subsequently melt under the influence of heat. Amorphous polymers are processed above their $T_g$ and semi crystalline polymers above their crystalline melt temperature ($T_m$ ). In both cases, carbon nanotubes are shear mixed with the polymer*[5]* .

Using this technique Jen *et al.* melted polymethylmethacrylate (PMMA) together with arc MWCNTs at a loading of 26wt% at 200C° in a lab moulder. The melt was compress molded, using a hydraulic press. The SEM images showed good dispersion of CNTs even at this high loading level*[41]* . In following the year Andrew *et al* demonstrated the fabrication of CVD MWCNTs polymer composites. They used high impact polystyrene and acrylonitrile–butadiene–styrene (ABS) polymers for their melt processed composites*[71]* . They prepared a master batch of the polymers and CNTs. The master batch was diluted to form a lower mass fraction film with melts of respective polymers and shear mixed. The composite films were prepared by compression molding. The same technique was also used by a number of other researchers *[37, 72, 73]*. Potschke *et al.* prepared a CVD MWCNTs/polycarbonate master batch melt by shear mixing at 260 C° in a mir-compounder*[74]* . They diluted the master batch with polycarbonate polymer in a micro-compounder*[74]* . They fabricated the composites by extrusion through a circular die. Their work revealed that small scale extrusion can be as efficient as large scale. Polymer degradation due to the high shear rate was also observed in their work. In 2004 Russell dry blended SWCNTs and MWCNTs with PMMA and extruded with twin blades at 130 C° through a cylindrical die*[75]* . In the same year Meincke *et al.* mixed polyamide-6, poly acrylonitrile butadiene styrene (ABS) and CVD-MWNTs in a twin screw extruder at 260 C°. This was followed by the cutting of the samples into pellets. The sample was inject molded to get composites with a good dispersion of CNTs*[76]* . In 2006 Ghose dry mixed phenylenethyl terminated imides and MWCNTs and inject molded it through hydrostatic pressure at 371C°*[77]* . They demonstrated the fabrication of polyimide nanocomposites containing up to 15 wt% MWCNTs without exceeding the maximum tolerable melt viscosity for composite processing. Alig *et al* fabricated MWCNTs composites by heat melting polypropylene (PP) (200-220 C°). They prepared a master batch and diluted the master batch further to 2, 3.5, 5 wt % by adding PP*[78]* .

### 2.4.3 Novel method of composites fabrication (very high mass fractions)

High viscosity in melt processing rendering good dispersions of CNTs and also melt blend of CNTs is difficult to process. In addition melt processing can cause polymer degradation *[74]*. While solution processing of CNTs is a famous tool for the fabrication

of CNT composites at higher concentrations, the nanotubes tend to bundle together. This causes a reduction in the mechanical properties *[5]*. To minimise these negative effects, a novel composite fabrication technique can be used called the buckypaper preparation technique i.e. filtration of a CNT solution through a filter membrane. Generally speaking, in this technique the CNTs are dispersed in large volumes of a solvent or polymer solution. The dispersion/solution is then filtered through a micromembrane under vacuum. CNTs/composites are deposited on the membrane and after drying a free standing film is peeled off the membrane. The CNTs concentration within the dispersion does not increase with time as usually happens in the case of conventional solution based process systems. Therefore very high CNTs loaded composite can be achieved with out significant aggregations of the CNTs. In 2003 Coleman *et al[79]* in their work they soaked the SWCNTs films in polyvinylalcohol (PVA), polyvinyl pyrolidone (PVP) and polystyrene (PS) solutions. The films obtained were called Buckypaper*[79]*. They observed the intercalation of up to 30wt % of the polymer in the porous CNT network. Intercalation is a process in which a polymer solution penetrates into the free volume of CNTs network by capillary action. In the following year Wang and co-researchers fabricated CNTs/epoxy composite by Buchner infiltration*[80]*. Firstly they prepared a CNT buckypaper. This was followed by infiltration of epoxy solution dissolved in ethanol through it. They noted a very good infiltration of epoxy through out the composite system. To get a thicker film, they placed several buckypapers on top of each other and pressed and cured them at 177C°. In recent years Blighe *et al.* (2008) demonstrated the fabrication of buckypapers with a variety of SWCNTs nanotubes*[81]* In their work they used pristine SWCNTs as well as a range of funtionalised nanotubes. All of the buckypaper were prepared without the incorporation of any polymer. The CNTs networks in all the buckypapers were held by physical interaction between the CNTs. Their work demonstrates that the films mechanical properties are dependent on CNTs junction densities i.e increasing number of CNTs junction increases mechanical properties i.e. stiffness and strength. In the same year Blighe and co researchers were able to prepare buckypaper by the filtration of chemical modified SWCNT/polyurethane/water dispersion through a micromembrane. The average diameter of the filtration membrane was 45 micrometer. In the same paper they discussed the preparation of layer by layer buckypaper composites as well. The work was break-through

in the mechanical reinforcement of polymers by CNTs. They demonstrated supper high increase in Young's modulus by a factor of 800 of polymer with addition of 0.75 mass fraction of CNTs. They also noted sharp decline in UTS and ductility with each increment of CNTs loading*[82]*. UTS is defined as the maximum observed stress in a stress strain curve

## 2.5 Models for fibre reinforced composites

Adding CNT to polymers increases both the modulus and strength. In order to predict these properties a number of different models have been suggested. Here, some of the models relevant to this work will be discussed.

### 2.5.1 Rule of Mixtures

The Young's Modulus ($Y_c$) of a composite can be predicted using the "Rule of Mixtures", if a number of conditions are satisfied*[48]*.

- The stress is perfectly transferred from matrix to fibre i.e. good bonding between the two.
- Fibres are aligned to the applied stress.
- Under all circumstances, both matrix and fibre are strained equally.
- Then the Young's modulus of the composite is given by:

$$Y_C = (Y_f - Y_m)V_f + Y_m \quad \text{Eq. 2.2}$$

where, $Y_f$ is the fibre modulus, $Y_m$ is the matrix modulus, $V_f$ is the fibre volume fraction.

Equation 2.2 is called the rule of mixtures*[48]*.

This model is for ideal conditions, but as the filler is usually much stiffer than the matrix, they cannot strain equally. Also, the fibres are usually randomly oriented in the matrix. This rule of mixtures has been modified for randomly oriented fibres by Cox*[83]* using the Krenchel expression:

$$Y_C = (\eta_o \eta_l Y_f - Y_m)V_f + Y_m \quad \text{Eq. 2.3}$$

where $\eta_o$ is the orientation efficiency factor (this has values of $\eta_o$=1 for aligned fibres, $\eta_o$=3/8 for fibres aligned in plane and $\eta_o$=1/5 for randomly oriented fibres*[84]* ), and where $\eta_l$ is the length efficiency factor and given by:

$$\eta_l = 1 - \frac{Tanh(a \cdot l / D)}{a \cdot l / D} \quad \text{Eq 2.4}$$

where $l$ is length and D is diameter of fiber and $a$ is given by

$$a = \sqrt{\frac{-3Y_m}{2Y_f \ln V_f}} \quad \text{Eq. 2.5}$$

Equation (2.2) can be modified to calculate the UTS of short fibre reinforced composites ($\sigma_C$).

$$\sigma_C = (\eta_s \sigma_f - \sigma_m) V_f + \sigma_m \quad \text{Eq. 2.6}$$

where $\eta_s$=(1-$l_c$/2l) and is called the strength efficiency factor, $\sigma_f$ is fibre strength, l is the fibre length and $l_c$ is the fibre's critical length. For effective reinforcement in composites filled with fibres, the fibres must have a certain minimum length called critical length ($l_c$ ). The critical length is given by

:

$$l_c = \frac{\sigma_f D}{2\tau}\left[1 - \frac{D_i^2}{D^2}\right] \quad \text{Eq. 2.7}$$

where $\tau$ is the fiber-matrix interfacial strength, D is the external diameter and $D_i$ is the internal diameter of the fibre respectively. For SWCNT there is almost no difference between the internal and external diameter however for MWCNT the difference depends on

the numberes of CNT walls which for example the internal diameter for MWCNT can be 8nm while external diameter for the same nanotube can be 20nm.

For real reinforcement the fibre length should be more than the critical length.

**Critical length**

In the case of fibre filled composite the filler must have some critical length ($l_c$) for effective mechanical reinforcements, which is defined by equation 2.7. For a composite filled with fibre have length equal to $l_c$ ($l=l_c$) then only axial centre of the fibre feel the maximum stress (Fig 2.17 B) while when $l > l_c$ then the reinforcements become more effective and stress transfers to a larger area of the fibre (Fig 2.17 C). However, when $l < l_c$ the stress cant be transfer to the fibre (Fig 2.17 A). A fibre having $l > 15l_c$, is called continuous fibre and the one have length lesser than 15 $l_c$ is termed as the discontinuous or short fibre*[48]*. The matrix filled with short fibres exhibits either no or very slight reinforcement because stress does not transfer efficiently to the filler*[48]*.

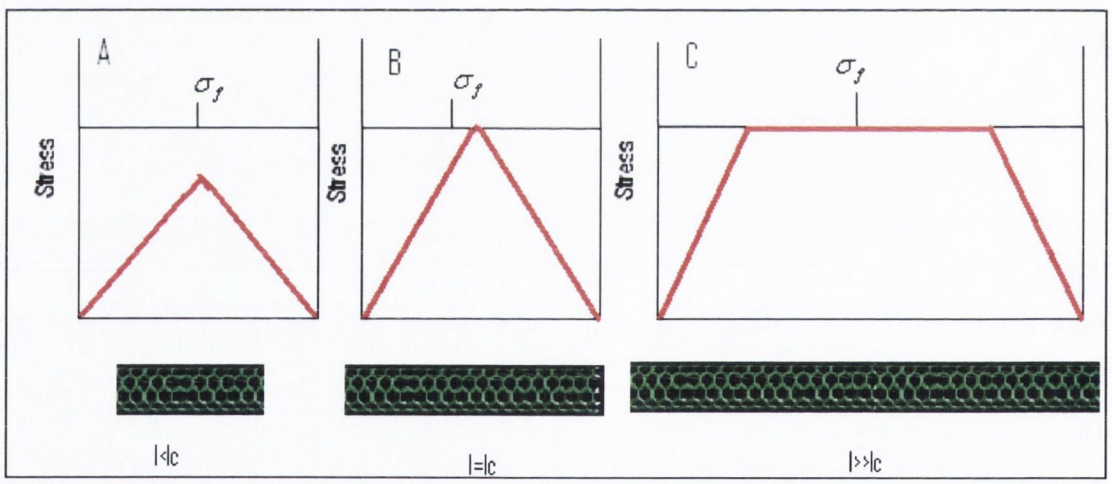


Fig 2.19 Illustration of stress position in fibre (reinforce composites) A) when $l = l_c$, B) $l >$ lc, C) $l >> l_c$ *[48]*

## 2.5.2 Halpin and Tsai model

This model is based on the work by Hills*[85]* to predict the Young's modulus of aligned short fibre composites*[86]* . The Young's modulus is given by:

$$Y_C = Y_m \frac{(1+\zeta\eta V_f)}{(1-\eta V_f)} \quad \text{Eq. 2.8}$$

where $\zeta = 2l/D$ and

$$\eta = \frac{Y_f / Y_m - 1}{Y_f / Y_m + 1} \quad \text{Eq. 2.9}$$

By modifying Equation (2.8) :

$$\frac{Y_C}{Y_m} = \frac{3}{8}\left[\frac{1+\zeta\eta_L V_f}{1-\eta_L V_f}\right] + \frac{5}{8}\left[\frac{1+2\eta_T V_f}{1-\eta_T V_f}\right] \quad \text{Eq. 2.10}$$

$$\text{where } \eta_L = \frac{Y_f / Y_m - 1}{Y_f / Y_m + \zeta} \quad \text{Eq. 2.11}$$

$$\text{and } \eta_T = \frac{Y_f / Y_m - 1}{Y_f / Y_m + 2} \quad \text{Eq. 2.12}$$

Equation (2.10) is the Halpin and Tsai equation for randomly oriented fibre composites. Halpin and Tsai equation is good for low mass fractions composites while rule of mixtures can be used for high mass fraction composites as well.

## 2.6 Requirement for effective reinforcement and role of funtionalised CNTs.

For effective reinforcement there are certain requirements which should be fulfilled. These are as

- Critical length
- Alignment of the filler material
- Good dispersion of the filler
- Stress transfer/ interfacial bonding between the filler and the matrix

**Critical length**

The critical length has been discussed earlier, the remaining factors will be discussed here.

**Alignment**

Composite prepared with aligned fibres exhibit higher mechanical properties than composites filled with randomly oriented fibres. The Young's modulus of aligned fibre composites can be higher by a factor of five *[5]*. These composites can have higher strength as well but the down side of these composites is anisotropy i.e composites shows good reinforcement in direction of alignment only. In the case of a fibre (composite) anisotropy does not matter.

**Dispersion**

One of the most important parameters for reinforcement in composites is uniform dispersion of the filler in the matrix. For mechanical reinforcement the effective penetration of adhesive resin among the filler fibres or particles is essential. In other words, wetting by the polymer of the maximum number and area of filler particles results in the maximum reinforcement of the composite. This can be achieved by the presence of a maximum numbers of individual CNTs per given volume in the composite system. One way to achieve a maximum number of individual CNTs and small bundles per given volumes is to disperse CNTs in an appropriate solvent. Pristine nanotubes remain in bundles but in solvents at very low concentration they can be exfoliate into individual tubes and small bundles *[65]*. At very higher concentrations CNTs do not stay suspended in a solvent and fall out*[87]*. To achieve good dispersion at high concentration researchers also use surfactants to disperse CNTs. Surfactants molecules have two ends one of which is compatible with solvent while other is phobic to the solvent and attached it self to CNT*[88]*. In this way a number of molecules (micelle) surrounds the CNT, exfoliate and make it dispersed in the solvent. On drying these surfactant molecules remain adhered to the CNT and form coating around it Due to the coating around the CNTs surfactants can have drawbacks in composites*[89, 90]* e.g coating around CNTs reduces mechanical and electrical properties. Thus pristine CNTs/solvent or pristine CNTs- surfactant/solvent can not be used for high mass fraction composite preparation due to aggregation of CNTs. In recent times it has been shown that chemically modified CNTs can be effective disperse in

various solvents at very high concentrations*[91, 92]* . Therefore high mass fraction CNTs composites with good CNTs dispersion can be prepared with chemically funtionalised CNTs.

**Stress transfer/ interfacial bonding**

Stress transfer to the filler is vital for composite reinforcement. Stress can be transferred to CNTs if there is good interfacial bonding between CNTs and matrix. The matrix can bind to CNTs either by physical bonding (Van der Waals forces) or mechanical interlocking*[93]* . Van der Waals forces are the weak attractive forces which exist among atoms, molecules, and surfaces. These are the primary bonds which exist between the polymer and CNTs in composites. Unlike chemical bonding these bonds are relatively weak. Adding to this, CNT bundles are also held by these weaker forces. Thus, in the case of composites applied stress usually does not transfer effectively to CNTs either because of CNT-polymer interface or CNT-CNT bonding. Mechanical interlocking is a process in which liquid, molten, solution based matrix is dried/cured in the nano/micro/ patches of filler. Thus the filler is bonded to polymer matrix by mechanical interlocking. In most cases CNTs have atomically smooth surfaces hence this kind of interaction is not possible in pristine CNTs. As with the issue of dispersion, again functionalised CNTs can have superior interfacial bonding properties to pristine CNTs. Functional groups of nanotubes can entangle with matrix chains. Adding to this, functionalities can form hydrogen bonding with matrix molecules*[57]* . Attached functional groups can react chemically and form chemical bonds and hence very good stress transfer and reinforcement*[94]* .

In an endeavor for such composites Yang *et al.* prepared CNTs composites using pristine MWCNTs and funtionalised MWCNTs as the filler and p(MMA-co–EMA) as the matrix. They did not observe any remarkable difference between funtionalised and nonfunctionalised CNTs*[95]* . Blak *et al.* funtionalised CVD MWCNT with polyproylene (PP). They fabricated composites by blending PP-CNTs with chlorinated PP*[96]* . Young's modulus was increased from 0.22 to 0.68 GPa. While strength and toughness was increased from 12.5 to 49 MPa and from 24 to 108 J/g respectively. Zhu *et al.* funtionalised SWNCTs with large organic group and blended it with epoxy resin *[97, 98]*. They covalently bonded these SWNCTs to epoxy. They noted an increase in Young modulus from 2.02 to 3.4 GPa

with a 4 wt% loading of CNTs. This corresponds to $dY/dV_f \sim 95$ GPa. An increase in strength from 83 to 102 MPa was also recorded. They also observed the fracture of CNTs. This suggests good stress transfer to the CNTs*[97, 98]* . Hwang chemically attached PMMA molecules to arc MWCNTs. These chemically modified CNTs were dispersed in PMMA matrix*[99]* . The resultant composite were reinforced by adding up to 20 wt% CNTs. They were able to significantly increase the modulus of composite to 29 GPa from 2.9 GPa with respect to polymer only sample. They observed enhancement in modulus with increase in CNTs loading even until 20 wt%. CNTs failure were observed by the ''sword and sheath'' method suggesting good interfacial stress transfer.

## 2.7 Mechanical properties of CNTs composites

As has been discussed in the previous chapter the primary purpose of a composites material is to prepare stiff, strong and tough yet light materials. To obtain such a material the polymer must fulfil the criteria of a good matrix.

Here the mechanical reinforcement is compared for work done by various researchers in terms of the increase in Young's modulus of polymer per volume fraction ($V_f$) of CNTs added. This values are expressed as $dY/dV_f$ . Y is the Young's modulus and $V_f$ is volume fraction of CNTs. The $dY/dV_f$ value can be extracted from experimental data of a composite or from series of composites with various mass fraction of CNTs (slope of Y vs $V_f$ ). $dY/dV_f$ can also be calculated using equation 2.1.

$$\frac{dYc}{dV_f} = \eta_o \eta_l Y_f - Y_m \quad 2.1 \; [5]$$

where $\eta_o$ is the orientation efficiency factor. This has values of $\eta_o$=1 for aligned fibres, $\eta_o$=3/8 for fibres aligned in plane and $\eta_o$=1/5 for randomly oriented fibres *[84]*

Shaffer was the first to fabricate solution based CNTs/polymer nanocomposites and study their mechanical behavior *[58]*. He prepared solution processed CVD-MWNTs-PVA composites with a filler loading level of 60 wt%. He used DMTA for mechanical

measurements. His study shows very small increase in the storage modulus of the polymer, the Young's modulus was increased from 6 GPa to 12 GPa with $dY/dV_f$ value ~ 4.7 GPa . It was found that above the glass transition temperature, the results were even better. In another study, Qian *et al.[67]* studied CVD-MWNT-polystyrene (PS) composites by tensile testing. They used 1 wt% of both short (~15μm) and long (~50μm) CVD-MWNTs and observed an increase in the Young's modulus from 1.2 GPa to 1.62 GPa and 1.69 GPa respectively, with a $dY/dV_f$ value of ~74 GPa. To understand the reinforcement mechanism they cracked the sample while observing it under scanning electron microscope (SEM).They noted the craze formation and observed that the crazes were bridged by the CNTs. Crazing is the phenomena of fine crack formation which may extend in a network on or under the surface or through a layer of plastic material*[100]*. When crazes reached 800 nm CNTs were either pulled out or fractured. This suggests that the interfacial bonding was not uniform or that the CNTs had weak points/defects. Safadi *et a.l[68]* also studied composites made with CVD-MWNT-PS using tensile testing. Their study showed a significant increase in the Young's modulus of the composite. Young's modulus increased by a factor greater than 2 compared to the polymer with a filler content of 2.5 vol% ($dY/dV_f$ ~ 122GPa), the pull out and the fracture of CNTs was also observed. While in another study Watts observed only the pull out of arc MWCNT from the matrix but no fracture*[101]* . These results suggests that CVD MWCNTs have low mechanical properties compare to arc MWCNTs. Cadek *et al.[39]* studied solution based polyvinylcarbazole (PVK) and PVA composites produced with arc-discharge MWNT. They found that the Young's modulus of the PVA was increased from 7 GPa to 12 .6 GPa with 0.6 vol.% of MWNTs. For PVK, the Young's modulus was increased from 2 GPa to 5.6 GPa with 4.8 vol % of MWNTs. Their DSC work revealed a linear increase in crystallinity of the PVA composite with increased CNT content, no such increase was noted for PVK samples. This suggested that the difference in reinforcement in PVA and PVK composites may be due to the presence of ordered structures at the polymer nanotube interface in PVA samples. Frankland also suggested the presence of an ordered structure at interface in her SWCNTs work*[17]* . Coleman *et al.* observed an increase in Young's modulus from 1.92 to 7.04 GPa in PVA-MWCNTS composites with a $dY/dV_f$ ~754 GPa*[36]* . Velasco *et al.* noted an increase in modulus from 0.71 GPa to 2.34GPa in arc MWCNTs/ methylethyl-methacrylate

co-polymer composites at 1wt% loading with a $dY/dV_f$ value ~272*[52]* . In another study, Ruan *et al.[102]* observed stress transfer to nanotubes using Raman spectroscopy. They used the D-band sensitivity of nanotubes to strain in the Raman spectra to show that significant stress was transferred to the nanotubes. Cadek *et al.[56]* used SWCNT, DWCNT, CVD-MWCNT and arc-MWNT as fillers in a PVA matrix. The outcome of this study was that the Young's modulus of the composite was observed to be directly related to the matrix-CNTs interfacial area, except for SWNTs. The result for SWCNT was explained in terms of bundle formation. Bundles reduce the interfacial area, and also CNTs in these bundles are bonded by weak Van der Waals forces, so the CNTs can slip easily under applied stress.

Jin *et al.[41]* fabricated PMMA-Arc-MWNT composites by melt processing and tested them by DTMA. For a filler load of 17 wt% they observed an increase in Young's modulus from 0.7 GPa to 1.63 GPa. In terms of $dY/dV_f$ this corresponds to 7 GPa, which is not significant reinforcement. Gorga *et al.[74]* studied the mechanical properties of polycarbonate-CVD-MWNT composites fabricated by melt processing. They observed a very small mechanical reinforcement, with a $dY/dV_f$ value of 2.4 GPa. Zhang *et al.[37, 73]* showed that the Young's modulus of polyamide-6 can be increased from 0.4 GPa to 1.24 GPa on addition of only 2 wt % CVD-MWNT, corresponding to $dY/dV_f$ value ~ 64 GPa.

Many of the thermoset polymers have higher mechanical properties than thermoplastics*[48]* . Also thermosets remain stable at elevated temperatures, while as the name indicates, thermoplastics lose their rigid structural integrity at $T_g$ or $T_m$. Owing to their superb mechanical properties and high aspect ratio CNTs are an attractive reinforcing filler for thermosets polymers. To understand the behavior of CNTs in a thermoset matrix, Ajayan *et al.[103]* fabricated and studied nanocomposites with a thermoset binder. In his epoxy-nanotubes work, the nanotubes were aligned using force produced by cutting the composite with a diamond knife. The values mentioned above are summarized in table 2.1

| Nanotube Type | Polymer | $Y_{Poly}$ (GPa) | $Y_{Max}$ (GPa) | $dY/dV_f$ (GPa) | Reference |
|---|---|---|---|---|---|
| CVD-MWCNT | PVA | ~6.3 | ~12.6 | ~4.7 | *[58]* |
| CVD-MWNTs | PS | 1.2 | 1.69 | ~74 | *[67]* |
| CVD-MWCNTs | PS | 1.53 | 3.4 | 122 | *[68]* |
| Arc-MWCNT | PVA | 7 | 12.6 | 990 | *[39]* |
| CVD-MWCNTs | PVA | 1.9 | 7.04 | 754 | *[36]* |
| Arch-MWCNTs | MEMA | 0.71 | 2.3 | 272 | *[52]* |
| Arc-MWNT | PVK | 2 | 5.8 | 75 | *[39]* |
| CVD_MVCNTs | PC | 0.8 | 1.04 | 2.4 | *[74]* |
| Arc-MWNT | PMAA | 0.7 | 1.63 | 7 | *[41]* |
| CVD-MWNT | PA-6 | 0.4 | 1.24 | 64 | *[37, 73]* |

Table. 2.1 Summary of mechanical properties of CNTs composites observed by various researchers.

## 2.8 Conclusion

Carbon nanotubes not only directly reinforce the polymer matrix because their excellent mechanical properties *[5]* but can indirectly enhance the mechanical properties by altering polymer morphology*[54, 55]* . Owing to theses unparallel properties, CNTs would be the potential filler for future composites. Having said that, there are certain issues with

CNTs which have to be addred for their effective utilisations. One issues with CNTs in use as filler is, their aggregation and poor dispersion. Although CNTs show very good dispersion in certain high boiling point organic solvent but at very low concentration*[65, 87]*. These high boiling point solvent can remain trapped in composite and reduce their mechanical properties*[104]* . At relatively high concentration CNTs tends to aggregate*[65, 87]* which is again hurdle in the utilising their properties. Bucky paper approach *[79]* can resolve this problem but again this method can not be used as industrial technique due the involvement of very large volume of solvent. Another problem with CNTs is their atomically smooth surface due to which mechanical interlocking and polymer chains entanglement is not possible hence less effective reinforcement. All theses issues can be resolved to quite a good extent by use of functionalised CNTs. Carbon nanotubes can be funtionalised with variety of functional groups which can then dispersed in number of low boiling point, high boiling point, organic and aqueous solvents, at high concentrations *[91, 92, 105]*. The attached functional groups can be large*[91]* enough to entangle with polymer chain hence imparting mechanical reinforcement. Functionalisation of CNTs can create defects in CNTs, at one hand this can reduce their mechanical properties of CNTs but at the other hand creating sites for mechanical interlocking. Therefore funtionalised CNTs would the potential filler of future composites.

## 2.9 Reference.


[1] C. Lee, X. Wei, J. W. Kysar, J. Hone, *Science* **2008**, *321*, 385.
[2] I. W. Frank, D. M. Tanenbaum, A. M. v. d. Zande, P. L. McEuen, *J. Vac. Sci. Technol. B,* **2007**. *6,* 2558,
[3] Kroto, e. a. H.W., *Nature* **1985**, *318*, 162.
[4] S. Iijima, *Nature* **1991**, *354*, 56.
[5] J. N. Coleman, U. Khan, W. J. Blau, Y. K. Gun'ko, *Corbon* **2006**, *44*, 1624.
[6] B. T. Kelly, *Physics of Graphite.*, Applied Science London, **1981**.
[7] K. Perepelkin, *Soviet materials science* **1972**, *8*, 198.
[8] R. Bacon, *Journal of Applied Physics* **1960**, *31*, 283.
[9] G. Overney, W. Zhong, D. Tomanek, *Zeitschrift fur physic D-atoms molecules and clusters* **1993**, *27*, 93.
[10] J. P. Lu, *Journal of Physics and Chemistry of Solids* **1997**, *58*, 1649.
[11] M. M. J. Treacy, T. W. Ebbesen, J. M. Gibson, *Nature* **1996**, *381*, 678.
[12] Eric W. Wong, Paul E. Sheehan, a. C. M. Lieber, *Science* **1997**, *277*, 1971.

[13] S. Jean-Paul, J. K. Andrzej, B. Jean-Marc, D. B. G. Andrew, S. Thomas, M. Karine, B. Sylvie, B. François, A. B. Nancy, F. Lásló, *Advanced Materials* **1999**, *11*, 161.
[14] R. Bernardo, T. K. Baker, K.J. Huttinger, Shaffer, J.L. Figueiredo, C. A. G.G., Tibbetts, a. Kinloch, *Carbon Fibers, Filaments and Composites*, Vol. 73, Kluwer Academic Publishers, **1990**.
[15] M Yu., L. Oleg, J. D. Mark, M. Katerina, F. K. Thomas, S. R. Rodney, *Science* **2000**, *287*, 637.
[16] J. P. Salvetat, G. A. D. Briggs, J. M. Bonard, R. R. Bacsa, A. J. Kulik, T. Stockli, N. A. Burnham, L. Forro, *Physical Review Letters* **1999**, *82*, 944.
[17] S. J. V. Frankland, A. Caglar, D. W. Brenner, M. Griebel, *Journal of Physical Chemistry B* **2002**, *106*, 3046.
[18] T. W. Ebbesen, P. M. Ajayan, *Nature* **1992**, *358*, 220.
[19] D. S. Bethune, C. H. Kiang, M. S. Devries, G. Gorman, R. Savoy, J. Vazquez, R. Beyers, *Nature* **1993**, *363*, 605.
[20] M. Takizawa, S. Bandow, T. Torii, S. Iijima, *Chemical Physics Letters* **1999**, *302*, 146.
[21] C. Liu, H. M. Cheng, H. T. Cong, F. L. G. Su, B. L. Zhou, M. S. Dresselhaus, *Advanced Materials* **2000**, *12*, 1190.
[22] T. Zhao, Y. Liu, *Carbon* **2004**, *42*, 2765.
[23] M. Cadek, R. Murphy, B. McCarthy, A. Drury, B. Lahr, R. C. Barklie, M. in het Panhuis, J. N. Coleman, W. J. Blau, *Carbon* **2002**, *40*, 923.
[24] M. Cadek, Vol. PhD, Trinity College University of Dublin, Dublin **2004**.
[25] D. Blond., in *School of Physics*, Vol. PhD, Trinity College University of Dublin, Dublin **2008**.
[26] K. Rupesh, B. Suryasarathi, *Journal of Minerals & Materials Characterization & Engineering* **2005**, *4*, 31.
[27] H. Dai, A. G. Rinzler, P. Nikolaev, A. Thess, D. T. Colbert, R. E. Smalley, *Chemical Physics Letters* **1996**, *260*, 471.
[28] B. Yakobson, R. Smalley, *American scientist* **1997**, *85*, 324.
[29] P. L. Walker, J. F. Rakszawski, G. R. Imperial, *J. Phys. Chem.* **1959**, *63*, 133.
[30] M. Jose-Yacaman, M. Miki-Yoshida, L. Rendon, J. G. Santiesteban, *Applied Physics Letters* **1993**, *62*, 202.
[31] C. Bower, W. Zhu, S. Jin, O. Zhou, *Applied Physics Letters* **2000**, *77*, 830.
[32] K. Mukul, A. Yoshinori, *Journal of Physics: Conference Series* **2007**, 643.
[33] G. Ortega-Cervantez, G. Rueda-Morales, J. Ortiz-López, *Microelectronics Journal* **2005**, *36*, 495.
[34] *Webster's New World Dictionary*, Wiley & Sons., New Yark **1988**.
[35] T. Hatakeyama., Z. L, *Handbook of thermal analysis*, John Wiley & sons Ltd, **1998**.
[36] J. N. Coleman, M.Cadek, R. B. ., V. N. ., K. P. R. ., C. B. ., A. F. ., J. B. N. ., Y. K. Gun'ko., W. J. . in *Advanced Functional Materials*, Vol. 14, **2004**, 791.
[37] W. De Zhang, L. Shen, I. Y. Phang, T. X. Liu, *Macromolecules* **2004**, *37*, 256.
[38] Y. Bin, M. Mine, A. Koganemaru, X. Jiang, M. Matsuo, *Polymer* **2006**, - *47*, 1308.
[39] M. Cadek, J. N. Coleman, V. Barron, K. Hedicke, W. J. Blau, *Applied Physics Letters* **2002**, *81*, 5123.
[40] A. B. Dalton, S. Collins, E. Munoz, J. M. Razal, V. H. Ebron, J. P. Ferraris, J. N. Coleman, B. G. Kim, R. H. Baughman, *Nature* **2003**, *423*, 703.

[41] Z Jin Pramoda KP, Xu G, G. SH, *Chemical physics letters* **2001**, *337*, 43.
[42] L Jin, Bower C, Z. O, *Applied physics letters* **1998**, *73*, 1197.
[43] B. David, W. William, Y. Karen, M. B. Fiona, K. Umar, A. Dorothée, C. Leslie, M. Joe, J. B. Werner, N. C. Jonathan, *Advanced Functional Materials* **2008**, *9999*, NA.
[44] S. M. Liff, N. Kumar, G. H. McKinley, *Nat Mater* **2007**, *6*, 76.
[45] K. Stefan, *Angewandte Chemie International Edition* **2002**, *41*, 2721.
[46] C. Ming, C. Weinong, W. Tusit, *Journal of Engineering Materials and Technology* **2005**, *127*, 197.
[47] P. J. Hanines, *Thermal method of analysis*, Blakie academinc & prfesional, **1995**.
[48] D. William, W. Callister., *Fundamentals of materials science and engineering, an introduction*, Wiley, New Yark **2003**.
[49] M. Celina, K. T. Gillen, R. A. Assink, *Polymer Degradation and Stability* **2005**, *90*, 395.
[50] M. Celina, J. M. Skutnik Elliott, S. T. Winters, R. A. Assink, L. M. Minier, *Polymer Degradation and Stability* **2006**, *91*, 1870.
[51] T. Ogasawara, Y. Ishida, T. Ishikawa, R. Yokota, *Composites Part A: Applied Science and Manufacturing* **2004**, *35*, 67.
[52] C. Velasco-Santos, A. L. Martinez-Hernandez, F. Fisher, R. Ruoff, V. M. Castano, *Journal of Physics D-Applied Physics* **2003**, *36*, 1423.
[53] X. Kornmann., L. Berglund, R. T. ., Mulhaupt, J. F. . *Polymer Engineering & Science* **2002**, *42*, 1815.
[54] J. N. Coleman, M. Cadek, K. P. Ryan, A. Fonseca, J. B. Nagy, W. J. Blau, M. S. Ferreira, *Polymer* **2006**, *47*, 8556.
[55] K. P. Ryan, M. Cadek, V. Nicolosi, D. Blond, M. Ruether, G. Armstrong, H. Swan, A. Fonseca, J. B. Nagy, W. K. Maser, W. J. Blau, J. N. Coleman, *Composites Science and Technology* **2007**, *67*, 1640.
[56] M. Cadek, J. N. Coleman, K. P. Ryan, V. Nicolosi, G. Bister, A. Fonseca, J. B. Nagy, K. Szostak, F. Beguin, W. J. Blau, *Nano Lett.* **2004**, *4*, 353.
[57] G. Nanda, C. Yong, *Macromolecular Chemistry and Physics* **2006**, *207*, 1773.
[58] Milo S. P. Shaffer, Alan H. Windle, *Advanced Materials* **1999**, *11*, 937.
[59] J. Xiong, Z. Zheng, X. Qin, M. Li, H. Li, X. Wang, *Carbon* **2006**, *44*, 2701.
[60] H. Xia, M. Song, *Journal of Materials Chemistry* **2006**, *16*, 1843.
[61] K. D. Ausman, R. Piner, O. Lourie, R. S. Ruoff, M. Korobov, *J. Phys. Chem. B* **2000**, *104*, 8911.
[62] X. L. Xie, K. Aloys, X. P. Zhou, F. D. Zeng, *Journal of Thermal Analysis and Calorimetry* **2003**, *74*, 317.
[63] C. A. Furtado, U. J. Kim, H. R. Gutierrez, L. Pan, E. C. Dickey, P. C. Eklund, *J. Am. Chem. Soc.* **2004**, *126*, 6095.
[64] J. Cao, Q. Wang, M. Rolandi, H. Dai, *Physical Review Letters* **2004**, *93*, 216803.
[65] S. Giordani, S. D. Bergin, V. Nicolosi, S. Lebedkin, M. M. Kappes, W. J. Blau, J. N. Coleman, *J. Phys. Chem. B* **2006**, *110*, 15708.
[66] J. N. Coleman, U. Khan, Y. K. Gun'ko, *Advanced Materials* **2006**, *18*, 689.
[67] D. Qian, E. C. Dickey, R. Andrews, T. Rantell, *Applied Physics Letters* **2000**, *76*, 2868.
[68] B. Safadi, R. Andrews, E. A. Grulke, *Journal of Applied Polymer Science* **2002**, *84*, 2660.

[69] G. Philip, A. Whitten ,G. Wallace, *Journal of Biomedical Materials Research Part B: Applied Biomaterials* **2007**, *82B*, 37.
[70] H. Cong, J. Zhang, M. Radosz, Y. Shen, *Journal of Membrane Science* **2007**, *294*, 178.
[71] R. Andrews, D. Jacques, D. L. Qian, T. Rantell, *Accounts of Chemical Research* **2002**, *35*, 1008.
[72] M. A. L. Manchado, L. Valentini, J. Biagiotti, J. M. Kenny, *Carbon* **2005**, *43*, 1499.
[73] T. X. Liu, I. Y. Phang, L. Shen, S. Y. Chow, W.-D. Zhang, *Macromolecules* **2004**, *37*, 7214.
[74] P. Potschke, A. R. Bhattacharyya, A. Janke, H. Goering, *Composite Interfaces* **2003**, *10*, 389.
[75] E. G. Russell, E. C. Robert, *Journal of Polymer Science Part B: Polymer Physics* **2004**, *42*, 2690.
[76] O. Meincke, D. Kaempfer, H. Weickmann, C. Friedrich, M. Vathauer, H. Warth, *Polymer* **2004**, *45*, 739.
[77] S. Ghose, K. A. Watson, K. J. Sun, J. M. Criss, E. J. Siochi, J. W. Connell, *Composites Science and Technology* **2006**, *66*, 1995.
[78] I. Alig, D. Lellinger, S. M. Dudkin, P. Pötschke, *Polymer* **2007**, *48*, 1020.
[79] J. N. Coleman, W. J. Blau, A. B. Dalton, E. Munoz, S. Collins, B. G. Kim, J. Razal, M. Selvidge, G. Vieiro, R. H. Baughman, *Applied Physics Letters* **2003**, *82*, 1682.
[80] Z. Wang, Z. Liang, B. Wang, C. Zhang, L. Kramer, *Composites Part A: Applied Science and Manufacturing* **2004**, *35*, 1225.
[81] F. M. Blighe, P. E. Lyons, S. De, W. J. Blau, J. N. Coleman, *Carbon* **2008**, *46*, 41.
[82] F. Blighe, W. a. Blau, J. Coleman, *Submitted*
[83] H. L. Cox, *British Journal of Applied Physics* **1952**, *3*, 72.
[84] H Krenchel, Copenhagan, *Fibre reinforcement:*, Akademisk Forlag, **1964**.
[85] R. Hill, *Journal of the Mechanics and Physics of Solids* **1964**, *12*, 199.
[86] J. C. Halpin Affdl, J. L. Kardos, *Polymer Engineering & Science* **1976**, *16*, 344.
[87] S. Giordani, S. Bergin, V. Nicolosi, W. J. Blau, J. N. Coleman, *physica status solidi (b)* **2006**, *243*, 3058.
[88] L. Vaisman, H. Wagner, G. Marom, *Advances in Colloid and Interface Science* **2006**, *128-130*, 37.
[89] N. Wilfrid, M. P. Maryse, A. D. Miaudet, Z. Cécile, P. Philippe, *Macromolecular Rapid Communications* **2006**, *27*, 1035.
[90] M. B. Bryning, D. E. Milkie, M. F. Islam, J. M. Kikkawa, A. G. Yodh, *Applied Physics Letters* **2005**, *87*, 161909.
[91] B. Zhao, H. Hu, A. Yu, D. Perea, R. C. Haddon, *J. Am. Chem. Soc.* **2005**, *127*, 8197.
[92] J. Amiran, V. Nicolosi, S. D. Bergin, U. Khan, P. E. Lyons, J. N. Coleman, *J. Phys. Chem. C* **2008**, *112*, 3519.
[93] C McClory, T. McNally, G. P. Brennan, J. Erskine, *Journal of Applied Polymer Science* **2007**, *105*, 1003.
[94] R. Sen, B. Zhao, D. Perea, M. E. Itkis, H. Hu, J. Love, E. Bekyarova, R. C. Haddon, *Nano Lett.* **2004**, *4*, 459.
[95] Y. Junwei, H. Jianhua, C. , Wang, , Q. Yujun, G. Zhixin, *Macromolecular Materials and Engineering* **2004**, *289*, 828.

[96] R. Blake, Y. K. Gun'ko, J. Coleman, M. Cadek, A. Fonseca, J. B. Nagy, W. J. Blau, *J. Am. Chem. Soc.* **2004**, *126*, 10226.
[97] J. Zhu, J. Kim, H. Peng, J. L. Margrave, V. N. Khabashesku, E. V. Barrera, *Nano Lett.* **2003**, *3*, 1107.
[98] H. P. J. Zhu, F. Rodriguez-Macias, J. L. Margrave, V. N. Khabashesku, A. M. Imam, K. Lozano, E. V. Barrera, *Advanced Functional Materials* **2004**, *14*, 643.
[99] G. L. Hwang, Y.-T. Shieh, K. C. Hwang, *Advanced Functional Materials* **2004**, *14*, 487.
[100] C. Harper, *Handbook of Plastics, Elastomer, And Comosites*, McGraw-Hill, Inc, New York **2002**.
[101] P. C. P. Watts, W. K. Hsu, *Nanotechnology* **2003**, L7.
[102] O. Lourie, H. D. Wagner, *Journal of Materials research* **1998**, *13*, 2418.
[103] C. Velasco-Santos, A. L. Martinez-Hernandez, F. T. Fisher, R. Ruoff, V. M. Castano, *Chem. Mater.* **2003**, *15*, 4470.
[104] U. Khan, K. Ryan, W. J. Blau, J. N. Coleman, *Composites Science and Technology* **2007**, *67*, 3158.
[105] S. Niyogi, M. A. Hamon, H. Hu, B. Zhao, P. Bhowmik, R. Sen, M. E. Itkis, R. C. Haddon, *Acc. Chem. Res.* **2002**, *35*, 1105.

# Chapter 3

## Materials and characterisation techniques

### 3.1 Introduction

This chapter discusses the materials used in this thesis and also outlines the characterisation techniques.

### 3.2 Carbon nanotubes

To understand and improve the mechanical properties of CNT nanocomposites, a variety of CNTs were used. A summary of their nature and origin is given in Table 3.1.

| Description | Production Method | Supplier | Functionality |
|---|---|---|---|
| SWCNT-Purified | HiPCO | www.cnanotech.com | N/A |
| SWCNT-PEG (P7) | CVD | www.carbonsolution.com | Polyethylene glycol (PEG) |
| SWCNT-PABS (P8) | CVD | www.carbonsolution.com | Polyaminobenzene Sulfonic Acid (PABS) |
| SWNT-ODA (P5) | CVD | www.carbonsolution.com | Octadecylamine (ODA) |
| VerythinMWCNT (9.5 nm)*[1]* | CVD | www.carbonsolution.com | N/A |
| ThickMWCNT(25 nm) *[2]* | CVD | www.carbonsolution.com | N/A |

Table 3.1 Different types of nanotubes prepared by high pressure carbon monoxide (HiPCO), chemical vapour deposition (CVD) techniques and suppliers.

## 3.3 Polymer matrices

**Polyvinyl alcohol (PVA)**

PVA is a thermoplastic polymer. PVA was used as the matrix in composites which will be discussed in chapter 4. It was supplied by Sigma-Aldrich (Aldrich: product code P-8136). PVA is prepared from polyvinyl acetate (PVAc) Figure 3.2. PVA is semi-crystalline polymer.

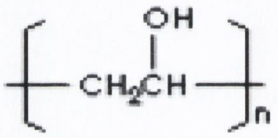

Fig. 3.1 Polyvinyalcohol (PVA)

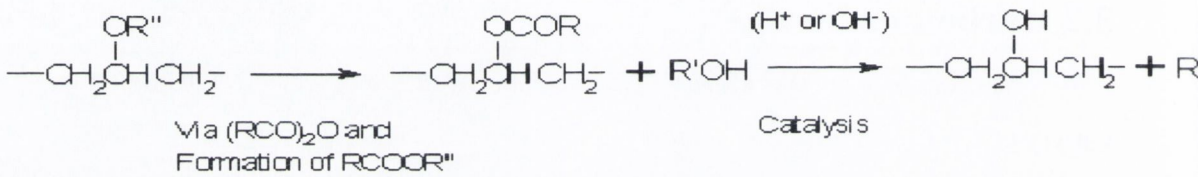


or

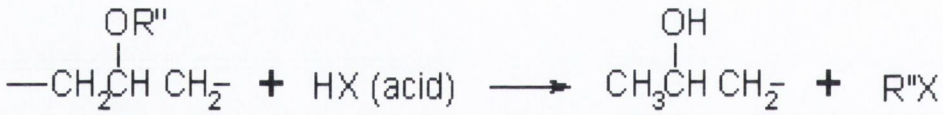


Fig 3.2 Two methods of PVA synthesis*[3]* .

**Polyurethane (PU) water dispersion**

This is a new class of thermoplastic elastomer, which was supplied in the form of highly viscous dispersion in water. The dispersion consists of an average particle size of ~ 3 micrometers. It was produced by Hydrosize*[4]* , product code U2-01. TPU is synthesised by chemically reacting a straight chain polyol and diisocyanate*[5]* . Thermoplastic polyurethanes are segment polymers. The polyol in TPU is very soft (with a very low $T_g$ ) and the diisocyanate part is relativity hard (with a high $T_g$ ) and so, these are referred to as soft segment (SS) and hard segment (HS) respectively. Due to the presence of hard and soft domains, these materials are also called segmented PU. The combination of

thermodynamically incompatible SS and HS gives rise to an interesting material*[5]* . The HS acts like filler and is mainly responsible for determining the stiffness and yield strength of TPU, while the SS accounts for very large deformation of TPU before break. These materials are analogous to spider silk in SS and HS morphology but unlike spider silk they have very low stiffness and yield strength because the HS are linked by weak hydrogen bonding. Scheme (Fig.3.3) shows TPU synthesis.

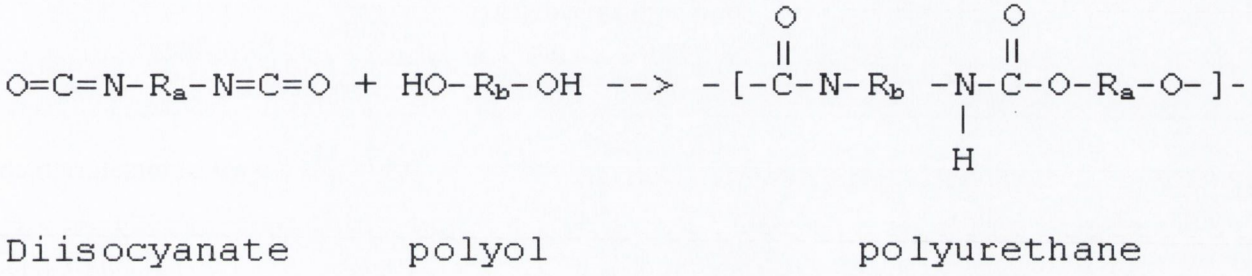


Fig 3.3 Polyurethane synthesis

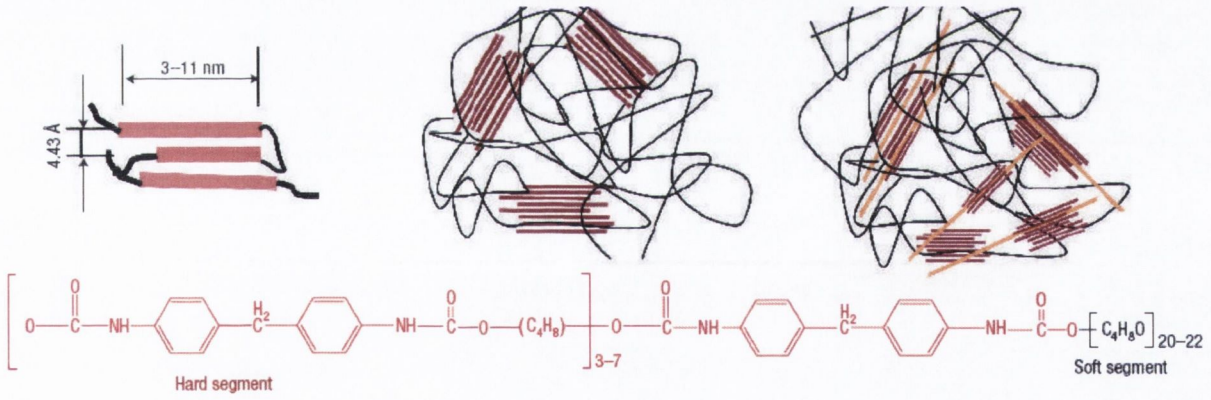


Fig 3.4 Typical TPU polymer *[6]*

## 3.4 Solvents

Depending on the nature of CNTs and polymer matrices, different organic solvents were used in this thesis. A summary of their physical properties are listed in Table 3.6.

| Solvent | Formula | MW (g/mol) | boiling point (°C) | melting point (°C) | density (g/mL) | Supplier |
|---|---|---|---|---|---|---|
| Dimethyl-formamide (DMF) | $C_3H_7NO$ | 73.09 | 153 | -61 | 0.944 | www.sigmaaldrich.com |
| Dimethyl sulfoxide (DMSO) | $C_2H_6OS$ | 78.13 | 189 | 18.4 | 1.092 | www.sigmaaldrich.com |
| *N*-methyl-2-pyrrolidinone (NMP) | $CH_5H_9NO$ | 99.13 | 202 | -24 | 1.033 | www.sigmaaldrich.com |
| Tetrahydrofuran (THF) | $C_4H_8O$ | 72.11 | 66 | -108.4 | 0.886 | www.sigmaaldrich.com |
| Water | $H_2O$ | 18.02 | 100.00 | 0.00 | 0.998 | In house |

Table 3.6 Physical properties of solvents

## 3.5 Characterisation techniques

### 3.5.1 Thermogravimetric analysis (TGA)

All thermogravimetric analysis in this thesis was done on a Perkin Elmer Pyris 1 TGA .

In this technique, the mass of a sample is monitored as function of temperature and plotted as a TGA curve. Figure 3.5A shows a typical TGA curve. In practice, a derivative weight loss curve is taken (Fig 3.5 B) which is referred as deferential thermogravimetric analysis (DTGA). Peak at ~ 50 °C in the DTGA plot (Fig 3.5 B) corresponds to the evaporation of

trapped solvent in the TPU, while around 376 and 506 arises due to the polymer degradations. TGA can be run under a range of atmospheres e.g oxygen, nitrogen.
This technique can be used for a variety of purposes e.g. oxidation, decomposition of substances etc*[7]* .

A modern TGA instrument consists of a number of common parts. Weight is monitored by a sensitive thermo balance. A digital recorder records variation in weight during a TGA run. A heating furnace made up of ceramic material is present to withstand high temperatures. Temperature is precisely controlled by a temperature programmer and a computer monitor displays the data.

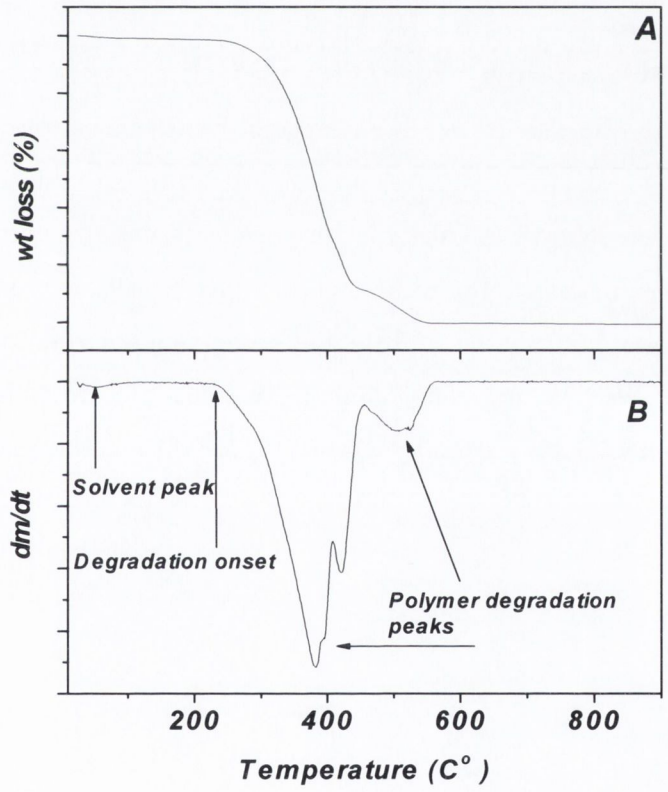


Fig. 3.5 A)TGA and B) DGTA of TPU shows solvent entrapment in polymer and polymer degradation temperature.

TGA can be used to determine a number of different properties of materials. Thermal stabilities of materials can be measured and compared under the required atmosphere. Oxidation or reduction of materials can be monitored. Solvent residues can also be elucidated from the DTGA curve. Life spans of materials can be estimated. The presence of volatile components in a sample can be determined from a TGA curve. TGA can also be used for analysing the kinetic features of all types of weight loss or gain, either with a view to predictive studies, or to understand the controlling chemistry. TGA can be used in combination with other techniques like mass spectroscopy to get very useful information. For example TGA in combination with mass spectrometry gives information about the degraded fragments. It can be used to find the presence of trapped solvent and the effect of this solvent on thermal stability of samples.

### 3.5.2 Differential Scanning calorimetry (DSC)

A DSC study was carried out to understand the effects of various kinds CNTs and CNT loadings on a polymer matrix. It was also used to understand the CNT solvent interaction in a given sample. All the DSC experiments were performed using a Perkin Elmer Diamond DSC machine. The technique, in which heat flow to materials is recorded against the temperature, is referred as differential scanning calorimetry (DSC). Using this method, the rate of heat flow to a sample and to a reference is independently measured over a range of temperature. Data is taken by monitoring the differential heat flow as a function of temperature (Fig 3.6).

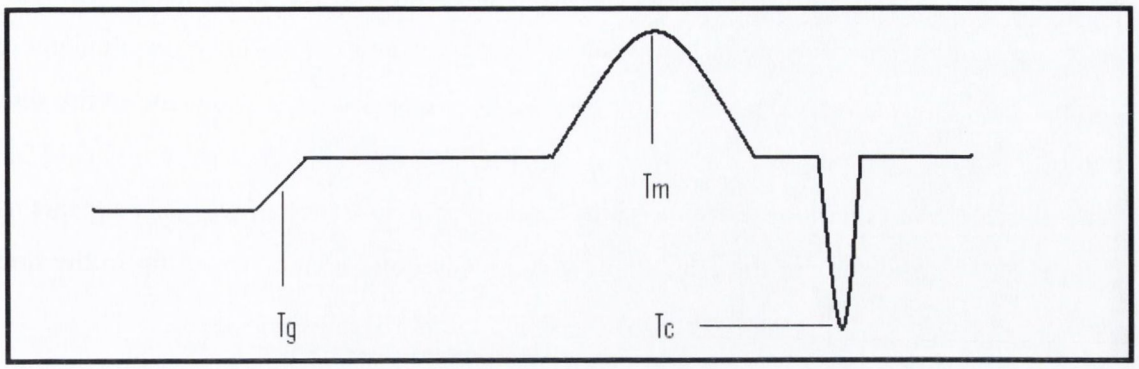


Fig. 3.6. Typical DSC curve of a polymer shows various thermal transition in polymer i.e. glass transition temperature ($T_g$), meting temperature ($T_m$), crystallisation temperature ($T_c$).

Numerous different thermal transitions are evident from DSC curves. It can be used to obtain glass transition temperatures ($T_g$) of amorphous and semicrystalline polymers. Melting points of materials can also be determined using DSC. Another useful application of DSC is its use in establishing the crystallisation time and temperature ($T_m$) and also percent crystallinity. Heats of fusion, reactions, specific heat and heat capacity can be found out with DSC. DSC is also used in determination of oxidative stability, rate and degree of curing and reaction kinetics.

This thesis mainly describes the $T_g$, $T_m$, and crystallinity of polymers and polymeric nanocomposites.

The heat capacity of a liquid is higher than the respective solid, so when an amorphous polymer is heated continuously, above its $T_g$, the polymer becomes rubbery or becomes a viscous liquid and the heat capacity suddenly increases. This appears as a step in DSC curve. The middle point of the step is taken as $T_g$ (Fig 3.4). The Glass transition is usually considered as a finger print for a particular polymer.

In the case of semicrystalline polymers, the ordered part/s of molecular chains in the polymer are more stable than the randomly coiled amorphous region. Extra heat is required to maintain a constant temperature rate as a DSC suddenly increases heat to keep the constant temperature rate until all the crystalline portion melts. This change appears as an endothermic peak on the DSC graph. Temperature at a maximum peak height is called $T_m$

(Fig 3.6). Integrating the area under the peak gives the change in enthalpy (ΔH) of a particular polymer or polymeric composite. The percentage crystallinity is calculated by comparing the measured (ΔH) value of a polymer to the theoretical (ΔH) value of the same, but 100% crystalline polymer. When a semicrystalline polymer's melt is cooled (Fig 3.6), some molecules lose a lot of energy to form low energy stable crystallites. This appears as a (down) exothermic peak in the DSC cooling run. The point of maximum dip in the down peak is described as the crystallisation temperature ($T_c$) (Fig 3.6).

### 3.5.3 Dynamic mechanical thermal analysis (DMTA)

When a polymeric material is strained within its elastic limit, after relaxation it should retain the pre-strain position. However, it never goes back to pre-strain position due the fact that materials lose some of their energy due to internal molecular friction and also because of dissipation as heat. Therefore a technique is needed to determine the dynamic or storage modulus usually denoted by $G$ or $E$ . Dynamic mechanical thermal analysis (DMTA) is used for this purpose. DMTA is a useful technique for characterising the properties of polymeric materials. The DMTA method normally provides plots of dynamic or storage modulus (G or E*)* and loss modulus G`` or E`` versus temperature (Fig. 3.7). The storage modulus, G, decreases with increasing temperature because with an increase in temperature the kinetic energy (KE) of polymer molecules also increases. This in turn decreases intermolecular attractive forces resulting in the polymer becoming less stiff. On the other hand, as the KE of molecules increases, intermolecular attractive forces decrease, subsequently the loss modulus (G``) increases. The loss modulus is a measure of the viscous behavior of material; therefore a higher loss modulus means a higher viscosity. Equation 3.1 relates the loss modulus to the viscosity.

$$\eta = \frac{G''}{\omega} \quad \text{Eq 3.1}$$

Where η is viscosity and ω is the oscillatory frequency.

If G``/G is plotted as function of temperature, the highest peak will appear at (dynamic) $T_g$ of a polymer (Fig. 3.8). G``/G is maximum at $T_g$ because at $T_g$ storage modulus remain minimum. As at Tg polymer molecules gain sufficient energy to move

freely thus the provided mechanical energy mostly utilises to make the polymer molecules flow against each other (friction) rather stretching them elastically.

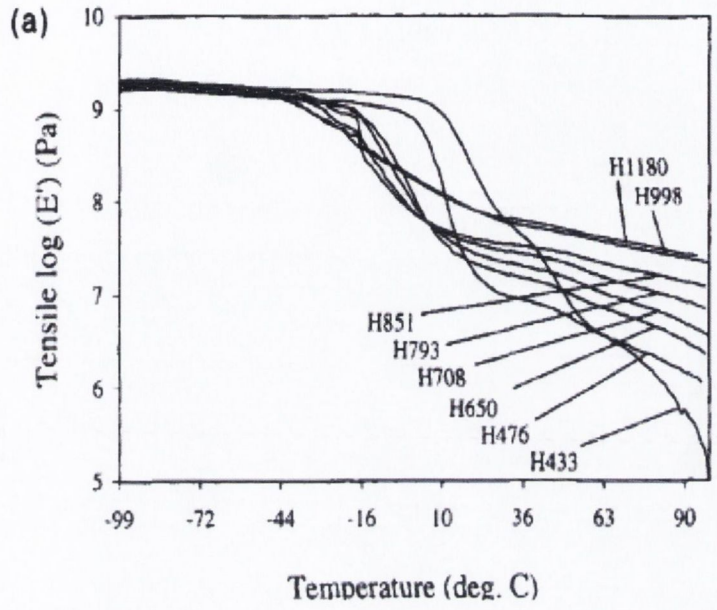


Fig 3.7 Storage modulus of series various PU elastomer. H433, H476... are codes for various types of TPU *[8]*

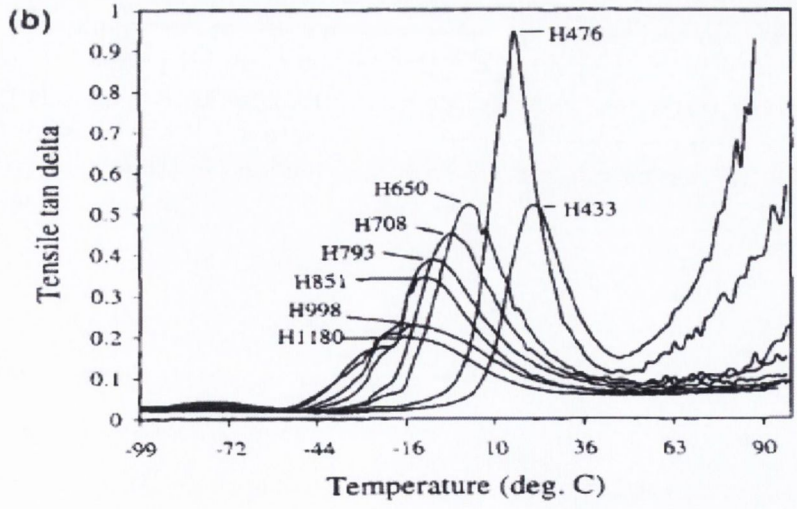


Fig 3.8 Plot of Tanδ of series TPU. H433, H476... are codes for various types of TPU *[8]*.

This is because at $T_g$ polymer molecules gain sufficient kinetic energy to overcome intermolecular interactions and are free to move. Above $T_g$, the polymer will become rubbery and most of the applied stress energy is utilised in irreversible deformation. G``/G is often denoted as *tan δ* illustrated in figure 3.9 (Fig).

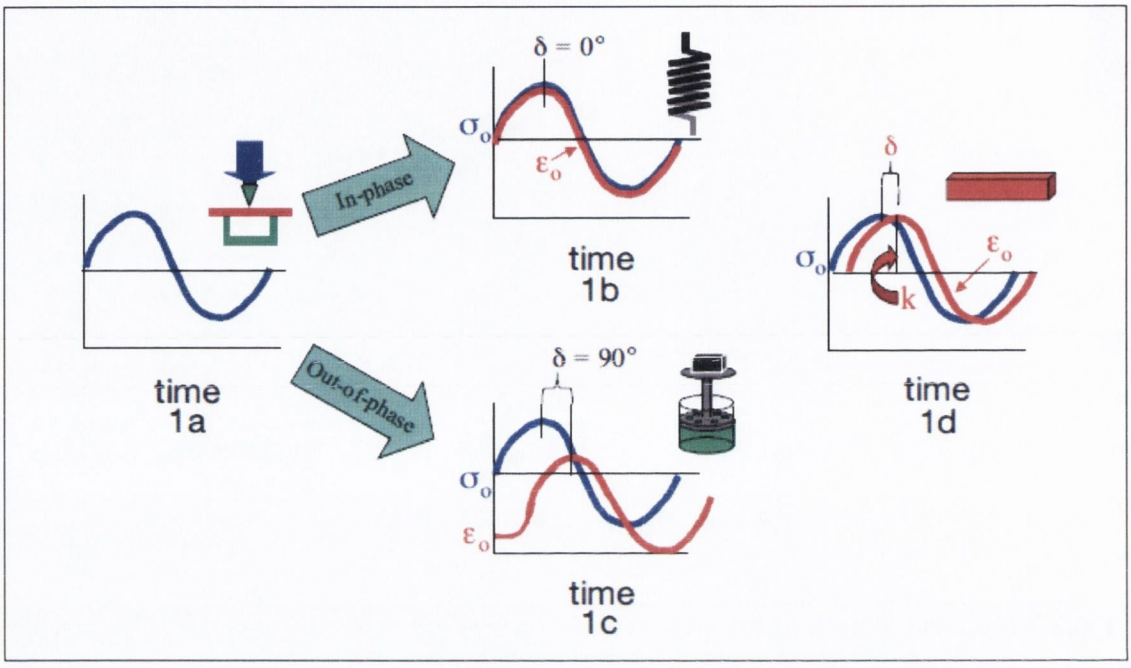


Fig 3.9 (reproduced from www.perkinelmer.com (1a) When a sample is subjected to a sinusoidal oscillating stress it responds in a similar strain wave provided the material stays within its elastic limits. When the material responds to the applied wave perfectly elastically, an in-phase storage, or elastic response is seen, (1b) while a viscous response gives an out-of-phase loss, or viscous response, (1c) Viscoelastic materials fall in between these two extremes (as shown in d). For the real sample in (d), the phase angle, δ, and the amplitude at peak, k, are the values used for the calculation of modulus, viscosity, damping, and other properties. Where σ is the stress and ε is the strain produced under the influence of applied stress.

### 3.5.4 Tensile testing (TT)

Tensile testing is the most widely used tool to investigate the mechanical properties of materials. Mechanical properties were measured using Zwick Roell tensile tester with 100 N load cell. In this thesis we have monitored stress-strain behavior of various CNTs polymeric composites. A sample is clamped in the jaws/head of a tensile tester. One of the jaws moves continuously against a static jaw to stretch the sample (until break). Applied force/stress is plotted as a function of strain. Such a plot is termed as stress-strain curve. Strain (ε) is given by equations 3.2 and 3.3.

$$\varepsilon = \frac{L_1 - L_0}{L_0} \qquad \text{Eq (3.2)}$$

where $\Delta L = L_1 - L_0$

Or

$$\varepsilon = \frac{\Delta L}{L_0} \qquad \text{Eq (3.3)}$$

Where $L_0$ is the initial length while $L_1$ is the final length of a sample.

Stress (σ) at a point is defined as the applied force per cross sectional area and given by equation 3.4.

$$\sigma = \frac{Force}{A} \qquad \text{Eq (3.4)}$$

where $A$ is cross sectional area and in case of a film sample, is given

as $A = W \times T_k$ Eq (3.5)

$W$ *is* width of sample and $T_k$ is thickness of sample.

Shown in Fig. 3.10 are the various regions in the stress-strain plot which are characteristic for various materials.

1) The initial part of stress-strain curve is usually linear ( Fig 3.9). This part of the curve is generally known as the elastic or proportional region. During stretching of a sample the inter atomic/molecular bonding distance slightly increases elastically. Therefore, the Young's modulus is a measure of inter atomic/molecular forces. The linearity in a stress-strain curve also represents the degree of order in a material which is why crystalline solids have linear elastic regions compared to amorphous solids. In some cases, the initial elastic part of a stress-strain curve may not be linear (see Fig 3.9) because of lower inter atomic/molecular attractive forces and lesser or no order. For this behavior the secant modulus is usually used. A secant is drawn from the origin to some point of

stress-strain curve and the slope is taken as secant modulus. In the elastic region, stress is increasing proportionally with increased strain or vice versa. This is because of constant strain of the polymer chain and filler in this part. The deformation in this region is reversible. The slope of the linear region is called Young's modulus. This is a parameter for measuring a material's stiffness. The area under the elastic region of the stress strain curve is usually termed as the resilience.

2) The point at which stress-strain curve no longer remains linear and an increase in strain occurs without an increase in stress is called the yield point and the stress at that point is called the yield point stress or yield stress *[9]*.

3) As stress is further increased beyond the elastic limit, the material starts to deform irreversibly. The region can be relatively flat (depending on the material). This part of the curve is called the viscous or plastic part. It continues until the material breaks. The strain at which the material breaks is termed as the strain at break ($\varepsilon_B$ ) and stress at that point is known as the strength at break and denoted as ($\sigma_B$.) The highest stress value in stress-strain curve is called the ultimate tensile strength (UTS). Strength at break ($\varepsilon_B$ ) and UTS may or may not be the same. If a material breaks at the UTS point both UTS and $\sigma_B$ will be the same, while if a material breaks at a lower stress value than UTS the UTS and $\sigma_B$ will be different (see Fig 3.9). The total area under the stress-strain curve is called strain energy or toughness of a material.

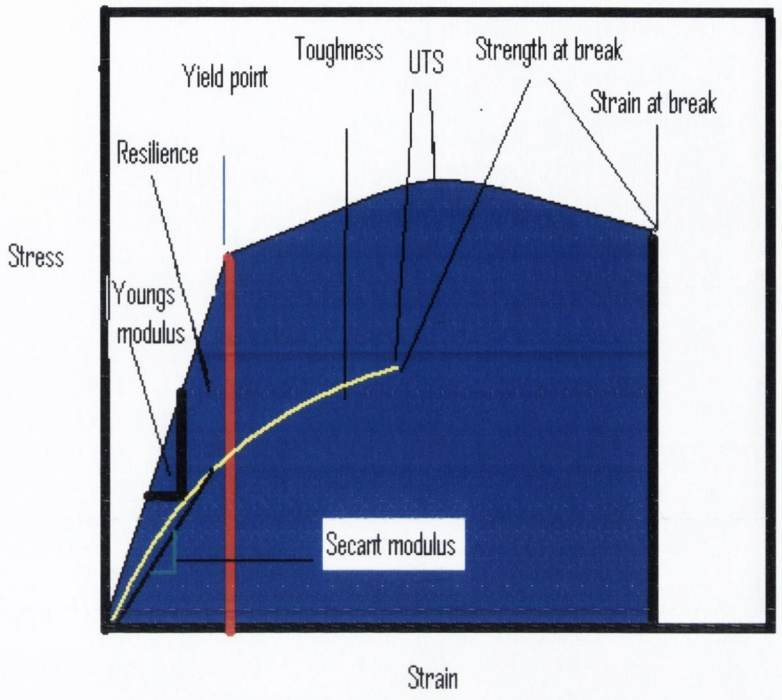


Fig. 3.10 Typical stress-strain curves.

## 3.6 References


[1] http://www.nanocyl.com/.

[2] K. P. Ryan, M. Cadek, V. Nicolosi, S. Walker, M. Ruether, A. Fonseca, J. B. Nagy, W. J. Blau, J. N. Coleman, *Synthetic Metals* **2006**, *156*, 332.

[3] D. Blond., in *School of Physics*, Vol. PhD Thesis, Trinity College University of Dublin, Dublin **2008**.

[4] http://www.hydrosize.com/.

[5] H.-D. Kim, T.-J. Lee, J.-H. Huh, D.-J. Lee, *Journal of Applied Polymer Science* **1999**, *73*, 345.

[6] S. M. Liff, N. Kumar, G. H. McKinley, *Nat Mater* **2007**, *6*, 76.

[7] T. Hatakeyama., Z. L, *Handbook of thermal analysis*, John Wiley & sons Ltd, **1998**.

[8] J. M. Darren, F. Gordon, G. M. Meijs, S. J. Renwick, P. Mccarthy, A. Gunatillake, *Journal of Applied Polymer Science* **1996**, *62*, 1377.

[9] C. Harper, *Handbook of Plastics, Elastomer, And Comosites*, McGraw-Hill, Inc, New York **2002**.

# Chapter 4

# The effect of solvent choice on the mechanical properties of carbon nanotube-polymer composites.

## 4.1 Introduction

Due to their superior mechanical properties, carbon nanotubes (CNTs) have long been mooted as the ultimate reinforcing filler in polymer based composites. However, the effective utilization of the mechanical properties of nanotubes composites depends on the quality of their dispersion and the level of polymer-nanotube interfacial bonding *[1, 2]*. A common technique for producing polymer-nanotube composites has been solution processing. In this technique, nanotubes and polymer are mixed in a common solvent. Nanotube dispersion relies on the interaction of the nanotubes with the polymer dispersant *[3]*. In general, solvent choice is motivated by the requirement that the polymer dispersant should be soluble in the solvent. Polyvinylalcohol (PVA) has been extensively used as a matrix for nanocomposites because of its solubility in a range of solvents including water *[4-8]*. In addition PVA is known to be a good dispersant of nanotubes *[5-7]*. In most of the CNTs-PVA studies water has been used as solvent *[4-6, 8-10]*.However, in recent times alternative solvents such as dimethylsulfoxide (DMSO) have been gaining popularity for fabrication of solution based composites *[11, 12]*. However, PVA is soluble in a wide range of solvents such as DMSO, N-methyl-2-pyrrolidone (NMP) and ethylene glycol *[12-15]*. The solvent choice can have significant effects on the morphology of the resultant solution cast polymer films. For example, the polymer crystallinity can vary greatly depending on whether the solvent used is a good or bad solvent for PVA *[14]*. Such solvent related effects are likely to have significant impact on the mechanical properties of solution processed polymer-nanotube films. In addition it has recently been shown that carbon

nanotubes can be dispersed in certain solvents without the need for polymer dispersants *[16-19]* . One of the most effective solvents studied was NMP *[16, 18, 20]*. This is significant as NMP is also a solvent for PVA. Thus, one would expect that PVA-CNTs formation in NMP would result in efficient nanotube dispersion resulting in very good quality composites.

The aim of the present study was to understand the effect of solvent choice on the mechanical properties of solution processed CNTs-polymer composites. This subject is poorly understood with the only study having been carried out on epoxy nanotube composites *[21]*. Three different solvents with different solubility parameters for PVA were used for fabrication and characterization of DCWNT-PVA composites. The resultant composites were found to have mechanical properties that depended significantly on solvent choice.

## 4.2 Sample preparation.

The double-walled nanotubes (DWCNTs) used here were grown by CVD with a nominal purity of 90% and purchased from Nanocyl (www.nanocyl.be: Nanocyl ®-2100). They had a mean diameter of 3.5 nm with lengths between 1-10 micron. Due to their large diameter they have very low density of ~750 kg/m$^3$. These particular nanotubes contain small amounts (<10%) metal oxide impurity. Polyvinyl alcohol was purchased from Aldrich (Aldrich: product code P-8136). The water used was deionised in-house while the NMP and DMSO solvents were spectroscopic grade (Aldrich). Solutions of polyvinylalcohol (PVA) were prepared using water, dimethylsulfoxide (DMSO) and N-methyl-2-pyrrolidone (NMP) as solvents, by sonication in a low power sonic bath (Ney Ultrasonik) for 4 hours. Each solution was divided in two and 0.25 wt % double walled nanotubes (DWCNTs) added to one of the portions to give a composite dispersion. Each composite dispersion was sonicated for 10 minutes using a high power ultrasonic tip processor, (model GEX600, 120W, 60kHz) followed by 2 hours in a sonic bath and again for 10 minutes under the sonic tip. These dispersions were then left undisturbed for 24 hours to allow any large nanotube aggregates or impurities to sediment out. Indeed, for each solvent, miniscule amounts of sediment (compared to the volume of nanotubes added

to each solution) could be observed after settling, suggesting that a very small fraction of the nanotube material had fallen out of solution. This sediment was then removed by decantation to another vial. Polymer only solutions and the CNTs-polymer dispersions were then drop cast into (40mm × 40mm × 10mm) Teflon trays. Films were then formed by drying in a vacuum oven at 60 °C. Two sets of freestanding films were obtained for each solvent-polymer and solvent-polymer-CNTs combination: (**a**) with one day drying time at 60 °C under vacuum and a second set (**b**) with 5 days drying under vacuum at the same temperature. After drying the films were stored for approximately 2 days in ambient conditions. This resulted in a small amount of water uptake by the polymer. The composite films had mass fractions of slightly less than 0.25 wt%. Taking the densities of PVA and DWCNTs to be 1300 and 750 kg/m$^3$, this results in volume fractions of $V_f$~0.4vol%.

A sample labeling scheme has been employed. This scheme is in three parts: The first part of the sample name can be "**a**" or "**b**" depending on whether the drying time was 1 day (**a**) or 5 days (**b**), the second part denotes the solvent, while the third part could be "**p**" or "**c**" depending on whether the sample was polymer or composite respectively. Thus "**a**DMSO**p**" denotes a polymer sample dried for 1 day, made using DMSO as solvent.

## 4.3 Characterisation techniques

Thermo gravimetric analysis (TGA) measurements were carried out for all the samples using a Perkin Elmer Pyris 1 TGA with a temperature scan rate of 10 °C/minute. In general TGA is used to monitor sample oxidation. However, in this case it is used to ascertain the level of solvent entrapment in the samples after drying. To assess the morphological properties of the samples, Differential Scanning Calorimetry (DSC) was performed using a Perkin Elmer Diamond DSC. Three heat runs were recorded for each sample by repeatedly heating from 0°C to 230°C at 40°C/min. Between each heating scan a cooling run from 230°C to 0°C at 40°C/min was also monitored. In each case, after the first heat run, the temperature was held at 230 °C for three minutes in an attempt to evaporate the trapped solvent. Dynamic Mechanical Thermal Analysis (DTMA) tests were performed on Perkin Elmer Diamond DMA. Uniform strips of dimension 2.5mm × 3mm × ~0.05mm, cut by means of a die cutter were used. Film thicknesses were measured using a digital micrometer. These experiments were run at temperature range from –30 °C to 170 °C with

a frequency of 1Hz. Tensile testing (TT) measurements were carried out using the same instrument as used for DMTA. Each reading for TT is the average of three individual measurements.

## 4.4 Results and discussion

### 4.4.1 TGA analysis

Thermo gravimetric analysis curves(sec 3.5.1, Fig 3.5) are plotted as derivative TGA curves (-dM/dT) in figure 4.1. In this format, the mass loss due to oxidization/evaporation of a given species appears as a peak. In the curves representing both polymer and composite samples, peaks in the region of 350 °C to 500 °C were observed. These are due to decomposition of PVA through elimination of water and pyrolysis *[22, 23]* while no peak was observed for CNT oxidation because of the extremely small quantities of CNTs in the samples. The peaks observed at approximately 190 °C, 175 °C and 100 °C in figure 4.1. a, b and c respectively are due to the evaporation of residual solvent left over from the sample preparation. These peaks are reasonably close to the positions of the solvent boiling points (BP) of 202 °C, 189 °C and 100 °C for NMP, DMSO and $H_2O$ respectively. The amount of trapped solvent was determined by calculating the area under each solvent peak. In addition, for the DMSO and NMP samples the small peak at 100 °C represents water that has diffused into the films from the atmosphere after film formation. It should be pointed out that for these samples, the mass of trapped solvent does not include this water content. Trapped solvent masses as a fraction of the total film mass are given in table 4.1 for all samples.

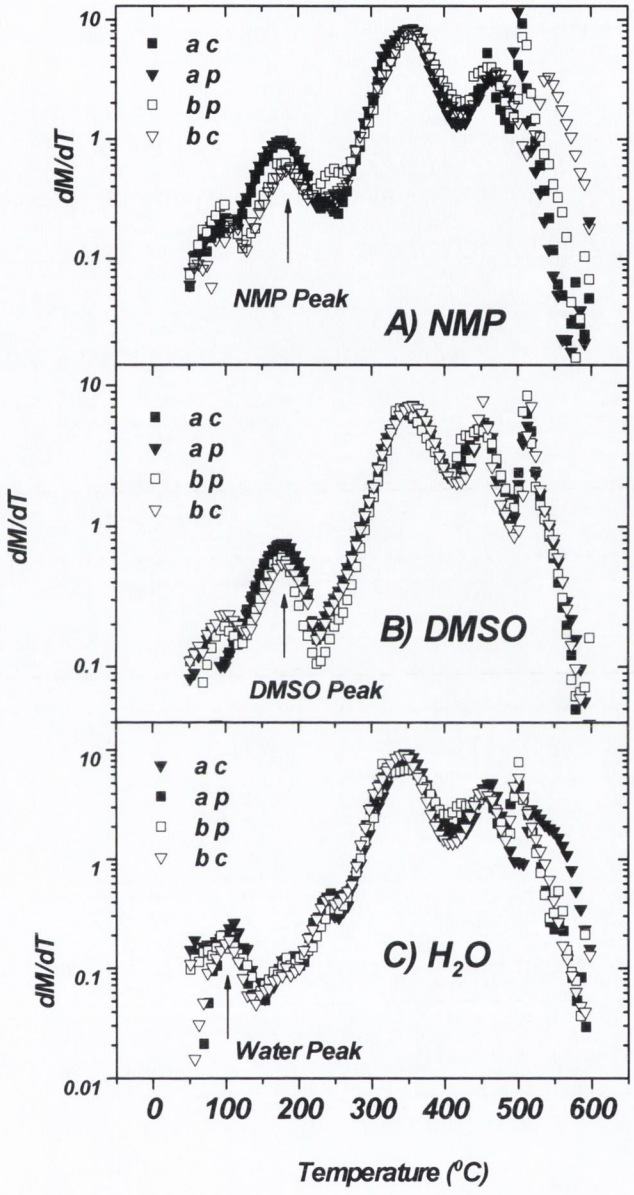


Fig. 4.1. Derivative TGA graphs of solution based DWCNT-PVA composites and polymer only samples. In each case the arrow highlights the solvent evaporation peak. Note that in all cases the y axis is presented logarithmically.

As shown in table 4.1, very little solvent remained trapped in the water samples. In all cases the water based samples retained less than 2% water. The amount of trapped water did not appear to correlate either with drying time or sample type (polymer/composite). It is

likely that most of the water actually evaporated during drying and the water observed by TGA is actually due to diffusion of water into the films after drying. This is supported by the fact that small quantities of water can be observed in the TGA curves for the DMSO and NMP based samples.

Significant quantities of solvent remained trapped in both DMSO and NMP based samples. In both cases the amount of trapped solvent was reduced for the longer drying time. However, in each case a factor of five increase in drying time resulted in less than a factor of two decrease in trapped solvent. In addition more solvent remained trapped in the NMP based samples than the DMSO based samples in keeping with NMP's higher boiling point.

| Solvent | Sample | Solvent content (%) | $T_g$ °C (static) | | | $T_g$ °C (dynamic) |
|---|---|---|---|---|---|---|
| | | | 1st run | 2nd run | 3rd run | |
| $H_2O$ | a p | 0.8 | 71 | 73 | 73 | 80 |
| | a c | 1.6 | 72 | 73 | 73 | - |
| | b p | 1.2 | 71 | 73 | 73 | 81 |
| | b c | 0.8 | 71 | 73 | 73 | 82 |
| DMSO | a p | 5.1 | 41 | 65 | 67 | 66 |
| | a c | 5.1 | 43 | 65 | 69 | 70 |
| | b p | 3.5 | 47 | 65 | 70 | 69 |
| | b c | 3.6 | 49 | 69 | 73 | 71 |
| NMP | a p | 7.2 | 37 | 70 | 72 | 67 |
| | a c | 7.1 | 46 | 70 | 71 | 63 |
| | b p | 3.8 | 47 | 70 | 72 | 77 |
| | b c | 3.7 | 55 | 71 | 72 | 75 |

Tab. 4.1. Trapped solvent content and both static (at first, second, third heat run) and dynamic glass transition temperature $T_g$ of solution based DWCNTs-PVA composites and polymer only samples

## 4.4.2 DSC study

Differential scanning calorimetry measurements (sec 3.5.2, Fig 3.6) were carried out on all samples in both heating and cooling mode. In all cases, a glass transition (figure 4.2) was observed between 35 °C and 75 °C depending on the sample and measurement mode. At higher temperatures (figure 4.1), phase transitions representing melting or crystallization were observed for heating or cooling cycles respectively. In the next section, we will consider the glass transition while in subsequent sections we will discuss the melting/crystallisation phase transitions.

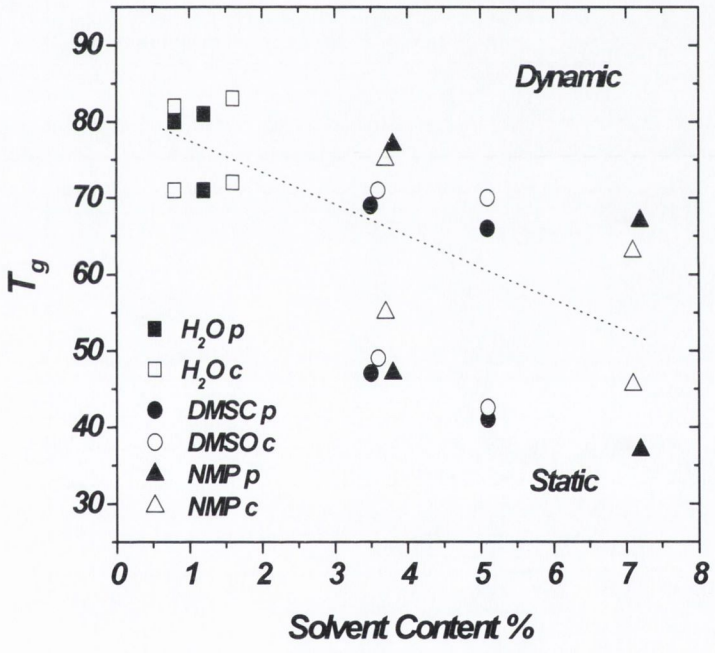


Fig. 4.2. $T_g$ of solution based CNT composites and polymer only samples as function of solvent content, suggesting plasticizing effect of trapped solvent. The dotted line separates the results of the static and dynamic measurements.

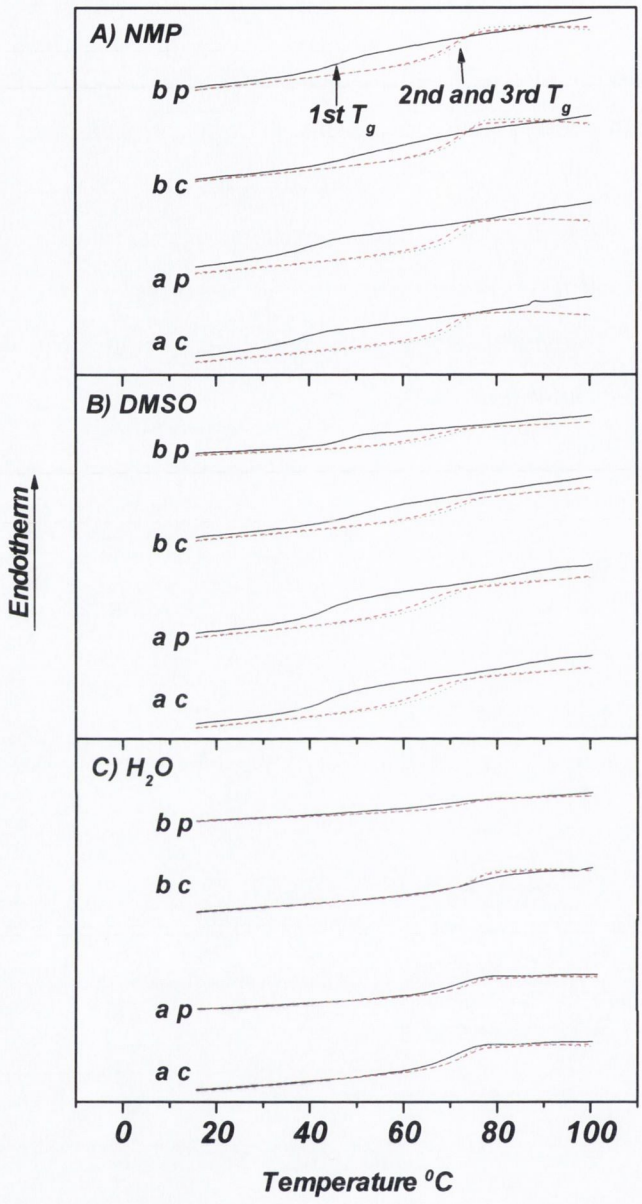


Fig.4.3. Low temperature portion of DSC curve for all three heat runs (first, second and third) for each sample. In each set of (three) lines the solid line represents the first heat run, the dashed line represents second heat run and the doted line represents the third heat run.

**The Glass Transition**

Shown in figure 4.3 are low temperature portions of the DSC curves relating to the glass transition for all samples. This transition occurs for polymers as the temperature is raised through the glass transition temperature and involves the onset of thermally induced chain segment motion and bond rotation. In each section the graphs have been shifted vertically into groups representing polymer-**a** sample, polymer-**b** sample, composite-**a** sample and composite-**b** sample. For each of these subsets the DSC curves for first, second and third heats have been superimposed.

In all cases the glass transition temperature, $T_g$, was measured as the midpoint of the region of increasing heat flow and is presented in table 4.1. We estimate that the quoted values of $T_g$ are accurate to with $\pm 2^{\circ}C$. It was observed that the $T_g$ for all the water samples remained almost the same (71 $^{\circ}C$- 73 $^{\circ}C$) in all three heat runs. This is because, as TGA showed, very little water remained trapped in these samples (see figure 4.1). The presence of small molecules in general and trapped solvent in particular, in polymer films tends to facilitate chain segment/side chain motion by disrupting inter-polymer interactions. This so-called plasticizing effect acts to lower $T_g$ compared to that which would be expected for the pure polymer. This phenomenon is illustrated in figure 4.2, which shows the $T_g$ measured during the first heat for all solvents plotted as a function of solvent content as measured by TGA. In general the $T_g$ tends to decrease with increasing solvent content.

As can be seen in table 4.1, in all four cases the $T_g$ of DMSO samples increased from first to third heat run. This reduction in plasticisation clearly shows a reduction in trapped solvent with successive heat runs due to solvent evaporation on heating. For the **b**DMSO**c** sample the $T_g$ was measured to be 73 $^{\circ}C$ during the third heat run. This is the same value as measured for the water samples on the third heat run suggesting that this is close to the glass transition temperature for this type of PVA in its dry state.

It was also found that $T_g$ of DMSO samples increased from polymer to composites by few degrees Celsius as has been observed by other authors *[24]*. This is probably due to bonding between polymer and CNTs which tends to restrict chain mobility, again resulting in an increase in $T_g$ for the composite samples*[25]*. The second and third $T_g$ of **a**DMSO and the second $T_g$ of **b**DMSO samples were lower than the second and third $T_g$ of water and

NMP samples which suggest the presence of residual DMSO even after the first heat run (see Tab. 4.1).

The glass transition temperature of all the NMP samples also increased from first to third heat run (see figure 4.3) because of evaporation of solvent, which reduced plasticizing effect. In all cases the $T_g$ was 71 °C-72 °C on the third heat run which is very close to the value of 73 °C observed for the water samples and the **b**DMSO**c** sample. This suggests that almost all of the NMP has evaporated by the third heat run.

As measured on the first heat run the $T_g$ of the NMP polymer samples was lower than that for the DMSO polymer samples in agreement with the fact that less solvent remained in the DMSO based samples. However, this is not the case for the composite samples where the $T_g$ for the NMP based samples exceeds that for the DMSO samples. This is despite the fact that less solvent remains trapped in the DMSO compared to the NMP samples. These facts are difficult to reconcile with the general rule that $T_g$ decreases with increasing solvent content. These results can be explained however if we assume that the NMP is mobile in the polymer during the drying phase (60°C) but tends to get sequestered at low-energy sites on the nanotubes surface on cooling. Evidence supporting the mobility of the NMP at 60°C will be discussed in section 4.3.1. This effect results in trapping of NMP at the polymer-nanotube interface. It should be pointed out that NMP is a good dispersant for nanotubes largely due to its high binding energy to the nanotube sidewall *[20]*. This suggests that any NMP molecules which come into contact with the polymer-nanotube interface may not be able to escape from these interfacial sites during the drying conditions used here.

Interfacial trapping of the NMP would reduce the amount of NMP trapped in the matrix polymer for a given total residual NMP content. If we assume that only matrix NMP can act as a plasticizing agent then we would expect a reduction in plactisization as a result of trapping of NMP at the interface. This is supported by the fact that the $T_g$s for the NMP based composite samples are much higher than their respective polymer only samples. This difference is much greater than the equivalent difference for the DMSO based samples. This suggests that the NMP based composites are drier than their respective composites even though the solvent contents are similar. Again this can be explained if we assume that significant quantities of NMP remain at the polymer-nanotube interface, leaving less

solvent in the bulk polymer. This interfacial NMP would be expected to reduce polymer-nanotube binding. This would result in greater than normal chain mobility at the nanotube interface. Thus, chain restriction is unlikely to play a significant role in the increase in $T_g$ for the NMP based samples. The solvent segregation at the interface is likely to be the dominant effect. This trapped interfacial NMP has an enormous impact on the mechanical properties of NMP based composites as will be discussed below.

| Solvent | Sample | Δ H (J/g) (error:±0.5J/g) | % Crystallinity (χ) | $T_m$ |
|---|---|---|---|---|
| $H_2O$ | a p | 30.8±0.5 | 22.2±0.4 | 196 |
| | a c | 33.4±0.5 | 24.1±0.4 | 195 |
| | b p | 33.3±0.5 | 24.0±0.4 | 195 |
| | b c | 32.6±0.5 | 23.5±0.4 | 190 |

Tab. 4.2 DSC data for first heat run for water based composites and polymer only samples.

**Crystallinity measurements on the first heat**

Shown in figure 4.4 are the high temperature portions of the DSC curves as measured on the first heat run. It is important to note that the first heat run probes the morphology of the material, as it exists immediately after film formation from solution. In all cases a melt peak is observed in the region of 180 °C - 210 °C. The enthalpy of melting ($\Delta H_m$) was found out by numerically integrating the area under the melt peak. The fractional crystallinity (χ) was calculated assuming the enthalpy of melting of 100% crystalline PVA to be 138.6 J/g *[26]*. All enthalpy and crystallinity data for the first heat runs are presented in table 4.2. The crystallinity of the **a**$H_2O$**p** polymer sample was measured to be 22%. The crystallinity of the **a**$H_2O$**c** composite sample was marginally higher at 24% as observed in other studies *[4-6]*. This represents an increase, normalized to nanotube content of $d\chi/dV_f \sim 4.8$. This value is similar to values reported for CVD-MWNT based composites but significantly lower than those reported for DWCNTs based composites *[5]*. The difference

is probably related to different sample preparation conditions. However in the case of the samples with longer drying time the crystallinity of **b**$H_2O$**p** was virtually identical to the **b**$H_2O$**c** sample. It is not clear at present why this is the case. The crystallinity was difficult to estimate in the DMSO and NMP based sample because, as TGA revealed, the residual solvents evaporate in the melt range of PVA preventing accurate measurement of the enthalpy of melting.

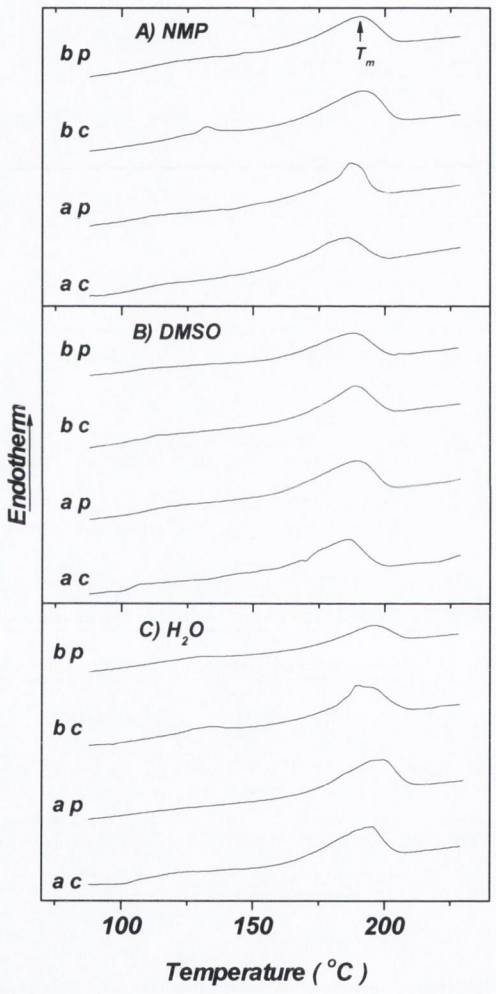


Fig. 4.4. High temperature portion of the DSC curves measured on the first heat for all samples.

**Crystallinity measurements on cooling**

After the first and second heat run, cooling runs were carried out for all samples as shown in figure 4.5. In addition subsequent heating and cooling cycles were measured. However we will only discuss crystallinity as measured from the recrystallisation phase transition observed during the cooling cycles. This is because cold crystallization was observed on the second and third heating cycles prior to melting. This cold crystallization peak tends to partially obscure the melt peak making enthalpy calculations difficult.

In all cases a recrystallisation peak is observed at high temperature followed by a glass transition at temperatures similar to these measured for the second heat. In all cases the crystallinity after re-crystallisation was measured from the area under the curve. These values are presented in table 4.3. In all cases the crystallinity was lower in the composites compared to the polymer only samples, possibly due to the hindering of the formation of PVA lamellae by the nanotubes. This reduction in crystallinity has previously been observed for PVA *[8]* and other polymers and has been attributed to nanotube enhanced thermal degradation of the polymer *[8]*. It should be pointed out that this is contrary to observations made both in this paper and in the literature for crystallinity measurements made on the first heat run *[5-7]*. This difference is not surprising as, for solution processed samples, the melt transition in first heat run measures melting of ordered structures formed during the solution drying phase. In contrast, the recrystallisation transition measured in the first cool (or the melt transition measured in the second heat) probes structures that are related to the melt phase of the polymer.

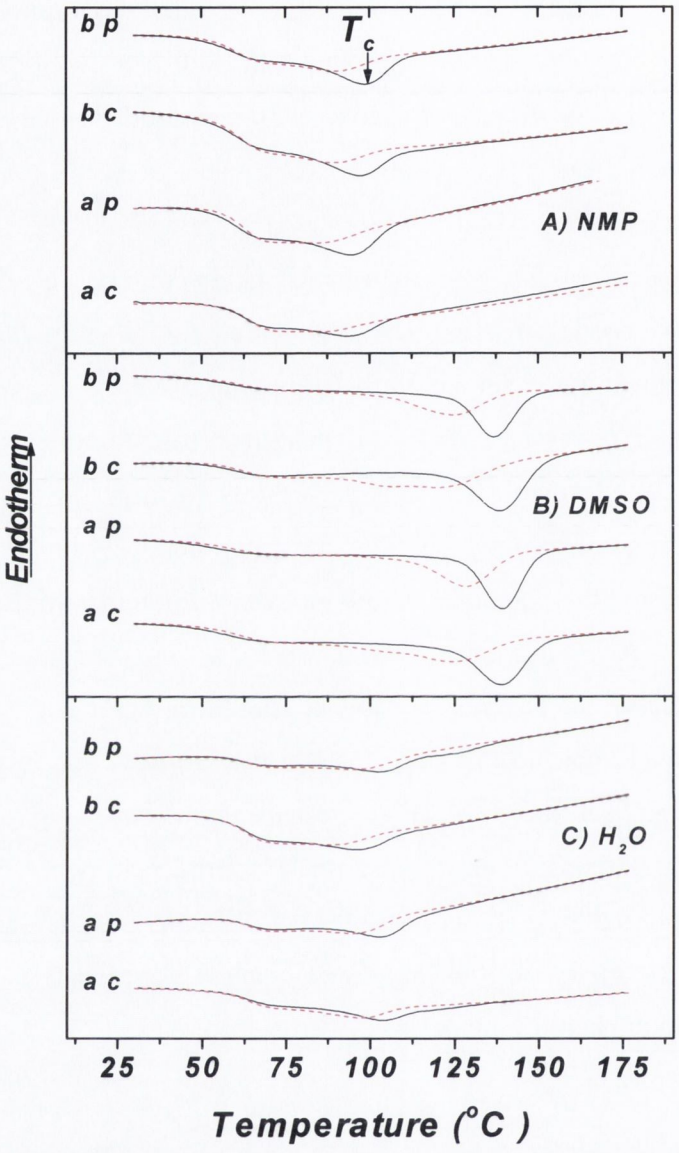


Fig. 4.5. First and second DSC cooling curves for each sample. Solid lines represent the first cooling step while dotted lines represent the second cooling step.

The cooling data also revealed that DMSO samples were much more crystalline compared to the water and NMP based samples. The data also indicated that DMSO samples re-crystallized at approximately 140 °C while water and NMP both re-crystallize at approximately 100 °C. One difference between the DMSO based samples and the others is

that, as revealed by the DSC study; small quantities of the solvent may remain even after a second heating cycle. Trapped DMSO molecules may act as nucleation sites for polymer crystallization in the same way that some dyes nucleate crystallinity in polymers *[27]*. The other reason may be some chemical reaction has been taken place between DMSO and PVA, which brought about chemical changes. The chemical changes in polymer matrix of solution based nanocomposites is due to the presence of residual solvent has previously been investigated previously as well *[21]*.

### 4.4.3 DMTA

For all samples dynamic mechanical thermal analysis (DMTA) was also carried out. However, the **a**$H_2O$**c** sample proved to be too brittle to obtain good results. DMTA is an oscillatory technique which gives the real and imaginary components of the elastic modulus as a function of temperature. The real part of the elastic modulus, usually called the storage modulus is shown for the NMP and DMSO based samples in figure 4.6.

As mentioned above, DMTA results were not obtained for the **a**$H_2O$**c** sample. However, the room temperature storage moduli for both water based polymer samples were similar, as expected, given the small deviation in trapped water content. The storage modulus of the **b**$H_2O$**c** sample was significantly higher than that of the equivalent polymer showing effective reinforcement as has been previously observed for water based PVA-NT composites.

As expected, an increase in storage modulus from polymer to composite was observed for the DMSO samples. The order of increase was **a**DMSO**c** > **b**DMSO**c** > **a**DMSO**p** > **b**DMSO**p**. This order holds true for all temperatures examined.

| Solvent | Sample | ΔH. (J/g) (error:±0.5J/g) | | %Crystallinity (χ) | $T_c$ | |
|---|---|---|---|---|---|---|
| | | 1st cool | 2nd cool | 1st cool | 1st cool | 2nd cool |
| $H_2O$ | a p | 6.5 | 3.8 | 4.7±0.4 | 101 | - |
| | a c | 5.5 | 2.3 | 3.9±0.4 | 101 | - |
| | b p | 5.6 | 4.2 | 4.0±0.4 | 101 | - |
| | b c | 3.7 | 1.8 | 2.6±0.4 | 100 | 100 |
| DMSO | a p | 23.0 | 18.5 | 16.5±0.4 | 141 | 130 |
| | a c | 20.0 | 17.2 | 14.4±0.4 | 141 | 126 |
| | b p | 22.6 | 18.9 | 16.2±0.4 | 141 | 126 |
| | b c | 17.8 | 14 | 12.8±0.4 | 139 | 124 |
| NMP | a p | 4.7 | - | 3.4±0.4 | 98 | 90 |
| | a c | 2.5 | - | 1.7±0.4 | 97 | 91 |
| | b p | 6.9 | - | 5±0.4 | 100 | 93 |
| | b c | 5.5 | 23 | 4±0.4 | 99 | 92 |

Tab. 4.3 DSC data of cooling run for solution based composites and polymer only samples.

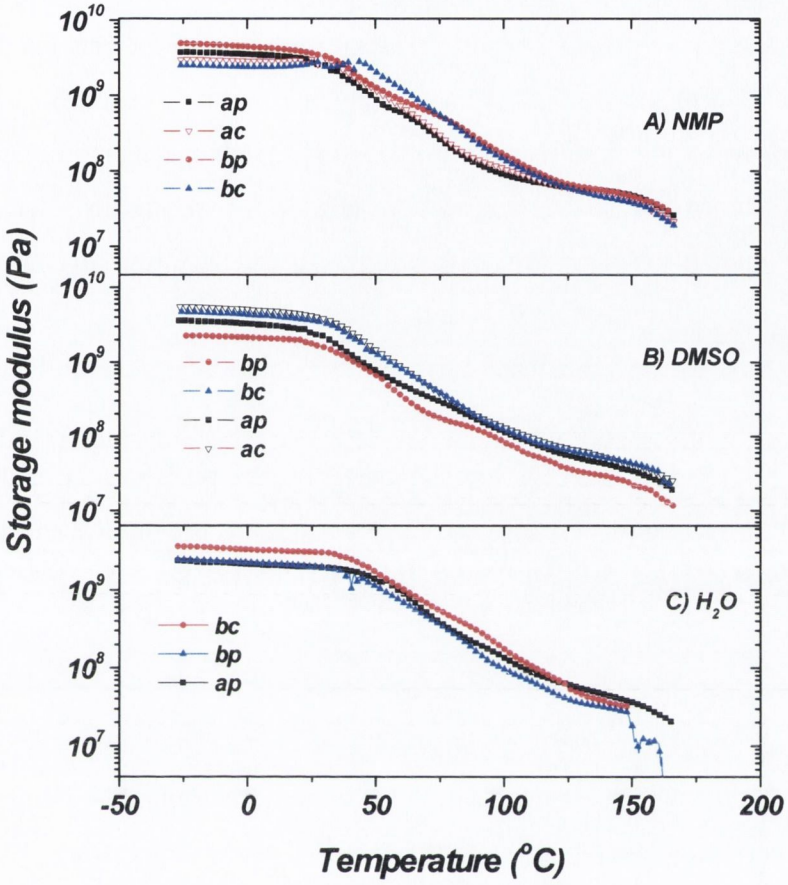


Fig. 4.6. Storage modulus as function of temperature of solution based DWCNT-PVA composites and polymer only samples.

Contrary to the behavior observed in the DMSO based samples, the storage modulus measured at room temperature decreased from polymer to composite in all NMP samples. This behavior is unexpected. NMP is known to be both a good solvent for PVA *[15]* and a good dispersant of nanotubes *[20].* As a result is had been expected that use of NMP as a solvent would result in a very good dispersion, resulting in excellent mechanical properties. The absence of reinforcement, in the presence of a good dispersion must mean that stress is not being transferred from polymer matrix to nanotube filler *[1, 2]*. However, PVA is known to bond well to nanotubes, resulting in good stress transfer *[6]* . This means some other factor must reduce the stress transfer in NMP based composites. This is almost

certainly due to entrapment of NMP at CNT-PVA interface as discussed above. The presence of trapped solvent must disrupt the polymer-nanotube bonding thus limiting the interfacial stress transfer. This is an important result. One might imagine that solvents such as NMP that tend to disperse nanotubes *[20]* would be good solvents to use in composite formation. However, such solvents are good dispersants for nanotubes precisely because they bind well to nanotubes *[20]*. This factor, however, results in solvent trapping at the polymer nanotube interface and the disruption of interfacial stress transfer.

However, it is interesting to note that the storage modulus of NMP based composites crosses over that of the respective polymer only samples at temperatures of ~25 °C and ~42°C for **a**NMP and **b**NMP samples respectively as shown in figure 4.6. This suggests that at elevated temperature the trapped NMP begins to desorb from the interface and become mobile in the polymer matrix. This allows the interfacial polymer to bind efficiently to the nanotube and allows the effective transfer of stress from polymer to nanotube.

**The dynamic glass transition temperature**

The energy dissipation during dynamic mechanical measurements is proportional to the ratio of the real and imaginary parts of the elastic modulus*[28]*. Better know as Tanδ, the energy dissipation tends to peak at the glass transition temperature, $T_g$. Shown in figure 4.7 is Tanδ as a function of temperature for all DMSO and NMP based samples. In all cases, a peak was observed indicating the presence of a glass transition. The glass transition temperatures measured using this dynamic technique is presented in table 4.1. In all cases these dynamic glass transition temperatures are greater than those measured by static means (DSC). This is due to the fact that, for viscoelastic materials in general, dynamic $T_g$ is dependent on the strain rate. The dynamic $T_g$s are plotted in figure 4.3 as a function of solvent content. It can be seen clearly that, as was the case for the static $T_g$s, the dynamic glass transition temperature tends to fall as the solvent content increases.

The dynamic $T_g$ of the **b**$H_2O$ samples increased slightly from polymer to composites. This trend has also been reported in many other studies as discussed above*[8, 24]*. In the DMSO based samples $T_g$ also increased from polymer to composites for both **a**DMSO and **b**DMSO samples.

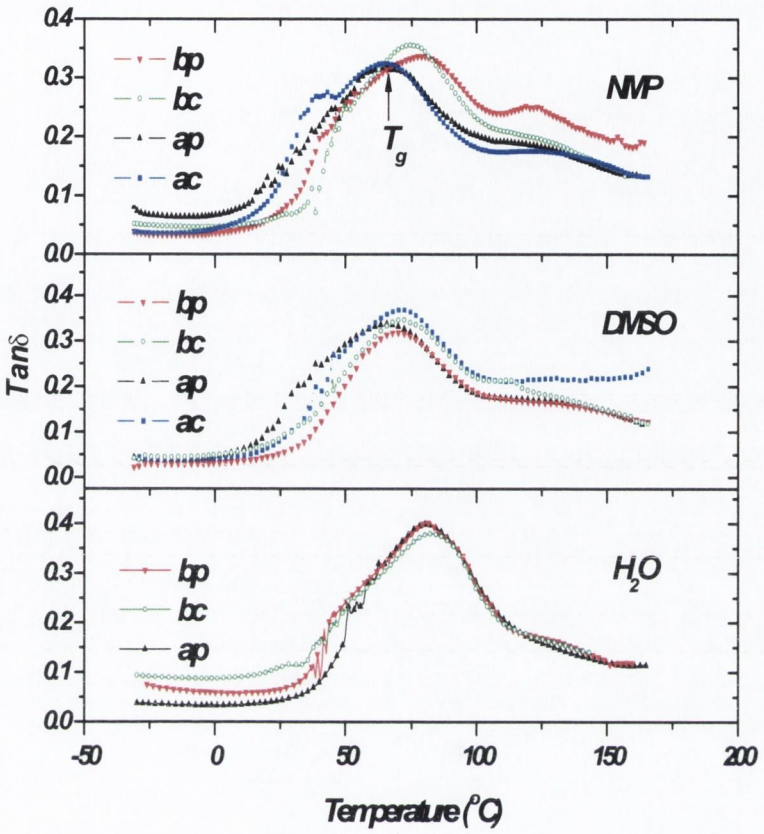


Fig. 4.7 Dynamic $T_g$ of composites and polymer only samples.

In the case of the NMP based samples however, the results were less straightforward. For these samples the composites $T_g$ were slightly lower than their respective polymer only samples, which is unexpected. This is in stark contrast to the static $T_g$ results as measured by DSC. The static $T_g$ results could be explained by the presence of trapped NMP at the polymer-nanotube interface. The main difference between the static (DSC) and dynamic (DMTA) measurements is that the dynamic $T_g$s tend to be significantly larger than their static counterparts as mentioned previously. However, as suggested by the storage modulus results, the NMP begins to desorb from the nanotube surface and become mobile at temperatures in the range between 25-42 °C. This suggests that at the higher temperatures (>63°C) where we observe the dynamic $T_g$ significant quantities of NMP may have

desorbed from the interface into the polymer matrix. If enough NMP desorbs, then the NMP content in the polymer matrix could exceed the NMP content in the polymer only samples resulting in a lower dynamic $T_g$ in the composite samples as is observed.

### 4.4.4 Tensile testing

Stress-strain measurements were made on all samples to investigate the static mechanical response. Representative stress-strain curves for each sample are shown in figure 4.8. It is immediately clear that the strain at break is lowest in the water based samples (table 4.4). This is consistent with the fact that the water based samples contained significantly less solvent compared to the other samples. Less residual water means less plasticization, resulting in more brittle materials and so lower strain at break. From these curves were extracted values for the Youngs modulus, the ultimate tensile strength and the strain at break. These values are presented in table 4.4. It should be pointed out that in all cases the Youngs moduli measured by static means were lower that the storage moduli at room temperature measured dynamically. This phenomenon has been observed in previous studies *[29]*.

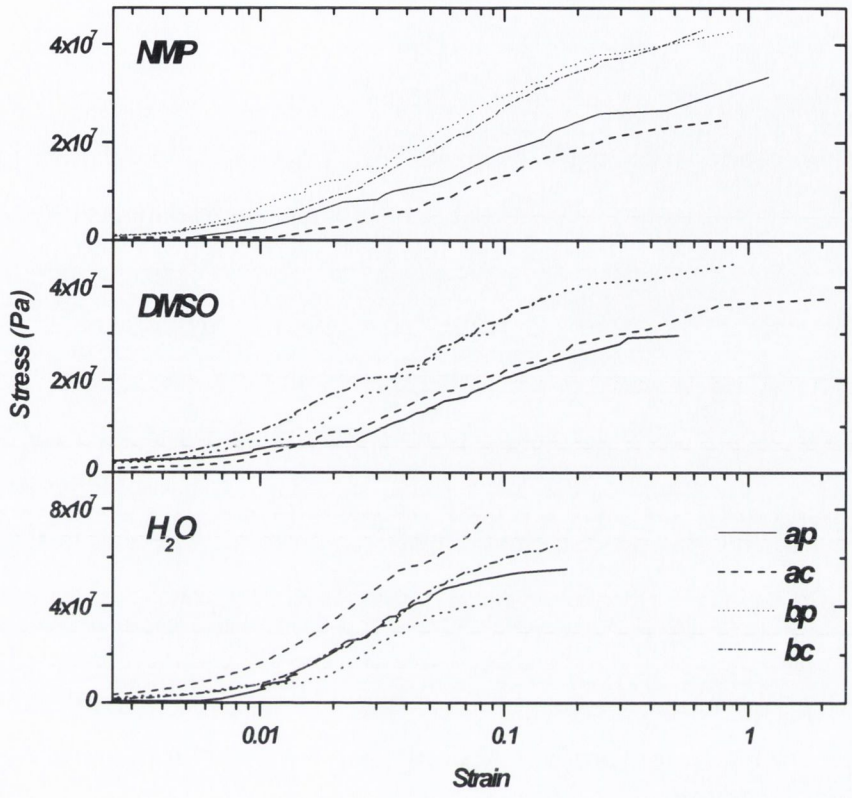


Fig. 4.8 Stress-strain curves for solution based composites and polymer only samples. Note that in all three graphs, the strain axis is plotted logarithmically.

For the water based samples, increases in both Young's modulus and strength were observed on the addition of nanotubes. However, these increases were much more significant for the **a**$H_2O$ samples. Interestingly, the **a**$H_2O$ samples also displayed an increase in crystallinity on the introduction of nanotubes. It has previously been suggested that nanotubes nucleate the formation of crystallinity in solution based PVA-CNT composites and that this nucleated crystallinity can act as an additional component of reinforcement *[1, 4, 6, 10, 30]*.The reinforcement of modulus *[1]*, as quantified by $dY/dV_f$, was ~240 and ~105 GPa for the **a**$H_20$ and **b**$H_2O$ samples respectively. The value of $dY/dV_f$~240 GPa for the **a**$H_2O$ samples is lower than previous measurements for DWCNT-PVA samples where nanotube induced crystallinity is present *[5]*. This is however

consistent with the fact that the rate of increase of crystallinity with volume fraction ($d\chi/dV_f$) measured here is lower than that quoted in ref *[5]* resulting in less induced-crystallinity based reinforcement. However, for the $bH_2O$ sample no nanotube induced crystallinity is present *[1]* and so the modulus reinforcement can only be due to the presence of nanotubes. Thus, the measured value of $dY/dV_f$ ~105 GPa is unexpectedly high. The reinforcement of strength, as quantified by $d\sigma/dV_f$, was~3.1 GPa for the $aH_2O$ sample. This is relatively low compared to the literature value of $d\sigma/dV_f$ ~40 GPa for MWCNT in PVA *[6]*, consistent with the low value of $d\chi/dV_f$ in the $aH_2O$ sample. No strength enhancement was observed within error for the $bH_2O$ sample. This may be correlated with the lack of nanotube-nucleated crystallinity in this sample.

In the case of the DMSO based samples, both moduli and strength values were significantly lower compared to the water based samples. Furthermore the strain at break was much higher than the water based samples. These effects are due to the plasticizing effect of trapped solvent. No increase in modulus within error was observed for the aDMSO samples on addition of nanotubes. However, a significant increase in strength of $d\sigma/dV_f$ ~5 GPa was observed. For the drier **b**DMSO samples, a significant increase in modulus was observed corresponding to $dY/dV_f$ ~105 GPa. This value is very similar to that measured for the $bH_2O$ samples, in the absence of induced crystallinity. The presence of induced crystallintiy could not be measured for the DMSO samples as the solvent evaporation masked the PVA melting peak in the crystallinity. However, we can speculate that the similarity in modulus reinforcement between the $bH_2O$ and **b**DMSO samples suggests that this figure represents the value appropriate to that for PVA with no contribution from nanotube induced crystallinity.

For the NMP based samples, both modulus and strength were lower in the composite samples compared to the polymer samples. This exactly the same trend observed for the room temperature storage modulus results again confirming the lack of stress transfer in the NMP based composites. We must reiterate that this is almost certainly due to the presence of interfacial NMP (see figure 4.9) whose presence is due to the strong affinity of NMP for carbon nanotubes. This underlines that fact that while NMP tends to successfully disperse nanotubes, its use in composite formation is ill advised unless care is taken to completely remove it from the sample.

| Solvent | Sample | Y-modulus (GPa) | Strain at break | UTS (MPa) | Storage modulus (GPa) |
|---|---|---|---|---|---|
| $H_2O$ | a p | 1.28 $\pm$ 0.1 | 0.18 | 54 $\pm$ 0.0 | 2.0 |
| | a c | 1.85 $\pm$ 0.01 | 0.09 | 78 $\pm$ 0.0 | - |
| | b p | 1.18 - | 0.10 | 42 - | 2.05 |
| | b c | 1.43 $\pm$ 0.03 | 0.19 | 49 $\pm$ 15 | 3.10 |
| DMSO | a p | 0.41 $\pm$ 0.01 | 0.51 | 29 $\pm$ 0.5 | 2.85 |
| | a c | 0.50 $\pm$ 0.05 | 0.63 | 35 $\pm$ 2 | 4.57 |
| | b p | 0.65 $\pm$ 0.05 | 0.91 | 44 $\pm$ 1 | 1.96 |
| | b c | 0.90 $\pm$ 0.0 | 1.1 | 38 $\pm$ 1 | 3.90 |
| NMP | a p | 0.35 $\pm$ 0.05 | 1.2 | 32 $\pm$ 1 | 3.18 |
| | a c | 0.24 $\pm$ 0.02 | 0.85 | 25 $\pm$ 1 | 2.92 |
| | b p | 0.78 $\pm$0.02 | 0.85 | 39 $\pm$ 3 | 4.00 |
| | b c | 0.46 $\pm$ 0.01 | 0.72 | 37 $\pm$ 4 | 2.49 |

Tab.4.4. Mechanical properties of DWCNT-PVA composites and polymer only samples.

One possible solution to this problem would be to use nanotube-like fillers whose walls are not smooth on the atomic scale. One example of such structures are coiled nanotubes as prepared by Lau et al *[31]*. These structures have graphite like surface so should be dispersible in NMP. However their curved surface should allow mechanical interlocking with the polymer matrix resulting in improved stress-transfer. The summery of solvent entrapment can be seen in animated figure 4.9.

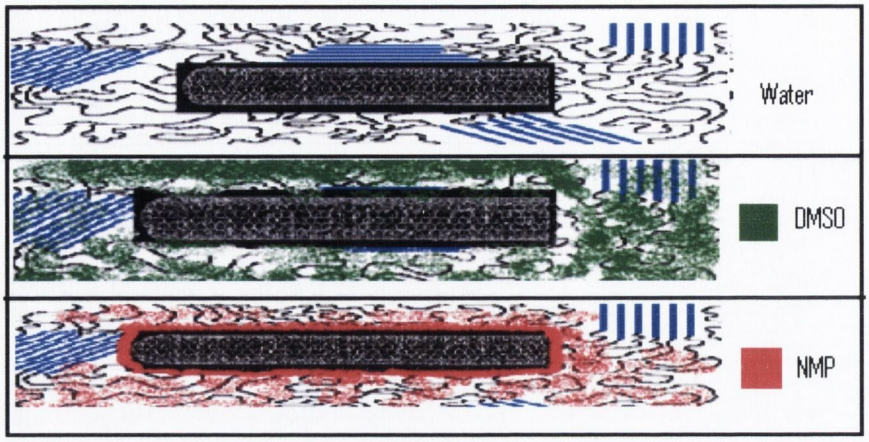


Fig 4.9 illustration solvent entrapment in matrix and at CNT-polymer interface (animated image)

## 4.5 Conclusion

Composites based on polyvinylalcohol as a matrix and double walled nanotubes as a filler have been produced by solution processing. Both polymer only films and polymer-nanotube composites were fabricated using three different solvents; water, DMSO and NMP. Thermo gravimetric measurements show that, after film formation, the amount of trapped solvent varied significantly with solvent type, drying time and presence or absence of nanotubes. Differential scanning calorimetry measurements show that to a first approximation the glass transition temperature decreases as residual solvent content increases. However, deviations from this behavior suggest that significant quantities of NMP are trapped at the polymer-nanotube interface. As was the case for the DMSO samples, both moduli and strength values for the NMP based samples were significantly lower compared to the water based samples. For both **a**NMP and **b**NMP samples, a significant reduction in both modulus and strength was observed on the addition of nanotubes. This is in direct correlation with the storage modulus measurements made at room temperature. This reduction in modulus and strength is most likely due to a complete lack of polymer-nanotube stress transfer. This is further evidence for the hypothesis of the presence of trapped NMP at the polymer-nanotube interface. Dynamical mechanical measurements show mechanical reinforcement on addition of nanotubes for water and DMSO based systems. Significantly, both modulus and strength were reduced at room

temperature on addition of nanotubes in NMP based systems. This is consistent with trapped interfacial NMP eliminating polymer-nanotube stress transfer. At higher temperatures the composite storage modulus surpassed the polymer modulus suggesting thermally induced desorption of NMP from the interface. Static mechanical measurements show increases in both strength and modulus on addition of nanotubes to water and DMSO based systems. However, as in the dynamic measurements, reductions in both modulus and strength were observed on introduction of nanotubes in the NMP based systems. Finally, increases in both modulus and strength appear to correlate with the presence of nanotube induced crystallinity in the water based composite systems. This study clearly shows that care must be taken when choosing solvents for polymer-nanotube composite formation.

## 4.6 References


[1] J. N. Coleman, U. Khan, W. J. Blau, Y. K. Gun'ko, *Corbon* **2006**, *44*, 1624.

[2] J. N. Coleman, U. Khan, Y. K. Gun'ko, *Advanced Materials* **2006**, *18*, 689.

[3] R. Murphy, J. N. Coleman, M. Cadek, B. McCarthy, M. Bent, A. Drury, R. C. Barklie, W. J. Blau, *J. Phys. Chem. B* **2002**, *106*, 3087.

[4] M. Cadek, J. N. Coleman, V. Barron, K. Hedicke, W. J. Blau, *Applied Physics Letters* **2002**, *81*, 5123.

[5] M. Cadek, J. N. Coleman, K. P. Ryan, V. Nicolosi, G. Bister, A. Fonseca, J. B. Nagy, K. Szostak, F. Beguin, W. J. Blau, *Nano Lett.* **2004**, *4*, 353.

[6] J. N. Coleman, M. Cadek, R. Blake, V. Nicolosi, K. P. Ryan, C. Belton, A. Fonseca, J. B. Nagy, Y. K. Gun'ko, W. J. Blau, in *Advanced Functional Materials*, Vol. 14, **2004**, 791.

[7] J. F. B. E. Kilbride and J. N. Coleman , P. Fournet, M. Cadek, A. Drury, and S. Hutzler, S. Roth ,W.J.Blau, *Journal Of applied Physics* **2002**, *92*, 4024.

[8] O. Probst, E. M. Moore, D. E. Resasco, B. P. Grady, *Polymer* **2004**, *45*, 4437.

[9] A. B. Dalton, S. Collins, E. Munoz, J. M. Razal, V. H. Ebron, J. P. Ferraris, J. N. Coleman, B. G. Kim, R. H. Baughman, *Nature* **2003**, *423*, 703.

[10] P. Miaudet, S. Badaire, M. Maugey, A. Derre, V. Pichot, P. Launois, P. Poulin, C. Zakri, *Nano Lett.* **2005**, *5*, 2212.

[11] X. Zhang, T. Liu, T. V. Sreekumar, S. Kumar, X. Hu, K. Smith, *Polymer* **2004**, *45*, 8801.

[12] Y. Bin, M. Mine, A. Koganemaru, X. Jiang, M. Matsuo, *Polymer* **2006**, *47*, 1308.

[13] Po-Da Hong, J.-H. C. H.-L. Wu, *Journal of Applied Polymer Science* **1998**, *69*, 2477.

[14] P.-D. Hong, C.-M. Chou, C.-H. He, *Polymer* **2001**, - *42*, 6105.

[15] Paresh P, FerdinandR, a. George, *Journal of Applied Polymer Science* **1979**, *23*, 2335.

[16] K. D. Ausman, R. Piner, O. Lourie, R. S. Ruoff, M. Korobov, *J. Phys. Chem. B* **2000**,
*104*, 8911.
[17] J. L. Bahr, E. T. Mickelson, M. J. Bronikowski, R. E. Smalley, J. M. Tour, *Chemical*
*Communications* **2001**, 193.
[18] C. A. Furtado, U. J. Kim, H. R. Gutierrez, L. Pan, E. C. Dickey, P. C. Eklund, *J. Am.*
*Chem. Soc.* **2004**, *126*, 6095.
[19] J. Cao, Q. Wang, M. Rolandi, H. Dai, *Physical Review Letters* **2004**, *93*, 216803.
[20] S. Giordani, S. D. Bergin, V. Nicolosi, S. Lebedkin, M. M. Kappes, W. J. Blau, J. N.
Coleman, *J. Phys. Chem. B* **2006**, *110*, 15708.
[21] K.-t. Lau, M. Lu, Chun-ki Lam, H.-y. Cheung, F.-L. Sheng, H.-L. Li, *Composites Science and Technology* **2005**, *65*, 719.
[22] B.J. Holland, J. N. Hay, *Polymer* **2001**, *42*, 6775.
[23] Jeffrey W. Gilmanl, David L. VanderHart, T. Kashiwagi', *American Chemical Society*
**1995**, 161.
[24] C. Velasco-Santos, A. L. Martinez-Hernandez, F. Fisher, R. Ruoff, V. M. Castano, *Journal of Physics D-Applied Physics* **2003**, *36*, 1423.
[25] L. H. Sperling, *Introduction to Physical Polymer Science.*, Wiley, **2001**.
[26] N. A., Peppas, P. J. Hansen, *Journal of Applied Polymer Science* **1982**, *27*, 4787.
[27] Z. L. T. Hatakeyama, *Handbook of thermal analysis*, John Wiley & sons Ltd, **1998**.
[28] I. Ward, a. J. Sweeney, *The Mechanical Properties of Solid Polymers*, Wiley, **2004**.
[29] A. Dufresne, M. Paillet, J. L. Putaux, R. Canet, F. Carmona, P. Delhaes, S. Cui, *Journal of Materials Science* **2002**, *37*, 3915.
[30] J. N. Coleman, M. Cadek, K. P. Ryan, A. Fonseca, J. B. Nagy, W. J. Blau, M. S. Ferreira, *Polymer* **2006**, *47*, 8556.
[31] K. T. Lau, M. Lu, D. Hui, *Composites Part B: Engineering* **2006**, *37*, 437.

# Chapter 5

## Mechanical reinforcement of thermoplastic polyurethane by functionalised SWCNTs

### 5.1 Introduction

Carbon nanotubes have excellent mechanical, electrical and thermal properties *[1-7]* Due to their unmatched properties, CNTs have been the subject of interest for use in composite materials since their discovery *[8]*. Numerous efforts have been made to utilise these properties in the fabrication of rigid plastic matrix composites*[9-12]* . The problem with plastic matrices is that at high volume/mass fractions they lose ductility and this may be accompanied by the reduction of other mechanical properties as well *[13]*. An alternative to rigid plastic matrices is elastomers. Among elastomers thermoplastic polyurethane (TPU) is on the versatile matrix. Thermoplastic polyurethane has a very high ductility. Another feature of TPU is its stress-strain recovery *[14]*. Unlike plastics, when they are stretched beyond the elastic limit, they can regain their shape on relaxation *[15]*. The shape recovery is due the presence of hard segment (HS) which acts as molecular spring for continuous soft segment (SS). The polyol or amine in TPU is very soft (with a very low $T_g$ ) and long chains while the diisocyanate part is relativity hard and short molecule (with a high $T_g$ ) and so, these are referred to as soft segment (SS) and hard segment (HS) respectively. The problem with TPU is its low stiffness and low stress in the plateau region of stress strain curves. TPU can be reinforced by addition of CNTs *[16-20]*.

One important parameter in composite reinforcement is good dispersion of the filler *[21]*. Pristine nanotubes can be dispersed very efficiently in solvents at very low concentration but at higher concentration they tend form bundles*[22, 23]* . These bundles are held by weak physical interactions and therefore create weak points in the composite

and result overall in weak composites. However this problem can be overcome by the use of functionalised CNTs. Very good dispersions of the functionalised CNTs can be achieved even at a very high concentrations compared with pristine CNTs *[24-27]*. Another requirement for good mechanical reinforcement is good stress transfer and interfacial bonding *[21]*. Strong interfacial bonding between a filler and matrix can be defined by mechanical interlocking or chemical reaction between them. Usually the CNTs are chemically inert and have an atomically smooth surface, this means mechanical interlocking and CNT-matrix reaction is rare. Again the functionalised CNTs have an advantage here due to the funtionalised groups attached to the CNTs. A polymer matrix can either entangle or chemically bond with the attached functional groups. Adding to this functionalisation of the CNTs creates defect in the CNTs, making them rough thus rendering them favourable for mechanical interlocking as well *[18]*. Functionalisation may weaken the CNTs but they are still strong enough to be used as filler for mechanical reinforcements.

Another very important aspect of choosing functionalised CNTs as filler for segmented TPU lies in its segmented nature. Hard and soft segments are thermodynamically incompatible*[21]* . The HS and SS within thermoplastic polyurethanes have different polarities *[28-31]*. Generally speaking the HS is hydrophilic while the SS is hydrophobic *[29]*. This strongly suggests that by selecting appropriate funtionalised CNTs, either HS or SS can be used to mechanically reinforce for a specific application. Recently Liff *et al.* have demonstrated the fabrication of nanoclay-TPU composites by restricting the nano filler to hard segment only *[29]*. Adding to this, both the hard and soft segment's mechanical properties can be tuned by mix CNTs approach which will be discussed in detail in Chapter 6. Hence, an efficient and compatible CNT- TPU solution based composite can be prepared on the basis of matching the solubility parameters of all three components, i.e. matrix, filler, and solvent *[32]*.

In the present work, keeping in mind the difference in hydrophobicities of HS and SS, three different types of functionalised-SWCNTs were used in two different solvents, water and THF to fabricate composites. All three composites exhibited different properties. These composites can be used as actuators/artificial muscles*[14, 33]* , extremely flexible electrodes *[34]* and sensors*[35]* .

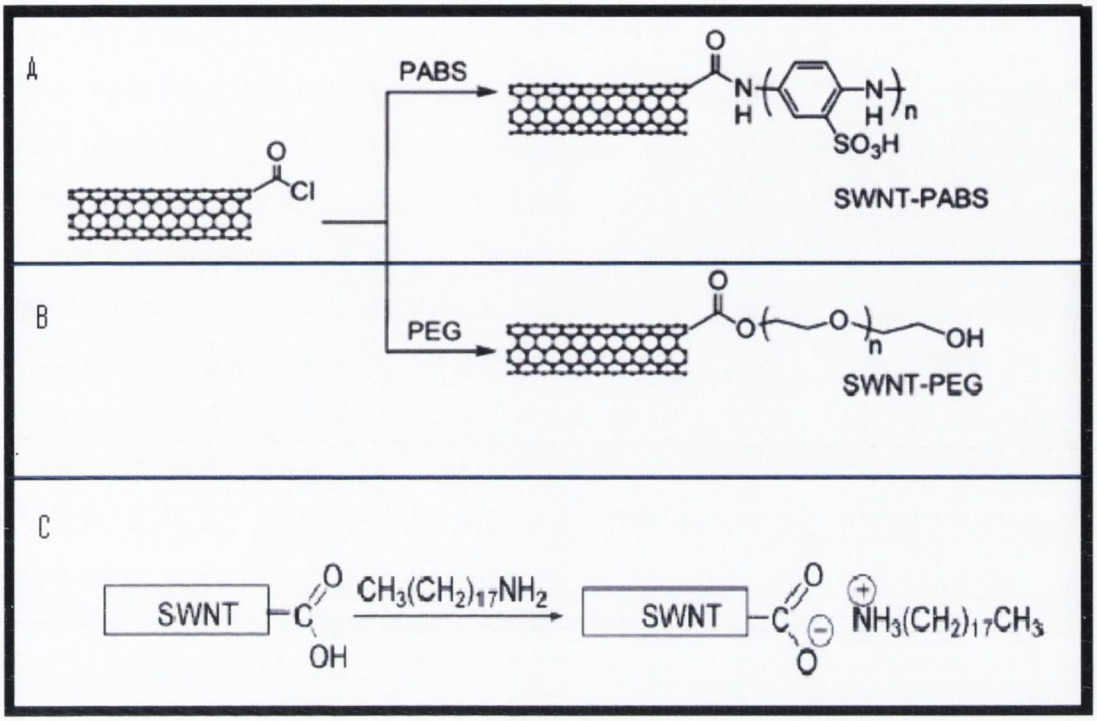


Fig. 5.1 Synthesis of functionalised SWCNTs *[24]* A) PABS-SWCNTs B)PEG-SWCNTs both of which are dispersible in water at high concentration. *[24]* C) ODA-SWCNTs are soluble in organic solvents at high concentration *[26]* .

## 5.2 Sample preparation

Thermoplastic polyurethane/$H_2O$ (product code U2-01.) emulsion was provided by Hydrosize® *[36]* with an average particle size ~ 3 μm. The dispersion was diluted to 50 mg/ml in deionised water. PEG-SWCNTs, PABS-SWCNTs and ODA-SWCNTs were purchased from Carbon Solutions, Inc. (Fig 5.1) *[37]*. Each of the PEG-SWCNTs and PABS-SWCNTs were dispersed in 10 ml of deionised water. Dispersions were made by energetic agitation of CNTs/$H_2O$ using an ultrasonic sonic tip (GEX600, 700W, 20%, 120 kHz) for 10 minutes. This was followed by 4 hours of sonication in an ultrasonic bath (Branson 1510 MT). Each of the CNT dispersions was then mixed with a prepared TPU/$H_2O$ emulsion using the same ultrasonic tip (5 minutes). These were the stock

solutions for the further work. Each of the stock composite solutions were diluted into a series of solutions. Each of these dilutions was sonicated for five minutes under the ultrasonic tip, followed by further sonication for 4 hours in the ultrasonic bath.

For the ODA-SWCNT system, the supplied TPU was dried at 60 °C for 3 days in Petri dishes. The dried TPU was cut into small pieces. A 50mg/ml TPU/THF solution was prepared at room temperature by magnetic stirring. The THF was purchased from Sigma Aldrich. The rest of the ODA-SWCNT composite solutions preparation procedure was the same as that which was carried out for water based systems .The only difference was that ultrasonication was undertaken in an ice beaker to avoid evaporation of the low boiling point THF. Composite and polymer only solutions were dropcast in 40 x 40 mm Teflon trays. The water-based solutions were dried at 60 °C in an oven for 12 hours, while the THF-based solutions were dried at room temperature for 12 hours followed by further heating at 60 °C for 2 hours. Free standing films were obtained. These films were cooled in ambient condition to stabilise them. Films were cut into strips using a die cutter with a fixed spacing of 2.25 mm. Thicknesses of the films were measured using a micrometer screw.

## 5.3 Results and discussion

### 5.3.1 Thermogravimetric analysis (TGA) analysis

Thermogravimetric analysis (TGA) was carried out using a Perkin Elmer Pyris 1 TGA. The temperature range was from 25 - 900 °C with scan of 10 °C /minute. TGA was carried out to assess the solvent entrapment in the sample and also to determine the onset of polymer degradations. The polymer TGA analysis study shows the presence of trapped solvent in the polymer. The TGA analysis also revealed that TPU starts degrading above 230 °C (Fig. 5.2). Once the degradation temperature was known, for all of the other thermal studies (DSC and DMTA) the maximum temperature was kept below 230 °C to avoid polymer degradation.

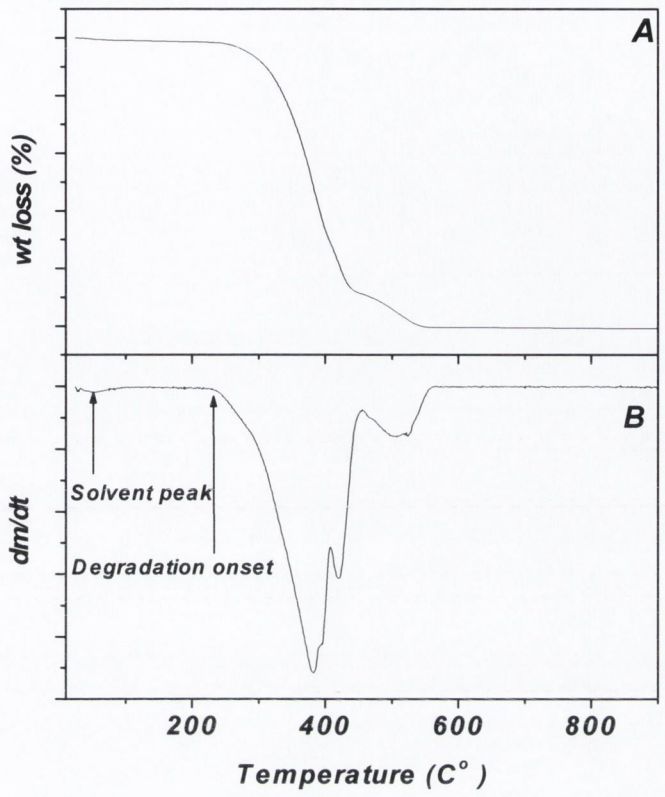


Fig. 5.2 A) TGA B) DTGA of PU/$H_2O$ sample, shows water entrapment and polymer degradation onset temperature.

## 5.3.2 DSC characterisation

DSC was carried out with a Perkin Elmer Diamond DSC with a heating scan rate of 20 °C/minute. For all samples the glass transition temperature ( ~ -25 °C) was very broad (Fig. 5.3). In all cases, no real difference was observed among composites and polymer only samples $T_g$.

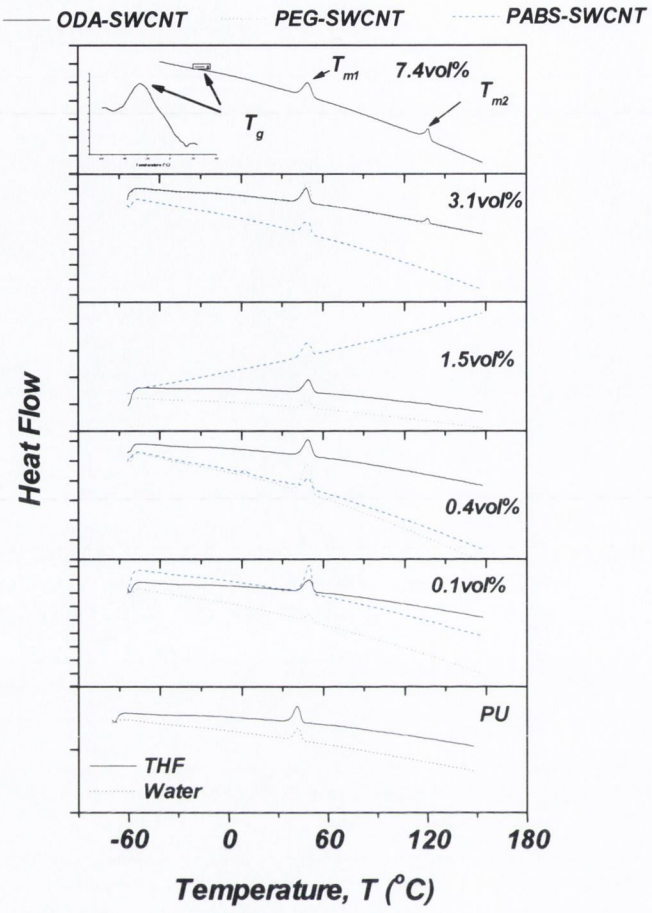


Fig. 5.3 DSC curves of TPU and functionalised SWCNTS composites.$T_{m1}$ is soft segment melting peak and $T_{m2}$ corresponds to HS melting nucleated by ODA-SWCNTs. Note: the plot on the top left is the derivative of $T_g$ part of DSC curve.

In all samples a crystalline melting peak $T_{m1}$ was observed at ~ 41 °C corresponding to the TPU soft segment melting (Fig.5.3). SS melting in the same temperature range has also been observed by various other researchers *[14, 18, 20, 28, 39-41]*. No difference of melting enthalpies was recorded between the ODA-SWCNT composites and the polymer only sample. The melting enthalpies of water dispersed PABS-SWCNT and PEG-SWCNT composites were higher than polymer only sample but with a lot of scatter (Fig. 5.4). This may be due to the evaporation of trapped/absorbed water (discussed in the next section) during the DSC heating run. The presence of trapped water has been revealed by TGA

(figure 5.2) as well. Another possibility is for higher enthalpies in water based composites compared to the respective polymer only samples. This may be due to the nucleation effect of these water dispersed CNTs. This infers the interaction of water dispersed CNTs with the SS.

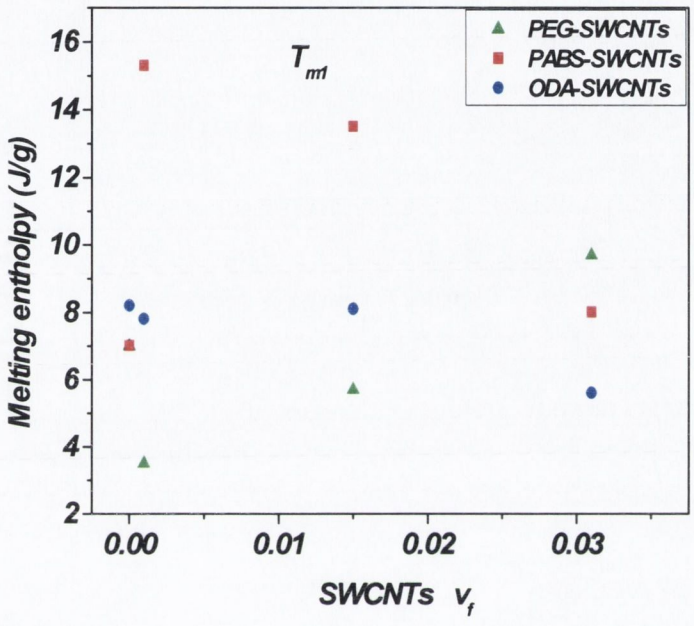


Fig 5.4 Melting enthalpy of functionalised SWCNT composites

The DSC study also revealed a second endothermic peak ($T_{m2}$) at 114 °C in ODA-SWCNT composites, while no such peak was observed in water-based composites. In the same temperature range in their TPU work, Liff *et al. [29]* observed a melting peak associated to the hard segment melting transition. The new peak may have arisen due to the nucleation of polydispersed HS crystallites by CNTs. Nucleation effects of CNTs in polymers have been reported elsewhere also *[42-44]*. This underlines the strong interaction of ODA-SWCNTs with the HS of TPU. $T_{m2}$ (second melting peak) started to appear at 2.5 wt % of CNTs. This second endothermic peak's enthalpies increased linearly with volume fraction of CNTs due to the increase in nucleation sites (Fig. 5.5). A linear increase in enthalpies has also been observed in other CNT-polymer work *[45]*.

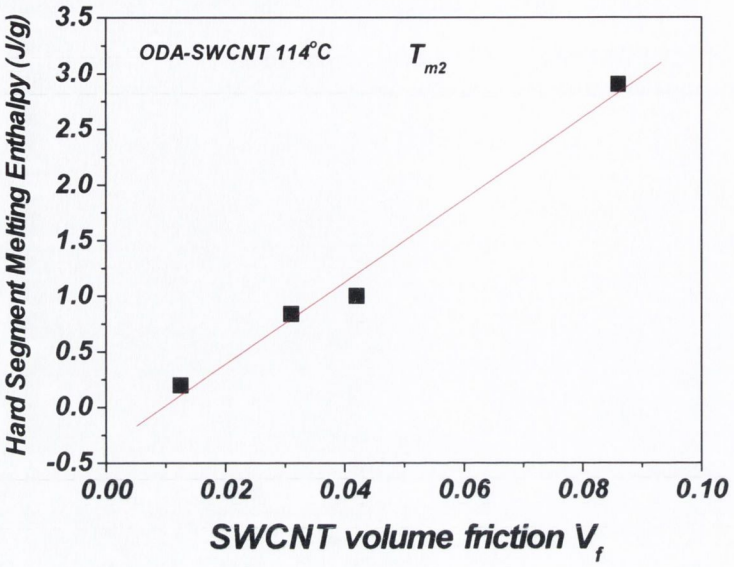


Fig. 5.5 DSC linear increase in melting enthalpies of TPU hard segment with introduction of ODA-SWCNTs.

**Cyclic DSC**

DSC was also performed on cyclically strained samples to find out the CNTs effect on strain induced crystallinity. In all strained samples, $T_{m1}$ was observed at the same temperature as was observed for non-strained samples, but the melting enthalpies were greatly reduced compared to their unstrained counterparts. The reduction was more pronounced in TPU/$H_2O$ samples compared to TPU/THF. Also, melting enthalpies were decreased slightly in successive cycles. The decrease in enthalpies can be associated with three reasons:

1) During cyclic deformation, internal friction of molecules generates heat energy which could melt relatively low melting point SS crystallites ($T_{m1}$).

2) Crystallites may be mechanically deformed and hence destroyed during the cyclic deformation of samples.

3) During cyclic deformation, due to the heating of the samples, evaporation of trapped water (associated to $T_{m1}$ crystallites) may occur.

The first two reasons seem less contributory, as can be seen in figure 5.6, as there is only a very slight difference in melting enthalpies of successive cycles within a sample. Also there is little difference between non-strained and cyclically deformed TPU/THF samples. Therefore, the third reason needs to be investigated in detail. If, the trapped/absorbed water is bonded to $T_{m1}$ crystallites and evaporates in the same temperature range, then this will contribute to overall (pseudo/apparent) crystallinity and vice versa. Cyclically strained samples can be relatively dried compare to non strained ones and that might be the reason that strained samples show low crystallinity. To investigate the actual reason for higher crystallinity in non-strained samples compared with cyclically strained samples, further experiments were carried out. DSC was conducted under the same experimental conditions as previously described. All non-strained water-based samples were further dried under vacuum at room temperature to avoid crystallites melting ($T_{m1}$). Similar to other non-vacuumed dried water samples, $T_{m1}$ appeared at around 41 °C for all samples. However, for the vacuum dried samples, $T_{m1}$ melting enthalpies were greatly reduced compared with the non-dried non-strained counterparts. For the polymer only sample, the melt enthalpy reduced from non-dried 7 J/g to 2.2 J/g (Vac dried). For the PABS and PEG-SWCNTs composite (1.55 vol%), the melt enthalpy reduced from non-dried 13.4 and 8 J/g to 4.8 and 3.3 J/g (Vac. dried) respectively. Enthalpies of the vacuum (Vac.) dried samples are also very close to the strained samples melting enthalpies (at third cycle) ~2.02-4.8 J/g i.e for the polymer and composites respectively (for comparison see tab 5.1). This reveals that the cyclically strained samples exhibit low crystalline melting enthalpies not because of heat melting of crystallites or mechanical deformation, but mainly because the samples contain less water due to the evaporating of water by heat generated during cyclic deformation. This also clearly indicates that absorbed/trapped water interferes with the $T_{m1}$ enthalpy.

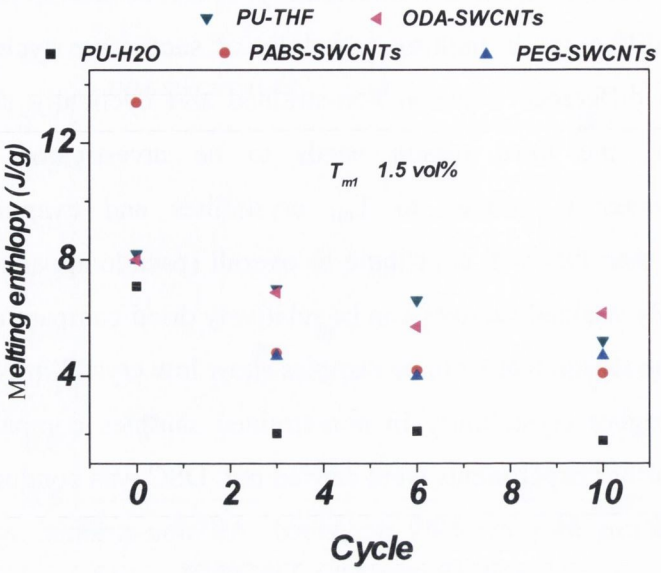


Fig 5.6 Melting enthalpies ($T_{m1}$) of cyclically deformed TPU and composites

TPU/$H_2O$ polymer only $T_{m1}$ melting enthalpy was around 2 J/g from the third to the tenth cycle. $T_{m1}$ for 1.55 vol% (2.5 wt %) PEG-SWCNT and PABS-SWCNT composites for the same cycles were in the range of 4.1- 4.8 J/g. These values are almost identical to the non strained Vac dried samples at the same vol% (CNTs), polymer =2.2, PEG-SWCNT =3.3, PABS =4.8 (see table 5.1). This strongly suggests that the composites were much more crystalline than pure polymer only samples in all cycles and the high crystallinity in composites is not associated with the trapped water. As has been underlined in the earlier paragraph, water can interfere with the $T_{m1}$ melting peaks and hence can give rise to (pseudo/apparent) high crystallinity . These water based hydrophilic CNT composites*[24]* can absorb and hold more water from the solution phase and from the atmosphere (compared to polymer only samples). However, non-strained vacuum dried samples (polymer and composites) have almost the same melting enthalpies as their strained counterparts (see table 5.1).Thus these results not only imply that water dispersed CNTs nucleate and increase crystallinity of SS*[20, 40]* , but during cyclic deformation the crystallites remain unaffected. In TPU/THF strained samples, analogous to water samples, $T_{m1}$ was observed at ~41 °C. Unlike the water samples, there was no large difference between the melting enthalpies of the polymer only sample and the ODA-SWCNT

composites. At the 3rd cycle, the composite with 2.5 wt% ODA-SWCNT $T_{m1}$ melting enthalpy was 6.88 J/g and for the polymer sample it was 6.6 J/g. This shows that the ODA-SWCNTs do not interact with the SS and hence there is no increase in SS crystallinity.

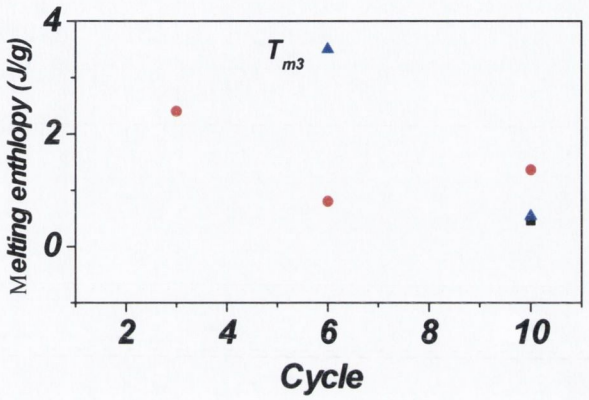


Fig. 5.7 Melting enthalpy ($T_{m3}$) of cyclically strained functionalised SWCT-TPU

Additionally to $T_{m1}$, another melting peak ($T_{m3}$) was observed at higher temperature, ~180 °C in cyclically strained composites samples (Fig 5.8). The reason for the appearance of the new peak is not clear at this point. This could either be due to the strain induced crystallization (SIC) or may be due to the degradation of the polymer.

| Sample | Non-dried<br>ΔH (J/g) | Vac. Dried<br>ΔH (J/g) | Cyc #3 deformed<br>ΔH (J/g) | $T_{m1}$ |
|---|---|---|---|---|
| PU-$H_2O$ (0 wt %) | 7 | 2.2 | 2 | 41 |
| PEG-SWCNTs 1.55 vol% (2.5 wt %) | 8 | 3.3 | 4.7 | 41 |
| PABS-SWCNTs 1.55 vol% (2.5 wt %) | 13.4 | 4.8 | 4.8 | 41 |

Tab. 5.1 Melting enthalpies of water based TPU composites

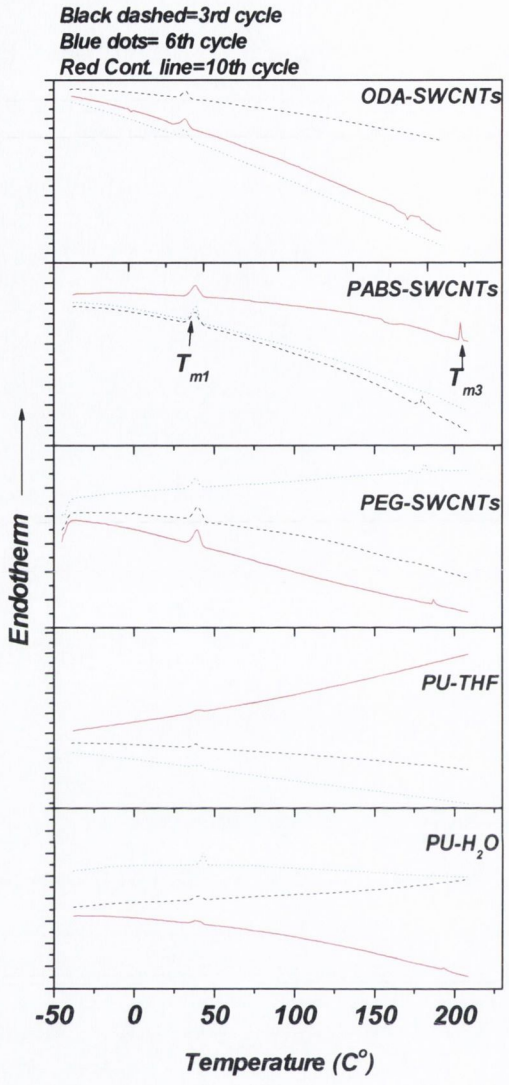


Fig. 5.8 DSC curves for cyclically deformed TPU and 1.55 vol% functionalised SWCNTs composites show the emergence of a new endothermic peak, $T_{m3}$.

## 5.3.3 Dynamic mechanical analysis

Dynamic thermal mechanical tests were carried out using a Perkin Elmer Diamond DMA. All the experiments were run in the temperature range from –60 °C to 170 °C with a frequency of 1Hertz.

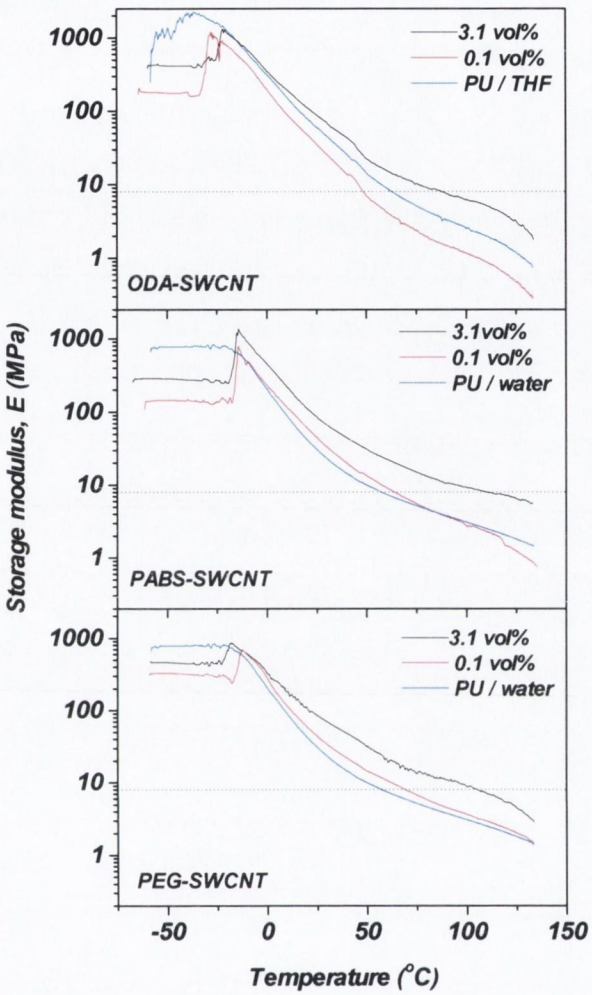


Fig. 5.9 Increase in storage modulus of TPU and composites fabricated with functionalised SWCNTs.

Interestingly, at low temperatures the storage moduli of all the composites were lower than their respective polymer only samples, as shown in figure 5.9. But at a certain temperature (-15 °C to -30 °C), the storage moduli of all composites increased sharply. This sharp increase of storage modulus in composites underlines the strain thickening effect of CNTs *[46]*. This is due to the fact that near $T_g$, polymer molecules get sufficient energy to move relatively freely and behave like a viscous fluid and hence can interact with the filler. For PABS-SWCNT composites, the storage modulus increased from 41 to 111 MPa, while for PEG-SWCNT composites it reached 102 MPa, both at 3.1 vol% (5 wt%) loading level.

This shows good interaction of CNTs with the polymer and stress transfer to the CNTs. For the same 3.1 vol% (5 wt%) ODA-SWCNT composite, the storage modulus was increased from 79 to 112MPa (compared to polymer). The higher storage modulus increase in the water based composites compared to the THF based composites might be because the PEG-SWCNT and PABS-SWCNT not only interact with the soft segment of TPU, but due to the presence of acidic (OH) functional groups, can form hydrogen bonds with the hard segment as well *[20]* which imparts extra reinforcement. This gives rise to the higher storage modulus compared to the THF based composite which shows a strong interaction with only the HS. For all composites, the storage modulus remains high compared to polymer only at all the temperature ranges. This suggests high temperature uses for these materials.

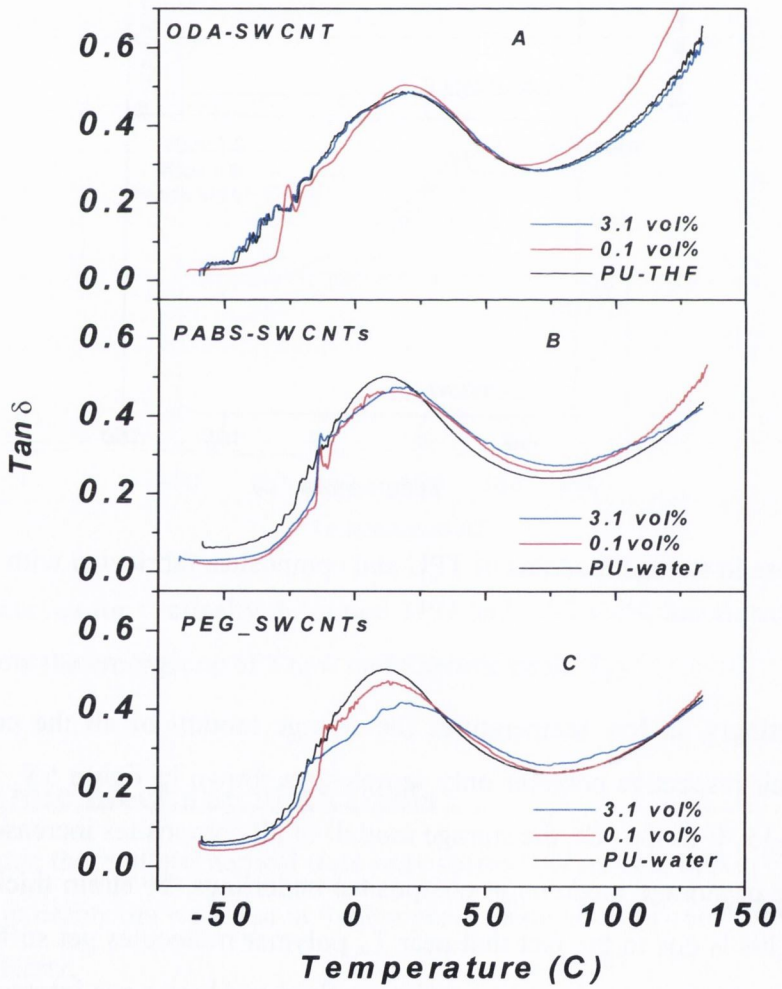


Fig. 5.10 Tan δ shows shifting of $T_g$ to higher temperature with the addition of water dispersible CNTs. This indicates SS interaction with these CNTs.

Shown in figure 5.10 Tan δ, is the ratio of the loss modulus to the storage modulus and when plotted as a function of temperature the highest peak in such a plot is referred to as $T_g$ (Dynamic). In general, the glass transition temperatures measured using DMTA are usually higher than those measured by the static method (DSC). This is because $T_g$ is strain rate dependent *[38]*. For plastics, the difference between the $T_g$ measured by the two thermal techniques is usually in range of 10 - 20 °C *[47]*. In the case of segmented elastomers, the difference in $T_g$ measured by the two techniques can be even larger, in the range 30 - 50 °C *[48, 49]*. The reason for this is that segmented elastomers have a very complicated morphology. Such a polymer consists of soft and hard segments. These two segments are thermodynamically incompatible *[31]* and have two different $T_g$s *[31]*. The matter is further complicated by the presence of soft and hard segment crystalline domains in the polymer which also affect the $T_g$ of the polymer. DSC is less sensitive compared to DMTA in resolving all these transitions. Thus DSC usually probes only the transition of the most abundant constituent of PU. This large difference between dynamic and static $T_g$s has been observed in other PU work as well. Darren *et al.* prepared polyurethanes with varying amounts of SS and HS and his work revealed the difference in $T_g$ measured with DSC and DMTA was ~ 30 °C *[48]*. While in TPU/PVC blends such a difference in $T_g$ for one of the samples was ~ 44 °C *[49]*.

For low volume fractions PEG-SWCNT and PABS-SWCNT composites, a small difference in $T_g$ (~11 – 14 °C) was recorded compared to TPU. In this work, the glass transition temperature for higher volume fraction composites fabricated with PEG-SWCNTs and PABS-SWCNTs was higher than their respective polymer only samples (Fig. 5.10). For PEG-SWCNTs 1.55 vol% (2.5 wt%) composites, the $T_g$ was increased by 6 °C, while for PABS-SWCNTs composites the $T_g$ was increased by 8 °C. However, for the ODA-SWCNTs the $T_g$ was unaffected by the introduction of CNTs. The bulk of TPU consists of soft segments *[40]*, hence any filler which interacts strongly with the polymer (soft segment) will increase the $T_g$ of the system *[38, 47, 50]* . Water dispersed CNTs may physically bond to the SS, hence restricting their mobility and causing an increase in $T_g$. Therefore, like the storage modulus, the $T_g$ also strongly indicates that the water dispersed CNTs show strong interactions with the soft segment at higher volume fractions.

### 5.3.4 Cyclic mechanical testing

All composites and polymer only samples were subjected to cyclic mechanical deformation tests to assess the effect of the CNTs on stress-strain recovery behavior. All samples were stretched to a preset strain (300 %) at a rate of 50mm/min. Samples were stabilised at this preset strain for 1 min followed by a relaxation at the same strain rate. This same step was repeated for a further 9 cycles. All the experiments were done at room temperature. Figure 5.11 shows a typical cyclic test.

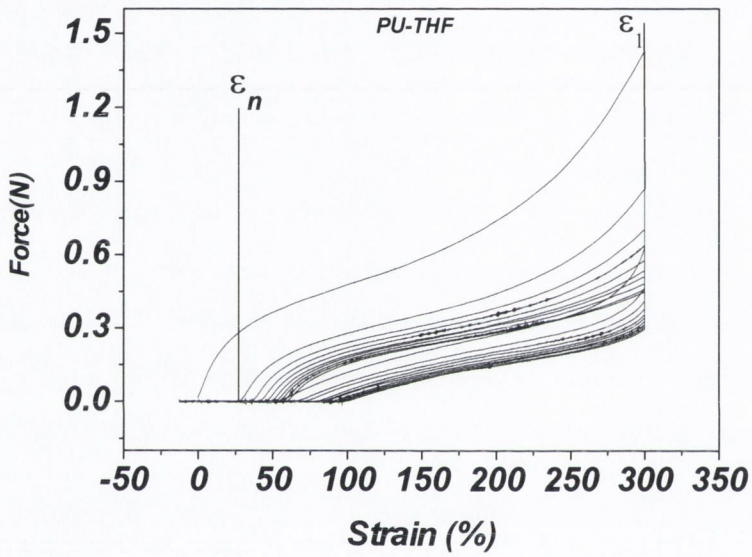


Fig. 5.11 Representative graph for the cyclic deformation of a TPU-THF sample.

Many of the materials when stretched to less than the breaking strain and beyond yield stress remain permanently deformed. However elastomers such as TPU, upon relaxation can more or less go back to the pre-strained position which is called strain recovery. In all samples, the first cycle was different to the rest of the cycles because of the deformation of the material beyond the elastic region. Strain recovery was measured in terms of recovered length per elongated length *[49]* using equation 5.1.

$$\text{Strain recovery} = \varepsilon_1 - \varepsilon_n / \varepsilon_1 \quad \text{Eq 5.1}$$

Where $\varepsilon_1$ is preset strain, and $\varepsilon_n$ strain at the nth of cycle shown in (Fig 5.11)

After the first cycle, the other cycles were almost identical to each other. In polymer only and low volume fraction samples, good strain recovery was observed (Fig. 5.12), but higher volume fraction composites did not recover fully. At 6.2 vol% (10 wt%) PEG-SWCNTs, the composites recover 56.7 % of the preset strain at the ninth cycle and PABS-SWCNT composites recover to 70 % at the same vol% and cycle. This suggests that the PABS-SWCNTs has a stronger interaction with the SS compared to the PEG-SWCNTs which prevent the return of the SS. ODA-SWCNT composites showed very good strain recovery as well. At 7 wt % these composites recovered to 71% of the preset strain after the 9th cycle.

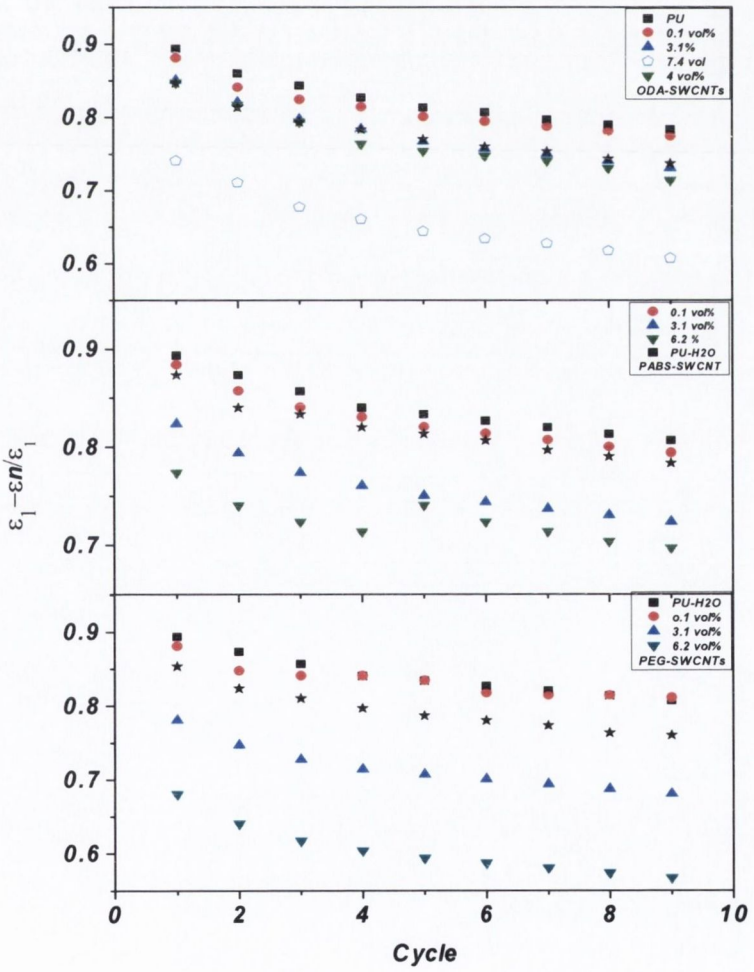


Fig. 5.12 Effect of CNTs type and loading on strain recovery behavior of TPU.

When TPU is stretched to less than the breaking strain, upon relaxation it can go back (to some extent) to the prestrain position. If the once stretched sample is stretched again it exhibits another yield point at lower stress value compared to the first cycle. This recovery is known as stress recovery (Eq 5.2). Stress recovery in successive cycles at particular strain value can be found out using equation 5.2.

$$\text{Stress recovery} = \sigma_1 / \sigma_n \quad \text{Eq 5.2}$$

Where $\sigma_1$ is the stress at 1$^{st}$ cycle and $\sigma_n$ is the stress at n$^{th}$ number cycle at 10 % strain. Stress values were taken at 10 % strain for the cycles. Stress recovery in TPU polymer only and low volume fraction composite samples were almost identical (Fig 5.13) and this has also been observed in another related work *[28]*. In all cases at the 10$^{th}$ cycle for high volume fractions, the composite samples lost more than 70 % of their initial stress at 10% strain. In general there was not much difference in stress recovery among all three types of composites. However, PABS-SWCNT composites showed slightly higher stress recovery, when compared to PEG-SWCNT and ODA-SWCNT at low $V_f$. At 3.1 vol% PABS-SWCNTs and PEG-SWCNTs the stress loss was 65% and 80% respectively. While for 3.1 vol%, ODA-SWCNT composite loss was 72%.

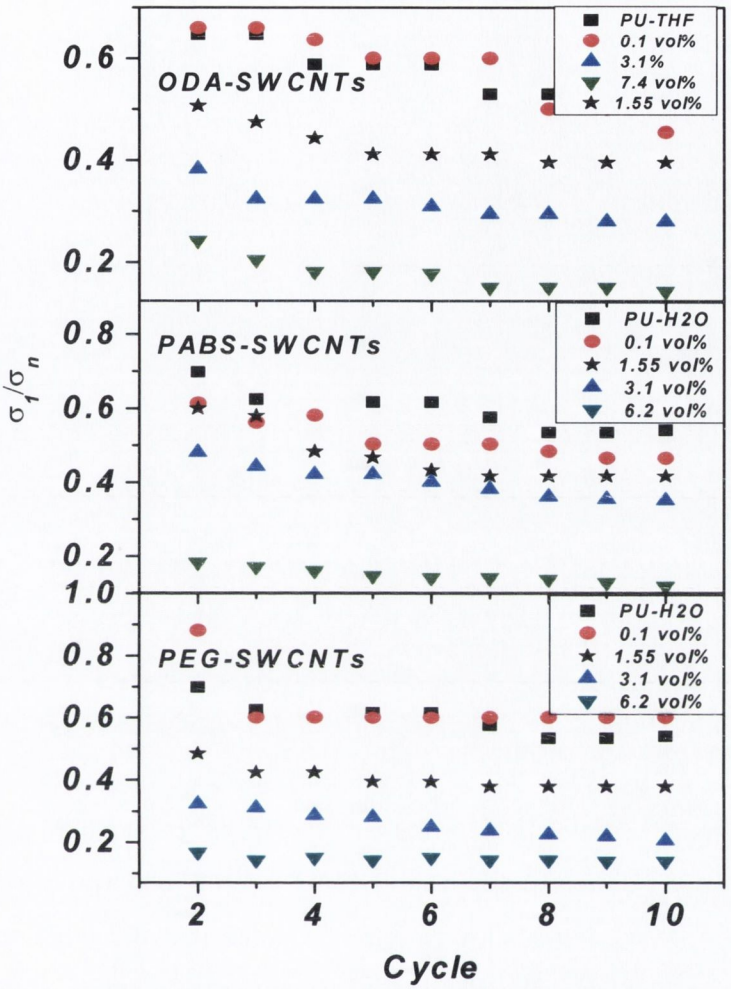


Fig. 5.13 Effect of CNT type and loading on the stress recovery behavior of TPU

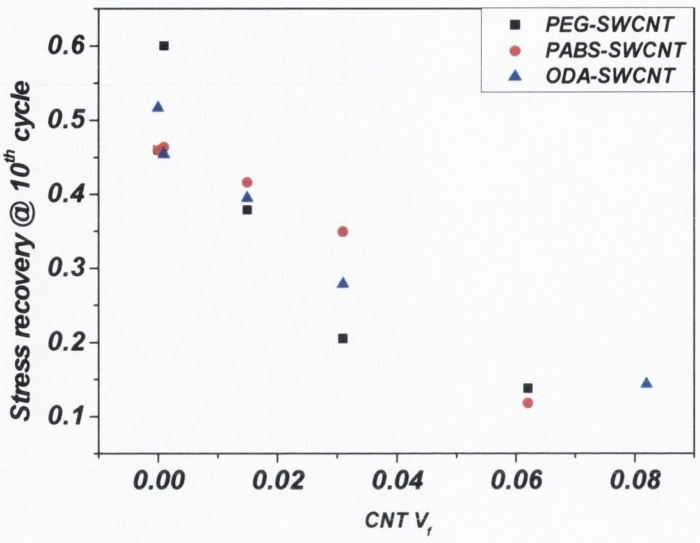


Fig 5.14 Stress recovery as function of $V_f$ at $10^{th}$ cycle.

Shown in figure 5.15 is the decrease in toughness (toughness has been defined in chapter 3.5.4) due to cyclic deformation. On the basis of the stress–strain results at each cycle, one would expect better toughness for ODA-SWCNT composites compared to the water based composites. Interestingly, the ODA-SWCNT composites have a lower toughness than water based composites. It must be noted that the toughness of TPU is mainly influenced by the slope of the plateau and strain hardening parts of the stress-strain curve. The slope of these two regions is mainly controlled by the SS mobility and the HS rotation ( see figure 5.16). Thus, good toughness in water based composites is due to their relatively higher sloped curves, which is because of the SS interaction with the water dispersed CNTs. A lower slope at these regions of the stress-strain curve accounts for lower toughness. Therefore, the lower toughness of the ODA-SWCNT composites indicates that these CNTs may facilitate SS mobility and HS rotation i.e. they do not restrict the SS mobility. The slope of the stress-strain curve at plateau region is shown in figure 5.17.

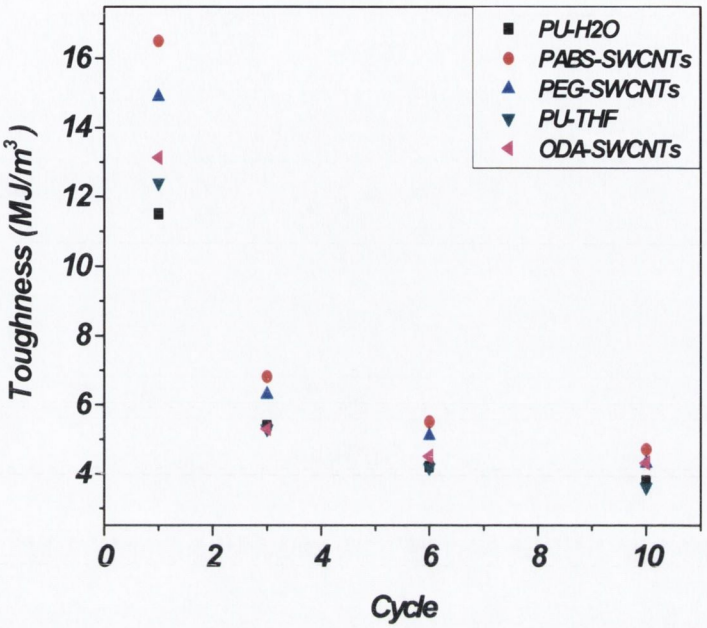


Fig. 5.15 Loss in toughness at successive mechanical deformations of TPU and its composites with 1.55 vol% (2.5 wt%) functionalised nanotubes.

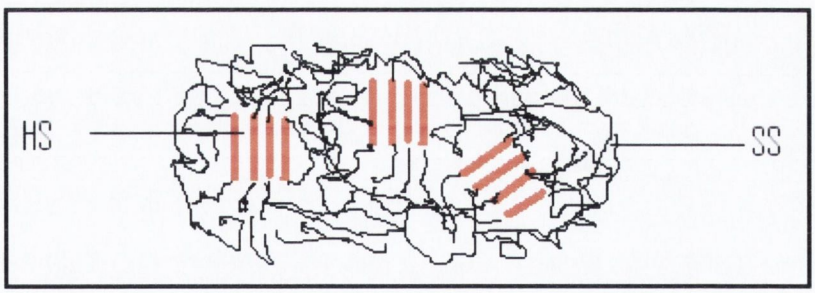


Fig 5.16. Shows TPU hard and soft segment domain.

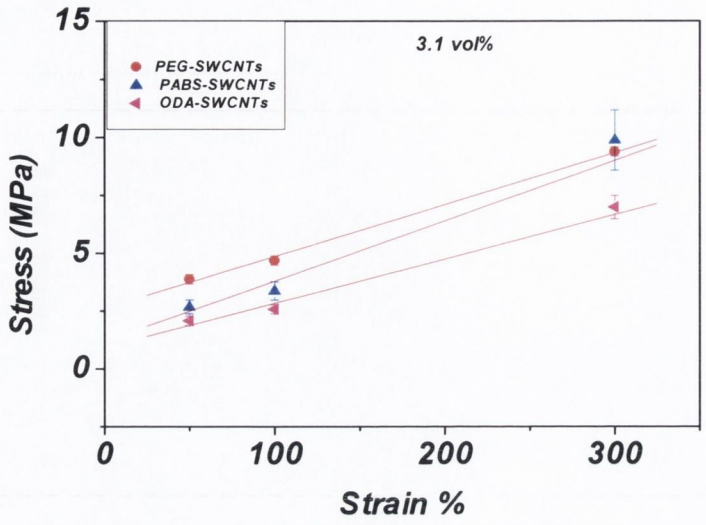


Fig. 5.17 Comparison of the plateau region in the stress-strain curve of TPU composites.

## 5.3.5 Mechanical

Shown in figure 5.18 are the representative stress-strain curves for the segmented TPU and composites, which can be divided into three parts *[29, 40]* .

1) Initial elastic deformation region up to the yield stress (see figure 5.19). Young's modulus in this part is associated with the constrained stretching, while the point where the linear stress-strain behavior stops is referred to as the yield point (or yield stress).

2) This is followed by the plateau region which starts from yield point and is associated with the stretching of the SS and the rotation and alignment of the HS segment.

3) The plateau region is followed by a steep part which arises due to strain hardening (SH) and strain induced crystallisation (SIC) of the SS.

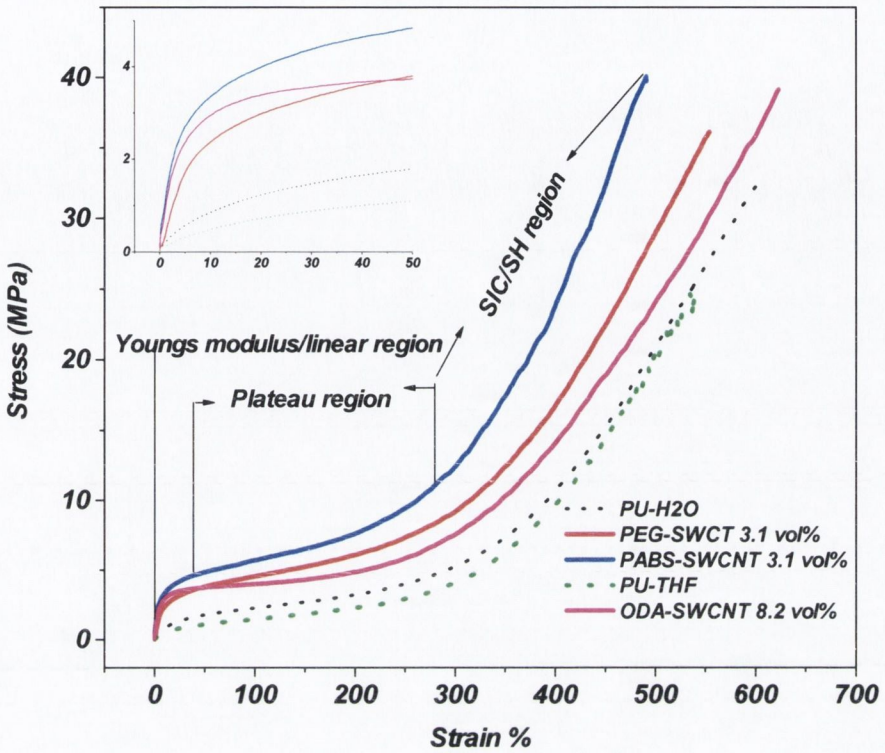


Fig. 5.18 Representative stress-strain curves of TPU and its composites made with functionalised SWCNTs.

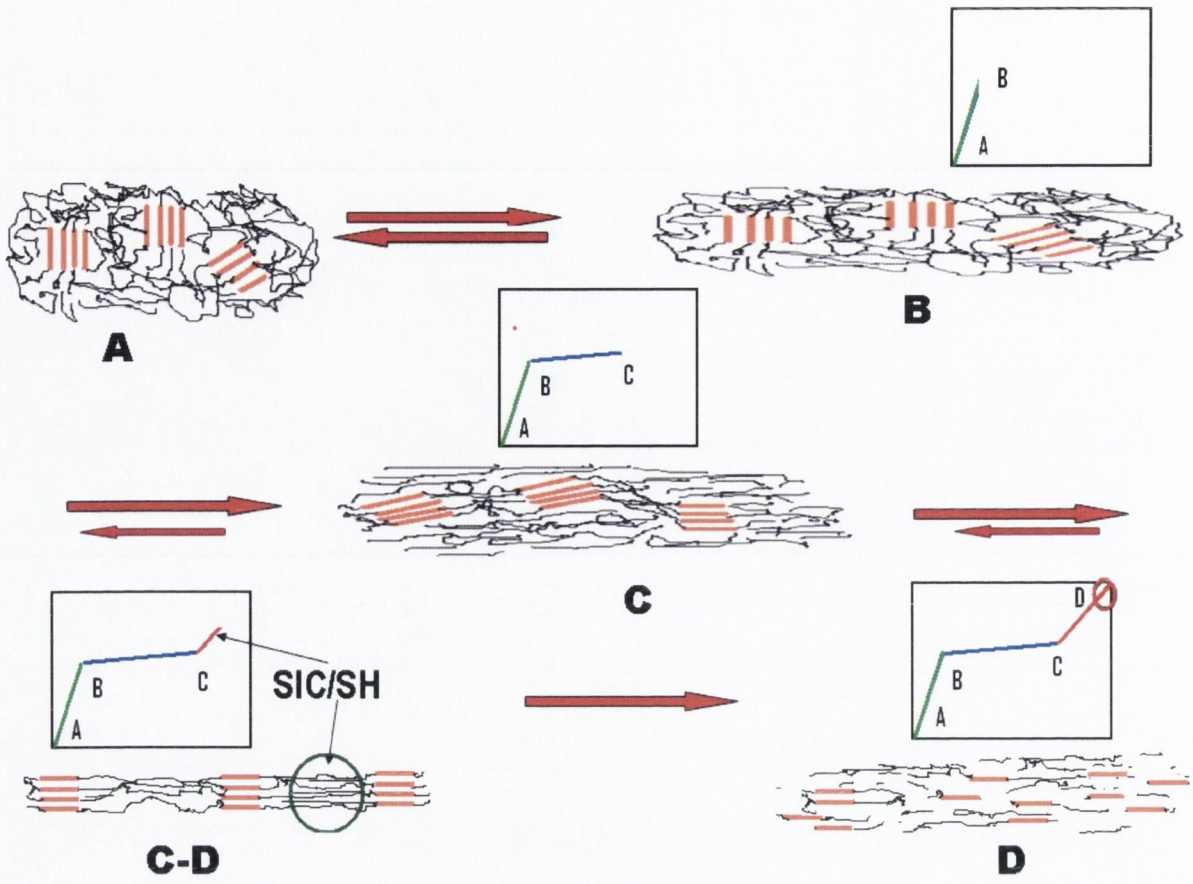


Fig. 5.19. Mechanical deformation mechanism in TPU (hard and soft segment). A-B shows the elastic deformation, B-C represents the elongation of SS, HS rotation and alignment in the direction of applied force. C-D infers further stretching of SS and alignment of SS and HS (SH/SIC). D Shows the UTS of TPU.

**Young's modulus**

For all three CNT types the Young's moduli of the composites were significantly increased compared to the value 12.58 MPa for polymer. PEG-SWCNT composites showed the largest increase in Young's modulus of all the composites. For PEG-CNTs 12.4 vol% (20 wt%) the Young's modulus was increased to almost 23 times the polymer only sample to 286 (MPa). At the same volume fraction PABS-CNTs composites exhibited an increase of 13 times. For ODA-SWCNTs, the samples' Young modulus (73.5 MPa) for the 8.2 vol% (13 wt%) composite had increased by 11.6 times compared to the polymer (6.32MPa). The Young's modulus then saturated at this value. The Young's modulus for the TPU polymer

is lower because these samples were prepared using THF as solvent instead of water. The relatively small values of Young's modulus for TPU/THF samples compared to the TPU/$H_2O$ samples suggest some morphological changes may have occurred or the THF may be trapped in the samples which then may act as plasticiser.

Usually elastomer reinforcement in term of Young's modulus is described by Guth's rule *[51]* as given in equation 5.3. Assuming the SWCNT aspect ratio as 300*[22, 27]* the Guth's rule does not agree with the experimental Young's modulus data. The same trend have been observed elsewhere *[14]*. Blighe et al also suggest that their data does not follow Guth's rule for a known CNTs aspect ratio*[32]*. However interestingly by assuming aspect ratios of ODA-SWCNT = 26, PABS-SWCNT = 28 and 40 all the samples measured here initially follow Guth's rule for the increase in Young's modulus (see figure 5.20) but deviate from Guth's rule for the volume fraction above 10 vol %. Likewise, in the work on TPU nanocomposites by Liff *et al.* the mechanical data follows Guth's rule at low $V_f$ *[29]*. This maybe due the aggregation of CNTs at high volume fractions. Another reason may lie in the segmented nature of TPU and the presence of functional groups on the CNTs. All the data presented here reveals that attached functional groups predominantly interact either with the HS or SS. Thus a particular type of functionalised CNT would predominantly reinforce either HS or SS not both the domains simultaneously and equally hence the data does not follow Guths rule.

$$Y_C = Y_{Elas}\left(1 + 0.067AV_f + 1.62A^2V_f{}^2\right) \quad [51] \text{ Eq. 5.3}$$

Where $Y_C$ and $Y_{Elas}$ are the composite and elastomer moduli, $A$ is the filler aspect ratio and $V_f$ is the volume fraction.

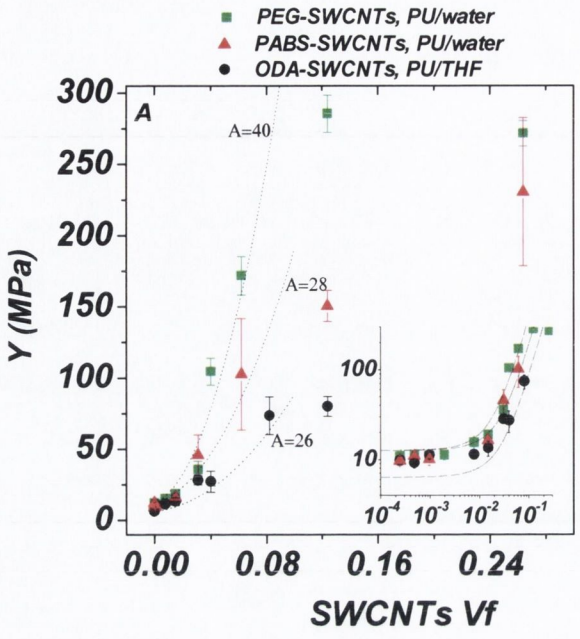


Fig. 5.20 Impact of functionalised SWCNTs on A) Young's modulus of TPU

The reinforcements measured here are significantly higher than in other similar work done with functionalised CNTs-PU. Buffa *et al.* fabricated functionalised-SWCNT–polyurethane composites. In their work they achieved an increase of ~ 3 times in Young's modulus at 20 wt% loading *[52]*. In another attempt, Gopal *et al. [20]* demonstrated an increase in Young's modulus of 7.4 times at this same CNT loading. They used functionalised MWCNTs in their polyurethane work, but the ductility was greatly reduced by a factor of 7. In a recent work *Liff et al.* achieved high reinforcement in their TPU-nanoclay work by restricting the nanoclay to the HS. This work suggests that by restricting nano filler to the HS, significant reinforcement can be achieved without sacrificing ductility at high filler loading *[29]*. Another contributory factor in the achievement of good reinforcement can be the enhancement in the crystallinity *[53, 54]*, as revealed by DSC and discussed earlier.

**Plateau region**

The initial part of this region corresponds to the yield stress. The yield stress (Fig. 5.21) for the water based composites is much higher than for the ODA-CNT composites.

For comparison reasons the stress at yield point is taken as the stress at 50% strain. The yield stress keeps increasing with the introduction of CNTs and it increases sharply in water-based composites for $V_f > 1.5$ %. For TPU/THF composites no such sharp increase was observed. For the PEG-SWCNTs composites 12.4 vol%, (20 wt %) the yield stress increased by 8.6 times compared to TPU (1.9 MPa), while at the same volume fraction for PABS- and ODA-SWCNT composites, the yield stress was increased by 5 and 3 times respectively. The high increase in yield stress in water-based composites may be due to the fact that the water dispersible CNTs are not only associated to the SS but these CNTs also have hydroxyl groups which can form hydrogen bonds with the HS *[20, 52]*. Therefore they can physically bond to the SS and HS and hence impart relatively more reinforcement to the sample. Another reason is that water-based TPU is not a solution but is a dispersion of micron sized TPU in water. During film formation in the free volume of the film, the water dispersed CNTs may form a network which could increase with increasing volume fraction and hence give a continuous increase in the Young's modulus and yield stress*[13]* .

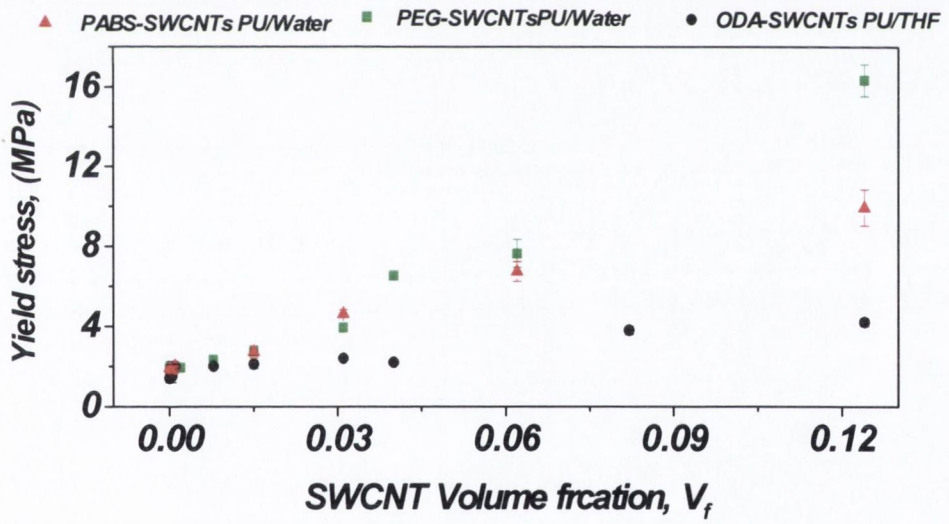


Fig. 5.21 Increase in yield stress of TPU with incorporation of CNTs

Stress throughout the second region (plateau region) of the stress-strain curve is much higher for the water-based composites (Fig 5.22). The stress keeps increasing with the addition of more water-dispersed CNTs. Interestingly, the ODA-SWCNT composites

remain flat for $V_f > 0.1$ % composites compared to the ODA-SWCNTs composites. As has been discussed already, this region is associated with the stretching of the SS accompanied by the rotation and alignment of the HS and CNTs. Water dispersible CNTs are mainly interacting with the SS. Therefore each addition of CNTs increases the bridging or physical crosslinking among the SS chains and thus not only decreases the SS mobility but also stiffens the soft segments and hence increases the slope of this region. The ODA-SWCNTs mainly restrict the HS and forms no bonding/bridging among the SS chains and therefore these regions are flat and there is less of an increase with the introduction of CNTs.

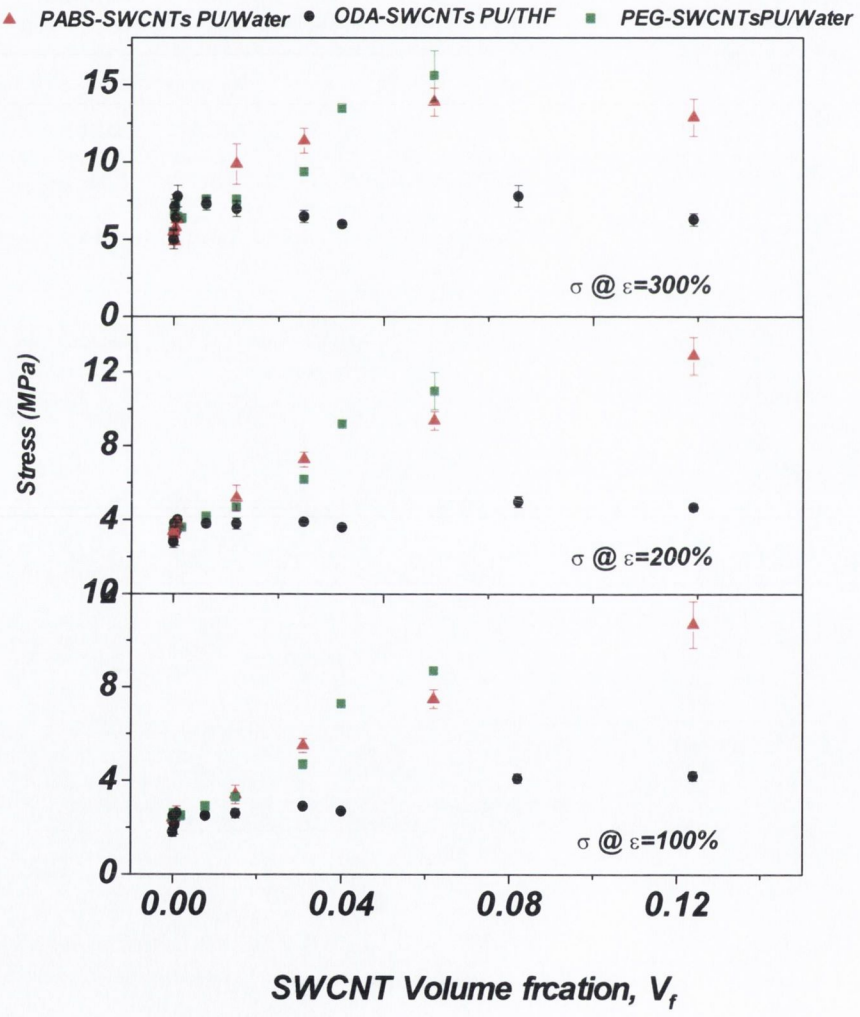


Fig. 5.22 Impact of functionalised SWCNTs on plateau region.

**Strain induced crystallisation/strain hardening**

Generally speaking, in TPU stress-strain curves the steepest region, which is followed by yield stress and soft segment straining region, is usually termed as the strain induced crystallisation or strain hardening region *[29, 40]*. The reason is, crystallites formed due to the strain act like a filler and hence increase the slope. Therefore the increased slope means more strain induced crystallites. The water based composite demonstrates enhanced SIC/SH compare to the ODA-SWCNTs composites. The highest SIC/SH slopes were observed in the case of PABS-SWCNTs composites (Fig. 5.23). Thus the mechanical results also point to the fact that PABS-SWCNTs and PEG-SWCNT enhance the strain induced crystallisation compared to ODA-SWCNTs. No significant change in SIC/SH slope were observed in TPU with the incorporation of ODA-SWCNTs. These results again infer the strong interaction of water dispersed CNTs with the SS. Higher slopes due to smaller diameter silicate particles in TPU-silicate nanocomposites can also be seen in Finnigan *et a.l [55]*.

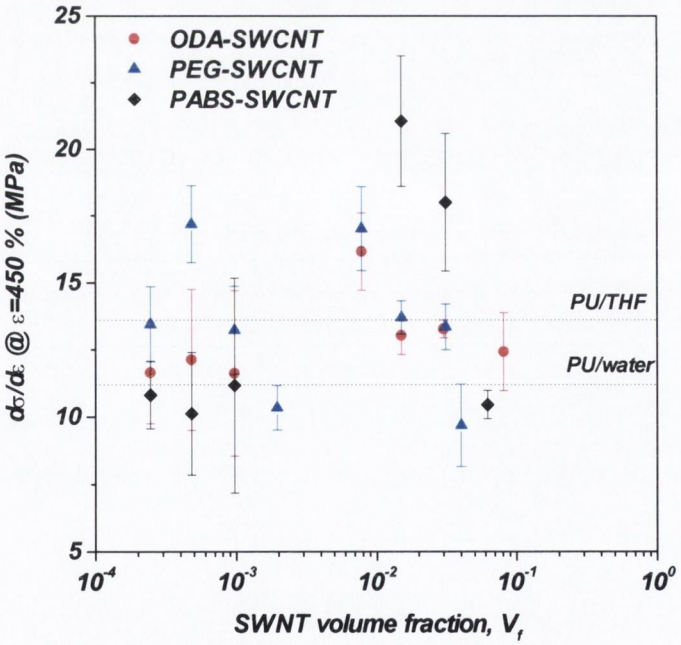


Fig. 5.23 Slopes of SIC/SH in all three types of composites shows effect of CNTs type on SIC/SH.

**Ultimate Tensile Strength**

In ODA-SWCNT composites, the strength at ultimate failure increases significantly, by 0.1 vol % (0.12 wt%), but then falls off slightly for $V_f > 1$ vol% and saturates at around 55 MPa. While in the case of PEG-SWCNTs and PABS-SWCNTs the strength is slightly enhanced, but rapidly decreases for $V_f > 1.5$. However, interestingly for ODA-SWCNTs composites strength does not collapse even at 20 wt% (12.4 vol%) compared to the polymer only sample. In all cases the composites with around 0.4 vol% CNTs showed the maximum UTS (Fig. 5.24).

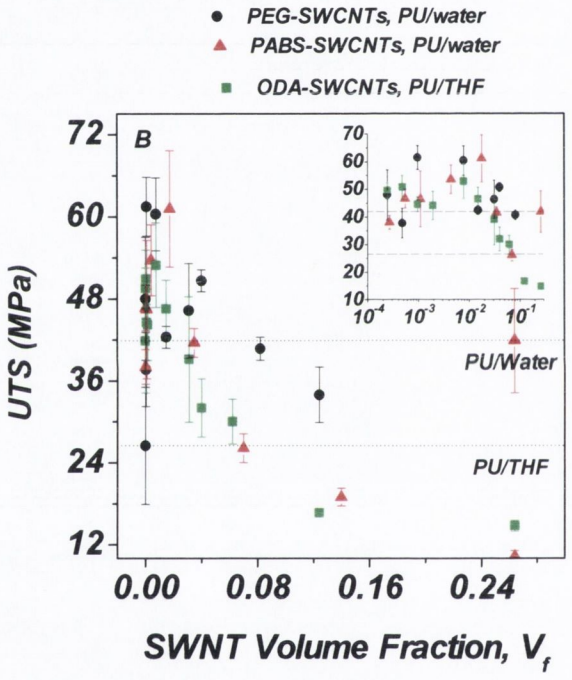


Fig. 5.24 Effect of functionalised CNTs on plateau region of the stress-strain curve of TPU. A continuous increase in stress implies the interaction of the water dispersed CNTs with the soft segment.

In these TPUs, the UTS occurs in the strain hardening region of the stress-strain curve. This part is dominated by the breakdown of the HS and SIC, SS stretching and breaking. The hard segment is brittle and breaks at low deformations because of local stresses *[40]*, therefore a filler which can impart reinforcement to the HS, will increase the

ultimate tensile strength. Thus the UTS data strongly infers that up to 0.4 vol% all the CNTs remain embedded in and reinforce the HS, but above 0.4 vol% the CNTs start to influence the SS. This is also supported by the sharp increase in Young's modulus and yield stress above 0.4 vol%. The UTS data further supports the argument that the ODA-SWCNTs mainly interact with the HS because they do not show a sharp decrease in UTS but rather saturation at high volume fractions.

**Strain at break**

In general, the low volume fraction composites and polymer only samples exhibited high strain at break values in excess of 400%, which is typical for a segmented PU *[18, 29, 40, 56]*. Compared to the polymer only, ODA-SWCNT composites exhibit significantly higher strain at break values ($\varepsilon_b$), saturating around 650%. Usually $\varepsilon_b$ decreases sharply at high CNT filler loadings *[18, 20]*, but surprisingly $\varepsilon_b$ remained high here, > 600%, even at very high volume fractions 12. 4 vol% (20 wt%) for the ODA-SWCNTs. The strain at break in segmented TPU remains high if the nano filler remains in or interacts only with the HS *[29]*. This suggests the restriction of these CNTs to the HS and more importantly the plasticising effect of these CNTs which facilitate the mobility of the SS and hence high ductility. In water based composites, with each increment in volume fraction of CNTs above 1 vol% a sharp reduction in strain at break was recorded. Large strains before breaking in polyurethane are due to SS stretching. Therefore any feature in the polymer which binds to the SS not only reinforces the sample by restricting the SS mobility, but has negative impact on the strain at break value. Thus a sharp decline in $\varepsilon_b$ is associated with CNT interactions with the SS. If the arguments of the HS and SS interaction are valid, then the higher volume fraction water based composite should have a higher $T_g$ while the ODA-SWCNT higher volume fraction composite samples should have the same (dynamic) $T_g$ compared to their polymer only samples, which is exactly the case (see figure 5.11). This assumption is further supported by the SIC/SH data plot (Fig 5.23). Slopes in the strain hardening region of the water based composites are much higher than for the ODA-SWCNTs due to the stiffness imparted by the filler bonding to the SS. Among water samples at higher volume fractions, PABS-SWCNT composites showed a sharper decline in $\varepsilon_b$ value compared to PEG-SWCNTs. Again the same reason can be assigned, as the

PABS-SWCNTs tend to interact with the SS more strongly than the PEG-SWCNTs. Also, the PABS-SWCNTs show higher SIC or strain hardening than the PEG-SWCNTs as revealed by the slope in the SIC or strain hardening region of the stress strain plot (Fig. 5.25). This makes the PABS-SWCNTs stiffer and less ductile (in SIC or SH region) than the PEG-SWCNTs composites.

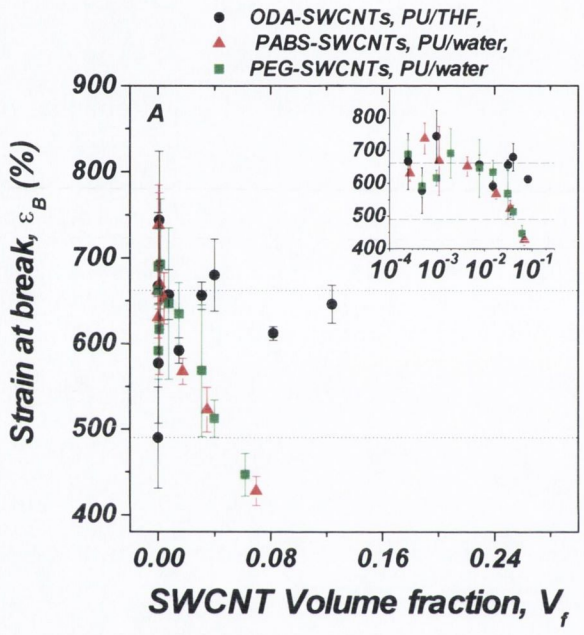


Fig. 5.25 Effect of functionalised SWCNTs loading on strain at break.

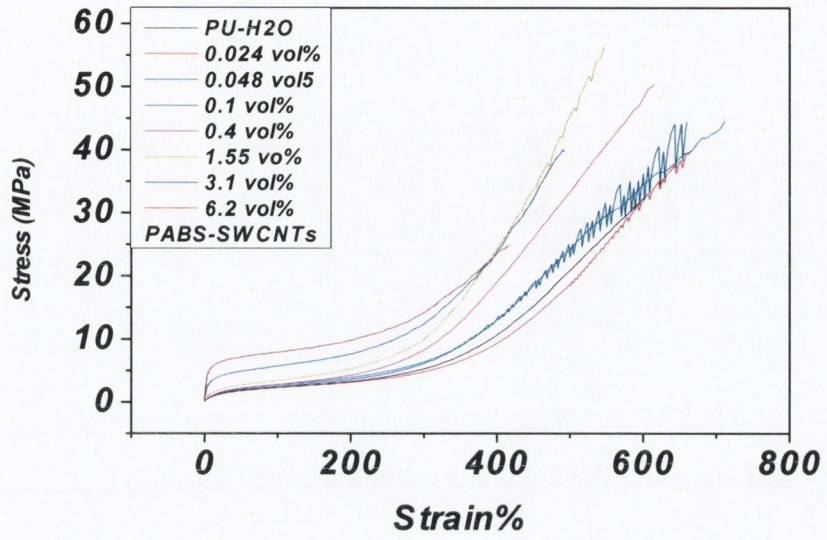


Fig. 5.26 Representative stress-strain curves of PABS-SWCNTs composites.

.

**Toughness**

The stiffness, yield strength, plateau region slope, and the stiffness of the strain crystallisation region can slightly influence the toughness within a particular TPU composites system, but the main contributors are the strain at break and UTS values. As the strain at break and UTS values are in the order, ODA-SWCNT>PEG-SWCNT/PABS-SWCNT composites so will be the toughness.

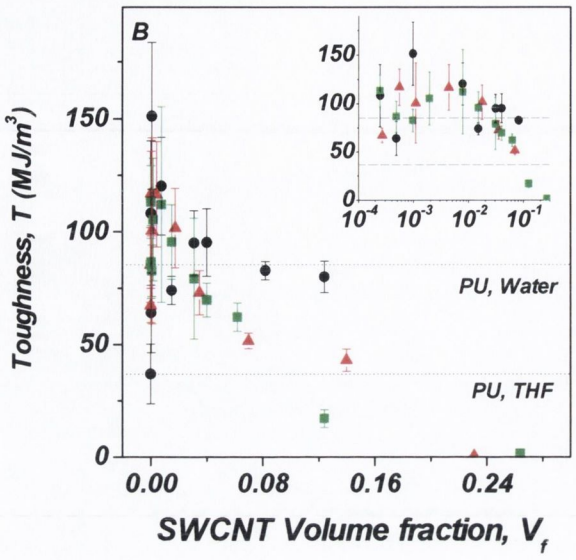


Fig. 5.27 Toughnesses of composites prepared with functionalised SWCNTs.

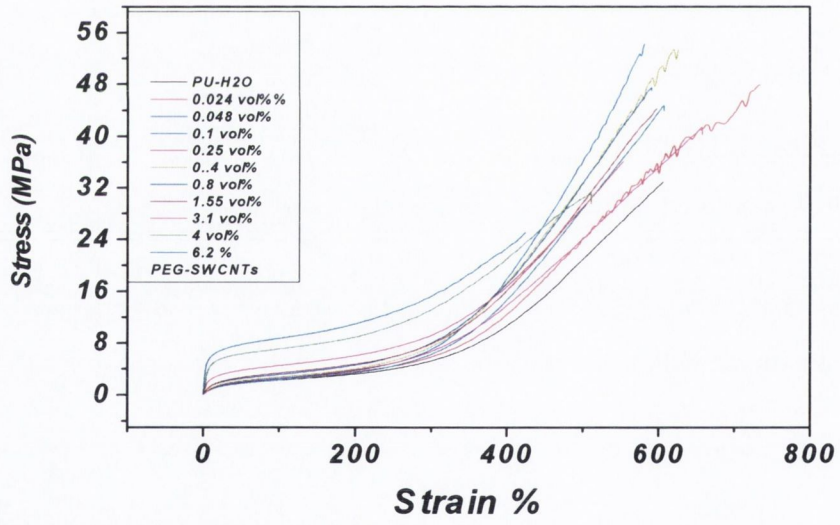


Fig. 5.28 Representative stress-strain curves of PEG-SWCNTs composites.

At low volume fractions, the ODA-SWCNT composites exhibited significantly higher toughness compared to the polymer only samples. For these composites the toughness initially increased sharply by a factor of 4.2, from 36 MJ/m$^3$ (0 wt%) to 151 MJ/m$^3$ (0.12 wt% or 0.1 vol%). The increase in the ODA-SWCNT samples' toughness

saturated around 80 $MJ/m^3$, while in the water based composites at low volume fractions, a relatively lower increase in toughness was observed. However, no saturation was observed, unlike for the ODA-SWCNT samples, and the toughness sharply decreased at high volume fractions. For the PEG-SWCNT composites, the toughness increased from 85.4 $MJ/m^3$ (0 vol/wt%) to a maximum of 113 $MJ/m^3$ and then decreased to 1.5 $MJ/m^3$ (20.5 vol% or 33 wt%) and for the PABS-SWCNTs the maximum was 117 $MJ/m^3$ and it then decreased to 0.5 $MJ/m^3$ (20.5 vol% or 33 wt%). The same reasons account for the increases or decreases in toughness as were already discussed for the strain at break.

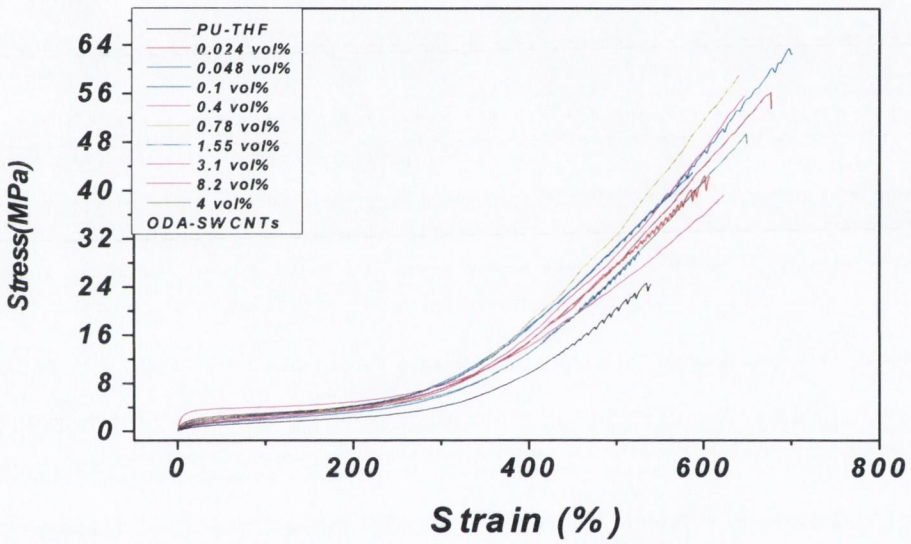


Fig. 5.29 Representative stress-strain curves of ODA-SWCNT composites.

## 5.4 Conclusion

Generally, the introduction of high volume fractions of CNTs to TPU is accompanied by a loss in mechanical properties due to the CNTs interactions with the TPU soft segments *[18, 20]*. In this work we were able to prepare very high volume fraction composites that exhibit excellent mechanical reinforcement. Importantly, even at very high volume fractions the stiffness, strength, and ductility were not decreased (for the ODA-SWCNT composites). This is because those functionalised CNTs, ODA-SWCNTs, mainly interact with the HS of the TPU. This shows that TPU can be significantly reinforced with

the appropriate CNTs at high loading of functionalised CNTs. The Young's modulus was increased by 22 times (for PEG-SWCNTs), the UTS doubled (for ODA-SWCNTs) and the toughness was improved by 4 times (for ODA-SWCNTs). It was also demonstrated that all three parts of the TPU stress-strain curve can me modified by the appropriate choice of CNTs.

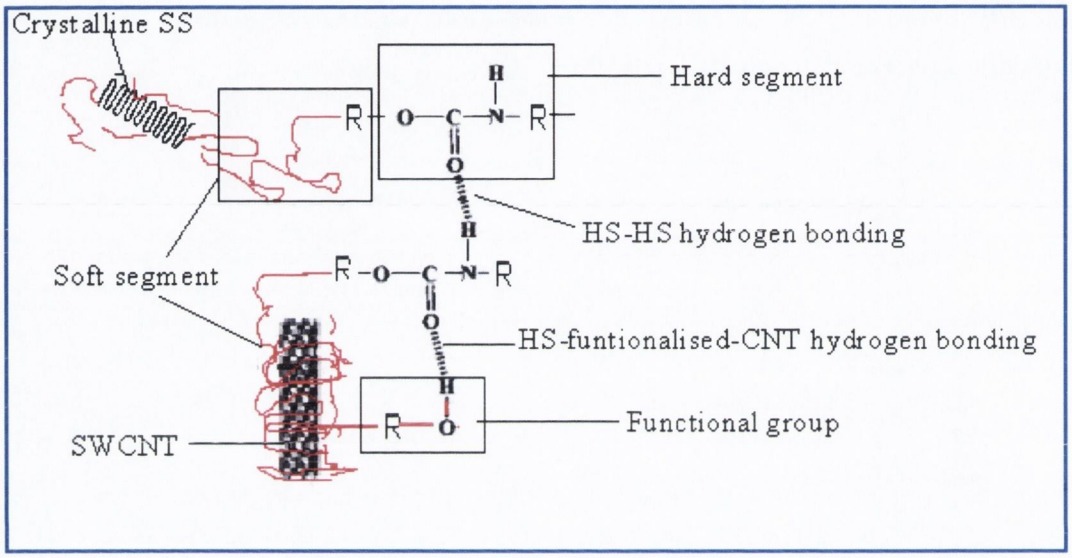


Fig 5.30 Schematic diagram illustrating hydrogen bonding among HS –HS and HS- water dispersed SWCNTs. The figure also shows water dispersed CNTs interaction with SS. This might be the reason for the water based composites high stiffness and yield stress compared to the ODA-SWCNT composites.

The increase in crystallinity of the SS on the introduction of water dispersed CNTs to TPU implies their affinity towards the SS. However, for ODA-SWCNT samples, no change in SS crystallinity is observed, while the nucleation of the HS polydispersed crystallites in the ODA-SWCNT composites indicates that these CNTs have a higher affinity towards the HS compared to the SS. DSC also shows the strain induced crystallisation in the water based samples. DSC on cyclic deformed samples reveals water association with the SS crystallites. The DSC study also indicates that the SS crystallites do not get destroyed during cyclic straining.

Cyclic mechanical deformation of the ODA-SWCNTs samples reveal good strain and stress recovery compared to the water based composites. By stretching TPU samples beyond their yield stress, CNTs and HS are rotated and try to align in the direction of the applied strain. Subsequently, on relaxation, the stress-strain recovery can be restricted by these aligned CNTs and HS and if the CNTs have any kind of bonding with the SS, this will also restrict recovery of the polymer. Thus, less stress and strain recovery in the water based composites indicates the interaction of these CNTs with the SS and vice versa for the ODA-CNTs.

Enhancement in the storage modulus of composites indicates good stress transfer. A higher increase in the storage modulus of water based composites compared to the THF based composites may be due to hydrogen bonding between HS and CNTs. The higher dynamic $T_g$ of the composites compared to the polymer, in the water based samples, suggests the restriction of molecular mobility due to the CNTs bonding to the SS (Fig. 5.30) Also, the higher $T_g$ in the water based composites infer that the majority of these CNTs must be embedded within the polymer (during the polymer particles fusion in the drying process). While no change in $T_g$ of the ODA-CNT composites underlines that there is no interaction between the SS and the ODA-SWCNTs.

The mechanical properties data is consistent with water dispersed CNTs interacting with the SS and the ODA-CNTs interacting with the HS. The water-based and THF-based composites show almost equivalent mechanical reinforcement up to 0.4 vol %, which suggests the presence of CNTs in the HS. The stress in the second (plateau) region of the stress-strain curve is much higher for the water samples, and keeps increasing with volume fraction of CNTs. For the ODA-SWCNTs, this region is lower and flat which reveals that these ODA-SWCNTs do not affect the soft-domain (as this region of the stress-strain curve is associated with SS stretching). The sharp decrease in the ductility and UTS and the sharp and continuous increase in the Young's modulus and yield stress (above 1 vol% CNTs) in the water-based samples indicates that the PEG-SWCNTs and PABS-SWCNTs have very strong interactions with the SS for $V_f > 1\%$, but at low volume fractions they can have interactions with the HS. The interaction with the hard segment may be due to the presence of hydroxyl groups in the water dispersible CNTs. Water based TPU is not a solution but is

a dispersion of micron sized TPU particles in water. Therefore, the sharp increase in Young's modulus, yield stress and the sharp decline in UTS and strain at break could be due to the network formation of water dispersed CNTs within the free volume of polymer *[13]*.

The saturation in the composite mechanical properties implies that the ODA-SWCNTs do not interact with the soft segment. The mechanical reinforcement in ODA-SWCNT composites is due to the HS interaction with the CNTs. Also, the ODA-SWCNTs are dispersed in TPU/THF and thus embedded within the polymer. Therefore no CNT network formation can occur and hence no sharp decline in the mechanical properties.

The reason that water dispersed CNTs show great affinity towards the soft segment is because PEG itself can be a soft segment in water born polyurethane, and in polyurethane in general *[57, 58]*, and hence, it is compatible with the PU soft segment. The alkyl groups in PABS can also have strong interactions with SS. The interaction of the ODA-SWCNTs with the HS is not clear.

It has been discussed earlier that TPU has hard and soft segment domains with different polarities. Both these segments have different affinities for various chemical groups. Therefore by changing the functionality of CNTs, mechanical properties can be altered as well. Therefore theses results suggest that a tuneable composite can achieved by the use of appropriate functionalised CNT.

## 5.5 References


[1] J. W. Che, T. Cagin, W. A. Goddard, *Nanotechnology* **2000**, *11*, 65.
[2] B. Savas, K. Young-Kyun, T. David, *Physical Review Letters* **2000**, *84*, 4613.
[3] B. Q. Wei, R. Vajtai, P. M. Ajayan, *Applied Physics Letters* **2001**, *79*, 1172.
[4] B. M. Kim, A. M. S. Fuhrer, *Journal of Physics: Condensed Matter* **2004**, *16*, R553.
[5] M. J. Biercuk, M. C. Llaguno, M. Radosavljevic, J. K. Hyun, A. T. Johnson, *Applied Physics Letters*, *80*, 2767.
[6] S. Xie, W. Li, Z. Pan, B. Chang, L. Sun, *Journal of Physics and Chemistry of Solids* **2000**, *61*, 1153.
[7] J. N. Coleman, U. Khan, Y. K. Gun'ko, *Advanced Materials* **2006**, *18*, 689.
[8] S. Iijima, *Nature* **1991**, *354*, 56.
[9] J. N. Coleman, M.Cadek, R. B. ., V. N. ., K. P. R. ., C. B. ., A. F. ., J. B. N. ., Y. K. Gun'ko., W. J. . in *Advanced Functional Materials*, Vol. 14, **2004**, 791.

[10] C. Velasco-Santos, A. L. Martinez-Hernandez, F. Fisher, R. Ruoff, V. M. Castano, *Journal of Physics D-Applied Physics* **2003**, *36*, 1423.
[11] H. D. Wagner, O. Lourie, Y. Feldman, R. Tenne, *Applied Physics Letters* **1998**, *72*, 188.
[12] B. E. Kilbride, J. N. Coleman, J. Fraysse , P. Fournet, M. Cadek, A. Drury, S. Hutzler, S. Roth , W. J. Blau, *Journal Of Applied Physics* **2002**, *92*, 4024.
[13] F. M. Blighe, W. J. Blau, J. N. Coleman, *Nanotechnology* **2008**, *accepted.*
[14] H. Koerner, G. Price, N. A. Pearce, M. Alexander, R. A. Vaia, *Nat Mater* **2004**, *3*, 115.
[15] M. Qinghao, H. Jinlian, Y. Lapyan, *Smart Materials and Structures* **2007**, 830.
[16] K. Jiyun, K. Hando, *Journal of Polymer Science Part A: Polymer Chemistry* **2005**, *43*, 3973.
[17] H. Xia., M. S. . *Soft Matter* **2005**, *1*, 386
[18] W. Chen, X. Tao, Y. Liu, *Composites Science and Technology* **2006**, *66*, 3029.
[19] H. Xia, M. Song, *Journal of Materials Chemistry* **2006**, *16*, 1843.
[20] H. J. Yoo, Y. C. Jung, N. G. Sahoo, J. W. Cho, *Journal of Macromolecular Science, Part B* **2006**, *45*, 441
[21] J. N. Coleman, U. Khan, W. J. Blau, Y. K. Gun'ko, *Corbon* **2006**, *44*, 1624.
[22] S. Giordani, S. D. Bergin, V. Nicolosi, S. Lebedkin, M. M. Kappes, W. J. Blau, J. N. Coleman, *J. Phys. Chem. B* **2006**, *110*, 15708.
[23] Giordani S., B. S., N. V, W. J. Blau, C. J. N, *physica status solidi (b)* **2006**, *243*, 3058.
[24] B. Zhao, H. Hu, A. Yu, D. Perea, R. C. Haddon, *J. Am. Chem. Soc.* **2005**, *127*, 8197.
[25] B. Zhao, H. H. R. , C. Haddon, *Advanced Functional Materials* **2004**, *14*, 71.
[26] S. Niyogi, M. A. Hamon, H. Hu, B. Zhao, P. Bhowmik, R. Sen, M. E. Itkis, R. C. Haddon, *Acc. Chem. Res.* **2002**, *35*, 1105.
[27] J. Amiran, V. Nicolosi, S. D. Bergin, U. Khan, P. E. Lyons, J. N. Coleman, *J. Phys. Chem. C* **2008**, *112*, 3519.
[28] L. T. J. Korley, B. D. Pate, E. L. Thomas, P. T. Hammond, *Polymer* **2006**, *47*, 3073.
[29] S. M. Liff, N. Kumar, G. H. McKinley, *Nat Mater* **2007**, *6*, 76.
[30] D. M. Crawford, R. G. Bass, T. W. Haas, *Thermochimica Acta* **1998**, *323*, 53.
[31] H.-D. Kim, T.-J. Lee, J.-H. Huh, D.-J. Lee, *Journal of Applied Polymer Science* **1999**, *73*, 345.
[32] F.M. Blighe,W. J. Blau, J. N Coleman, *Nanotechnology* **2008**, 415709.
[33] H. Paik, N. Seo Goo, *Smart Materials and Structures* **2006**, *15*, 1476.
[34] B. Valery, S. Srikanth, K. Ramesh, A. Massood, *Applied Physics Letters* **2006**, *88*, 164101.
[35] Y. Luo, C. Wang, Z. Li, *Synthetic Metals* **2007**, *157*, 390.
[36] http://www.hydrosize.com/.
[37] http://www.carbonsolution.com.
[38] T. Hatakeyama., Z. L, *Handbook of thermal analysis*, John Wiley & sons Ltd, **1998**.
[39] H. M. Jeong, J. B. Lee, S. Y. Lee, B. K. Kim, *Journal of Materials Science* **2000**, *35*, 279.
[40] H. Koerner, W. Liu, M. Alexander, P. Mirau, H. Dowty, R. A. Vaia, *Polymer* **2005**, *46*, 4405.

[41] H. Koerner, J. J. Kelley, R. A. Vaia, *Macromolecules* **2008**, *41*, 4709.
[42] A. R. Bhattacharyya, T. V. Sreekumar, T. Liu, S. Kumar, L. M. Ericson, R. H. Hauge, R. E. Smalley, *Polymer* **2003**, *44*, 2373.
[43] J. Sandler, G. Broza, M. Nolte, K. Schulte, Y. M. Lam, M. S. P. Shaffer, *Journal of Macromolecular Science-Physics* **2003**, *B42*, 479.
[44] X. L. Xie, K. Aloys, X. P. Zhou, F. D. Zeng, *Journal of Thermal Analysis and Calorimetry* **2003**, *74*, 317.
[45] M. Cadek, J. N. Coleman, K. P. Ryan, V. Nicolosi, G. Bister, A. Fonseca, J. B. Nagy, K. Szostak, F. Beguin, W. J. Blau, *Nano Lett.* **2004**, *4*, 353.
[46] S. H. Kim, G. H. Sim, K. H. Ahn, S. Lee, *Korea-Australia Rheology Journal* **2002**, *14*, 49.
[47] U. Khan, K. Ryan, W. J. Blau, J. N. Coleman, *Composites Science and Technology* **2007**, *67*, 3158.
[48] J. M. Darren, F. Gordon, G. M. Meijs, S. J. Renwick, P. Mccarthy, A. Gunatillake, *Journal of Applied Polymer Science* **1996**, *62*, 1377.
[49] H. M. Jeong, J. H. Song, S. Y. Lee, B. K. Kim, *Journal of Materials Science* **2001**, *36*, 5457.
[50] L. H. Sperling, *Introduction to Physical Polymer Science.*, Wiley, **2001**.
[51] G. Eugene, *Journal of Applied Physics* **1945**, *16*, 20.
[52] B. Fabian, A. Gustavo, B. P. Abraham, D. R. Grady, *Journal of Polymer Science Part B: Polymer Physics* **2007**, *45*, 490.
[53] J. N. Coleman, M. Cadek, K. P. Ryan, A. Fonseca, J. B. Nagy, W. J. Blau, M. S. Ferreira, *Polymer* **2006**, *47*, 8556.
[54] I. Ward., *Mechanical properties of solid polymers*, Wiley, New York: **1971**.
[55] B. Finnigan, K. Jack, K. Campbell, P. Halley, R. Truss, P. Casey, D. Cookson, S. King, D. Martin, *Macromolecules* **2005**, *38*, 7386.
[56] F. Yeh, B. S. Hsiao, B. B. Sauer, S. Michel, H. W. Siesler, *Macromolecules* **2003**, *36*, 1940.
[57] Y. Meng-Shung, T. Ping-Yuan, *Journal of Applied Polymer Science* **2003**, *90*, 233.
[58] P. Santhosh, T. Vasudevan, A. Gopalan, K.-P. Lee, *Journal of Power Sources* **2006**, *160*, 609.

# Chapter 6

## Preparation of thermoplastic polyurethane composites with pristine and functionalised mixed carbon nanotubes

## 6.1 Introduction

Many studies have been devoted towards the goal of achieving strong, stiff, yet tough composite materials. Among natural materials, spider silk is the most extraordinary material, with a strength of up to 1.7 GPa and still a strain at failure ~ 70-1000 % *[1, 2]*, thus it has an extraordinarily high toughness *[3]*. Despite this, spider silk still has a lower density than steel by a factor of ~ 6 *[4]*. These amazing mechanical properties of spider silk are due to the morphological arrangement of its (protein) block copolymer chains*[1]*. Spider silk has two distinct regions: a hard nanocrystalline region that is embedded in a soft rubbery segment *[5]*. The combination of the hard segments (HS) and the soft segments (SS) gives rise to the morphology of a composite material, resembling an elastomer loaded with stiff and strong nano filler. The nanocrystalline part acts like a molecular spring and needs a lot of force to deform to failure *[6]*. This molecular spring like character of the HS is also responsible for the stress-strain recovery in spider silk.

The understanding of the molecular architecture of spider silk, and hence the reinforcement mechanism, has recently attracted scientists to the use of thermoplastic polyurethane (TPU) because of its analogy to spider silk. TPU also consists of both hard and soft segments *[7]*. The hard segments form small crystalline domains in the polymer and they are physically cross-linked *[8]*. TPU is usually a very ductile polymer which needs a large energy to break, like spider silk. Though TPU resembles spider silk in toughness *[3]* and with its soft segment and hard segment morphology, the drawback with TPU is, unlike spider silk, the stiffness and yield point are usually low due to the weak physical interactions among crystallites of the hard segments and the continuous soft

segments. The hard segments determine the stiffness and yield stress of the TPU. Increases in the hard segment content increase the stiffness at the expense of the ductility and ultimate tensile strength *[8, 9]* due to the extensive cross-linking of the polymer which hinders the SS mobility.

To increase the stiffness and yield stress of TPU without increasing the hard segment content and hence sacrificing ductility, nano fillers are usually incorporated into the system *[10]*. Carbon nanotubes would be the ideal choice due to their superior mechanical properties. Numerous other studies have been made to utilise CNTs as efficient fillers in polymers *[11-14]* . Work also has been done using thermoset elastomers as the matrix with CNTs as the filler *[15-17]* . The problem with thermoset composite systems is continuous viscosity build-up, poor dispersion and difficulties in processing due to the continuous cross-linking chemical reactions.

In this work, TPU was mechanically reinforced by incorporating different types of pristine CNTs. A maximum loading limit for each pristine CNT type was always reached, limiting the reinforcement possible due to the coating of CNTs around polymer particles. To increase the maximum loading a novel approach was tried. Functionalised CNTs were mixed with the pristine CNTs, which enhanced the overall CNTs dispersion, increased the maximum loading limit and as a result enhanced the mechanical properties.

## 6.2 Sample preparation

For this study, thermoplastic polyurethane/$H_2O$ (product code U2-01.) emulsion was provided by Hydrosize® *[18]* with an average particle size of ~ 3 μm. Polyethyleneglycol functionalised single wall carbon nanotubes (PEG-SWCNT) were purchased from Carbon Solutions, Inc (Fig. 6.1) *[19]*. Pristine HiPCO SWCNTs were purchased from Carbon Nanotechnologies Inc *[20]*. Very thin multiwall carbon nanotubes (VthinMWCNTs) and thick multiwall carbon nanotubes (ThickMWCNTs) were provided by Nanocyl *[21]*. Basically, four types of composites solutions were fabricated, 1) with pristine SWCNTs 2) with pristine VthinMWCNTs 3) with pristine MWCNTs and 4) with mixture of pristine VthinMWCNTs, ThickMWCNTs and PEG-SWCNTs in equal mass fractions. The TPU/$H_2O$ dispersion was diluted to 40 mg/ml in deionised water. The CNTs were added to TPU/$H_2O$, and the composite solutions were made by energetic agitation of CNTs/$H_2O$

using an ultrasonic sonic tip (GEX600, 700W, 20%, 120 kHz) for 10 minutes. The dispersion was further sonicated for 4 hours in a low energy ultrasonic bath (Branson 1510 MT). These were used as the stock solutions for the composite preparation. This stock solution was then diluted into a series of solutions using the ultrasonic tip (5 minutes) between dilutions. This was again followed by a 4 hour ultrasonic bath sonication. The prepared solutions were then dropcast into 40 X 40 mm teflon trays and dried in an oven for 12 hours at 60 °C. Free standing films were obtained and used for further characterisation. Film thicknesses were measured using a micrometer screw.

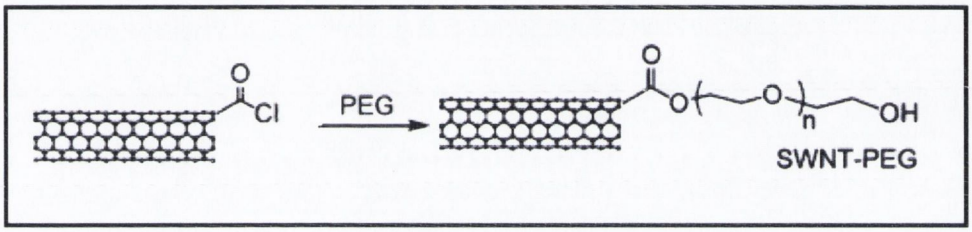


Fig. 6.1 Chemical synthesis and proposed structure of PEG-SWCNTs*[22]* .

## 6.3 Results and discussion

Three different kinds of composite were fabricated with pristine SWCNT, VthinMWCNT, and thick MWCNTs and tested for mechanical reinforcements. The volume fraction of CNT in each film was calculated from the mass fraction using the densities, $\rho$ = 1100 kg/m$^3$ for TPU*[18]* , $\rho$ = 1500 kg/m$^3$ for SWCNT*[23]* , $\rho$ = 1750 kg/m$^3$ for VthinMWCNT and $\rho$ = 2150 kg/m$^3$ Thick MWNT*[24]* for. The external diameter of these tubes previously measured, are in the order of SWCNT (~1nm) and less than VthinMWCNT (9.5 nm)*[21]* and ThickMWCNT (25 nm)*[25]* .

As has been mentioned in the previous chapter, the stress-strain curve for a typical segmented thermoplastic TPU can be divided into three main parts *[26, 27]*.

1) Initial part - corresponds to stiffness of the material
2) Plateau part
3) The plateau part is followed by a steep part which corresponds to strain hardening and strain induced crystallisation.

The mechanical properties are discussed in terms of reinforcement in the stated three parts.

**Young's modulus of pristine nanotubes**

Representative stress-strain curves for the SWCNTs are shown in figure 6.2.With each addition of SWCNTs to the polymer, the Young's modulus increases more or less linearly. The maximum Young's modulus for the SWCNT composites was 68.5 MPa at 3.6 vol% (5 wt%) compared to the polymer only sample value of 18.1 MPa. This is an increase of 3.8 times compared to the polymer. Beyond 3.6 vol% (5 wt%), the films show very poor dispersion of the CNTs and no continuous composites were achievable.

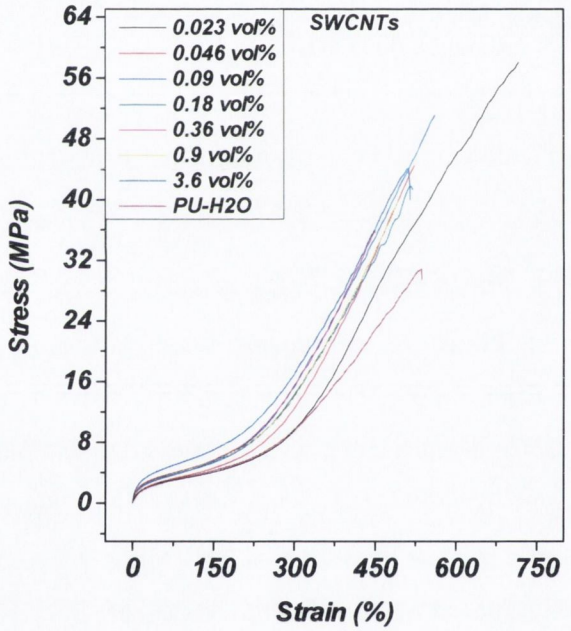


Fig. 6.2 Representative stress-strain curves for the pristine SWCNT composites shows enhancement of the mechanical properties in all three parts.

Shown in figure 6.3 are representative stress-strain curves for the very thin multiwall (VthinMWCNTs) composites. These follow almost the same trend as the SWCNTs, i.e the Young's modulus increases with increasing volume fraction of CNTs (Fig. 6.5). The composites loaded with 3.1 vol% (5 wt%) VthinMWCNTs exhibits the highest increase of

4 times the Young's modulus of the polymer only sample (from 18.1 to 73.7 MPa). However, unlike the SWCNTs, it was possible to obtain a relatively well dispersed and slightly higher volume fraction film, with 4.37 vol% (7 wt%) CNT loading. The Young's modulus at 4.37 vol% (7 wt%) loading was 82.25 MPa. Above 4.37 vol%, it was not possible to fabricate continuous and well dispersed composites loaded with VthinMWCNTs.

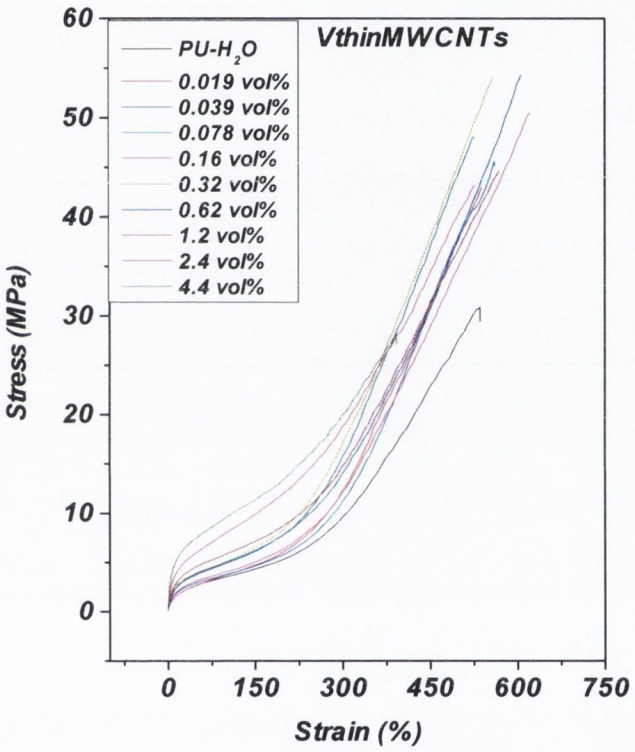


Fig. 6.3 Representative stress-strain curves for very thin multiwall carbon nanotubes.

Representative stress-strain curves for the ThickMWCNTs are shown in figure 6.4. For the thick multiwall carbon nanotubes (ThickMWCNTs), the maximum Young's (93.75 MPa) modulus was observed for the composite loaded with 7 wt% (3.36 vol%) CNTs. At 3.36 vol% (7 wt%), the Young's modulus was increased by a factor of 5 from the polymer only sample Young's modulus of 18.1 MPa. The increase in Young's modulus with increasing CNTs loading follows almost the same trends as were observed in the SWCNTs

and the VthinMWCNTs. It was possible to fabricate 4.8 vol% (10 wt% ) MWCNT composites, but the Young's modulus was slightly decreased.

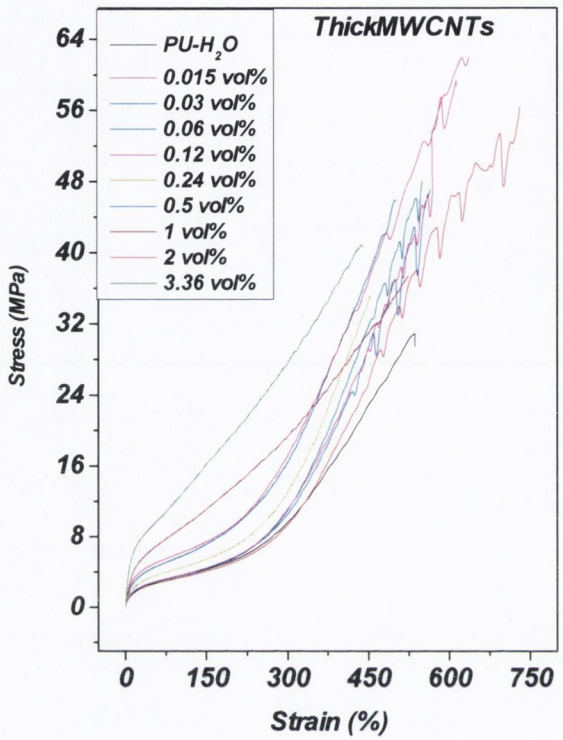


Fig 6.4 Representative stress-strain curves for Thick multi wall carbon nanotubes.

The elastomer reinforcement is usually predicted by Guth's rule *[28]*, as given in equation 5.1.

$$Y_C = Y_{Elas}\left(1 + 0.067AV_f + 1.62A^2V_f{}^2\right) \qquad \text{Eq. 5.1}$$

where $Y_C$ and $Y_{Elas}$ are the composite and elastomer moduli, $A$ is the filler aspect ratio and $V_f$ is the volume fraction.

From the previous measurements carried out in the same group in Trinity College, the aspect ratios of the SWCNTs have been measured to be ~ 900 using TEM and AFM*[29]* and for the MWCNTs 100-200 *[30]* . Assuming the SWCNT aspect ratio as 900 and for a MWCNT aspect ratio as,100 the, Guth's equation only agrees at low CNTs loading levels and does not agree with the experimental data at high loading (Fig 6.5). SWCNTs starts to deviate from Guth's rule for vol > 0.01 vol % (0.12 wt%),

VthinMWCNT at 0.78 vol% (1.25 wt%) and ThickMWCNT 2.5 wt% (1.2 vol%) (Fig. 6.5). This suggest that up to these CNT $V_f$s the CNTs may remain embedded in the polymer with no CNT network formation. Therefore composites can be defined by filler-polymer interactions.

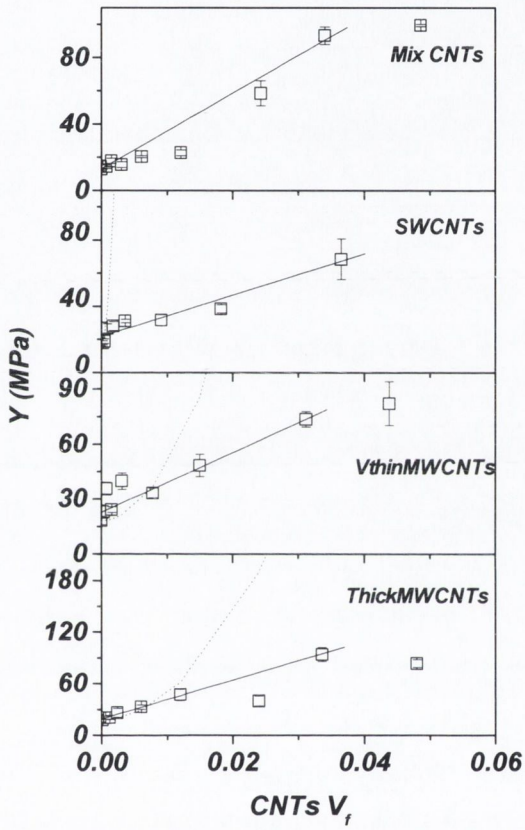


Fig. 6.5. Young's moduli of composites fabricated with various kind of CNTs. Note: the hollow symbols represents the experimental Young's modulus, while the dotted line represents the Young's modulus predicted by Guth's rule.

Other equations which can also be used for estimating the mechanical properties of the fibre reinforced composites are the rule of mixtures (equation 5.2) and the Halpin–Tsai equations (mentioned in chapter 2). The Halpin-Tsai equation is has been shown to work well for low volume fraction samples *[31]*. The composites fabricated in this work were loaded with relatively high volume fractions of CNTs. Thus, we use the rule of mixtures equation in terms of $dY/dV_f$ values (Eq.5.2 and 5.3).

$$Y_C = (\eta_o \eta_l Y_f - Y_m) V_f + Y_m \quad \text{Eq 5.2 } [32, 33]$$

where $\eta_o$ is the orientation efficiency factor. This has values of $\eta_o$=1 for aligned fibres, $\eta_o$=3/8 for fibres aligned in plane and $\eta_o$=1/5 for randomly oriented fibres *[34]*

or

$$\frac{dY_c}{dV_f} = \eta_o \eta_l Y_f - Y_m \quad \text{Eq 5.3 } [31]$$

For the SWCNT samples, the experimental $dY/dV_f$ value obtained by a linear fit to the data in figure 6.5 is ~1.3 GPa. For single wall carbon nanotubes, the Young's modulus can be in the range of 320-1000 GPa*[35, 36]* . Therefore, for SWCNT composites, the $dY/dV_f$ value should correspond to ~120-375 GPa. The experimental $dY/dV_f$ value obtained here for the SWCNTs is significantly lower than the theoretical values. However, in similar work Chen *et al.* fabricated SWCNTs-polyurethane composites and achieved a reasonably similar $dY/dV_f$ value to our work i.e. ~1.9 GPa *[37]*. In another work, Fabian *et al.* showed an increase in Young's modulus from ~ 140 to 210MPa with a 2.5 wt% SWCNTs loading in polyurethane *[38]*. This corresponds to a 1.5 times increase in the Young's modulus. Their $dY/dV_f$ value is ~ 4 GPa, which is close to the value presented in this work, but is also significantly lower than the theoretical values. Xia *et al.* also prepared SWCNTs-PU composites *[39]*. They were able to increase the Young's modulus of polyurethane from 7.94 to 11.77 MPa. This is equivalent to a $dY/dV_f$ ~ 0.8 GPa. In the same paper they have also discussed the fabrication of the SWCNTs-grafted polyurethane composites. The reinforcement they got for the SWCNT-grafted-PU was slightly better than for non-grafted composites. The Young's modulus for the 0.7 wt% grafted-SWCNTs (chemically bonded to the polymer backbone) composite was 22.1 MPa *[39]*. This corresponds to $dY/dV_f$ of 2.8 MPa, again close to the $dY/dV_f$ value for SWCNTs measured here and still far below than the theoretically predicted values. Haddon *et al.* prepared a SWCNT-PU composite membrane by the fibre electrospinning technique*[40]* . The maximum Young's modulus which they achieved in their work was ~ 26 MPa (for 1 wt% SWCNT loading) compared to the polymer only membrane modulus of 6 MPa *[40]*. The $dY/dV_f$ value corresponds to ~ 2.8 GPa which is again close to our $dY/dV_f$ value. Thus the Rule of mixtures *[32, 33]* does not fit to the SWCNTs data. Again this may be due to the formation of CNT networks.

The $dY/dV_f$ values extracted from the linear fit to the VthinMWCNTs-TPU composites data is ~1.6 GPa (Fig. 6.5). In the case of ThickMWCNTs-TPU samples, it is 2.3 GPa (Fig 6.5). If we consider the MWCNT's Young's modulus to be in the range of 10-500 GPa *[41]*, then according to the rule of mixtures, the $dY/dV_f$ value should be in the range of ~ 3.75 – 187 GPa. Therefore, if the majority of the MWCNTs Young's modulus are in the lower range, 10 GPa, then the MWCNTs experimental $dY/dV_f$ value is close to the rule of mixtures value. The $dY/dV_f$ presented in this work does not significantly differ from those reported in the literature. Sahoo *et al.* showed a large enhancement in the Young's modulus in their MWCNT-PU work. They observed an increase in Young's modulus by a factor of 7.4, compared to the polymer only sample of 50 MPa, at 20 wt % CNT loading *[16]*. The $dY/dV_f$ value extracted from their work is ~3.6 GPa. Chen and coworkers reinforced PU with MWCNTs. They observed a linear increase in the Young's modulus with increasing volume fraction of the CNTs. Their work gives a $dY/dV_f$ value of ~ 1.3 GPa.

The fact that the SWCNTs show a lower increase in Young's modulus may be because the SWCNTs tend to form bundles at higher concentrations and thus it may be related to poor dispersion of the SWCNTs *[29, 42]*. However, in the MWCNT composite samples, at high volume fractions the ThickMWCNTs show a higher Young's modulus compared to the VthinMWCNTs. This is surprising because Cadek *et al.* in their CNT-PVA work showed that the mechanical properties of MWCNT composites were directly proportional to the surface area of the CNTs *[14]*. Again, dispersion might be an issue here or the difference may be due to the nature of the polymer used in their work.

**Maximum loading limit for pristine composite.**

In each type of pristine carbon nanotube, (SWCNT, VthinMWCNT, ThickMWCNT) there was always a maximum limit beyond which the fabrication of good continuous composites was not possible. This may be due to CNT network formation and poor dispersion. For the SWCNT composites, the highest volume fraction composite prepared was 3.6 vol% (5 wt%). In the case of the VthinMWCNTs, the limit was 4.37 vol% (7 wt% ) and for the ThickMWCNTs the maximum achievable loading was 4.8 vol% 1(0 wt%). This suggests that the maximum loading limit scales with the diameter of the CNTs.

One reason for the maximum loading limit may be the aggregation of CNTs at high volume fractions *[31]*. The other more convincing reason lies in the nature of TPU used. The polymer used in this work was in the form of micron sized particles dispersed in water. During the drying/curing process these particles fuse together to form a continuous polymer film. During the sonication process of the CNT-TPU composite in water solution, the hydrophobic CNTs *[43]* form a network around the hydrophobic polymer particles, which is illustrated in the figure 6.6. During the drying/curing process the dispersions with the low volume fractions of CNTs partially encapsulate the polymer particles, thus leaving uncovered areas on the polymer particles. These uncovered areas can touch between neighboring particles and can fuse together into a single mass. Therefore, at low volume fraction, the CNTs are engulfed in the polymer particles and become well embedded in the composite. With the increase in CNT volume fraction, the CNT coating around the polymer particles also increases. Subsequently, there comes the stage when most of the polymer particles' surface area becomes encapsulated by the CNTs (Fig 6.7). Therefore, the particles can not fuse with the neighboring particles and hence they can not form a good, continuous film. This CNT network formation has also been proposed by Blighe *et al.* in their CNT-TPU study *[44]*.

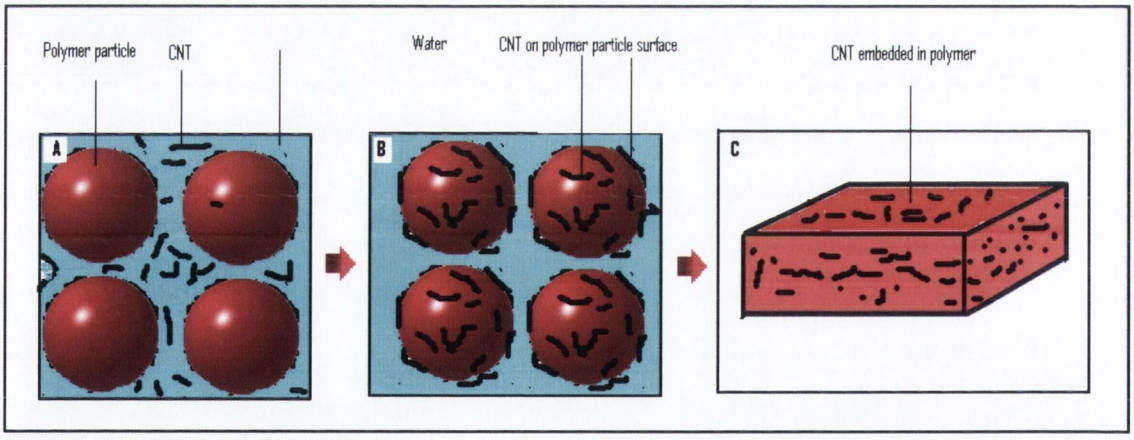


Fig. 6.6 A) Shows the low volume fraction CNT dispersion in TPU/$H_2O$ before sonication.

B) Adsorption of CNTs on the TPU particles due the hydrophobic nature of CNTs and TPU particles.

C) CNT-TPU composite after drying, shows the engulfing of the CNTs by polymer particles due to their fusion into a single mass.

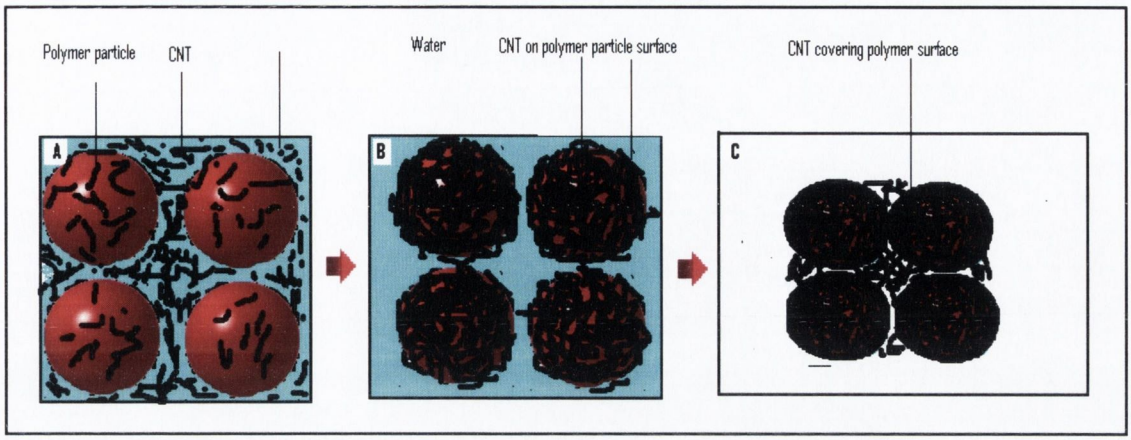


Fig 6.7. A) Shows the high volume fraction CNT dispersion in TPU/$H_2O$ before sonication.

B) Adsorption of CNTs on the TPU particles due the hydrophobic nature of CNTs. This diagram illustrates that at high concentrations polymer-polymer interaction are not possible due to the presence of CNT networks around the polymer particles. The CNT networks prevent polymer particles fusing together.

The phenomena are also evident from Young's modulus data where the Guth's rule is valid for the very low fraction volume fractions samples (see Fig. 6.5). The data reveals that, at very low volume fractions, the CNTs remain embedded in the polymer and the mechanical properties can be defined by the polymer–CNT interactions. While at the higher volume fractions the CNTs form a network in the polymer and hence the mechanical properties can not be defined by Guth's Rule for the filler-polymer interactions. The Young's modulus experimental data for both types of the MWCNTs follows the Guth's equation, up until relatively high volume fractions values, in comparison with SWCNTs. This is consistent with the fact that, at a given volume fraction, the SWCNTs cover more surface of the polymer particle/s in comparison with the MWCNTs.

To confirm the CNT network formation phenomena around the polymer particles an experiment was carried out. A high volume fraction 18.7 vol% (30 wt%) of VthinMWCNTs-TPU/water composite solution was sonicated. After 5 minutes of

sonication, all the CNTs-TPU were observed to be in large single lumps in a, more or less, clear water solution (see Fig 6.8). This reveals that, due to the hydrophobic nature of the CNTs, they tend to adhere to the hydrophobic polymer *[45]* particles, rather than remaining dispersed in water, and encapsulate the polymer particles. Therefore, at high volume fractions, the polymer particles can not touch and fuse to each other and the particles are primarily held together by CNT-CNT interactions, as illustrated in figure 6.7. Thus we can not get a composite film at the higher volume fractions but instead get beads of polymer coated with CNTs. However, at low concentrations there can be bare/uncovered areas on the polymer particle surface which can make contact to neighboring particles and fuse together (Fig 6.6).

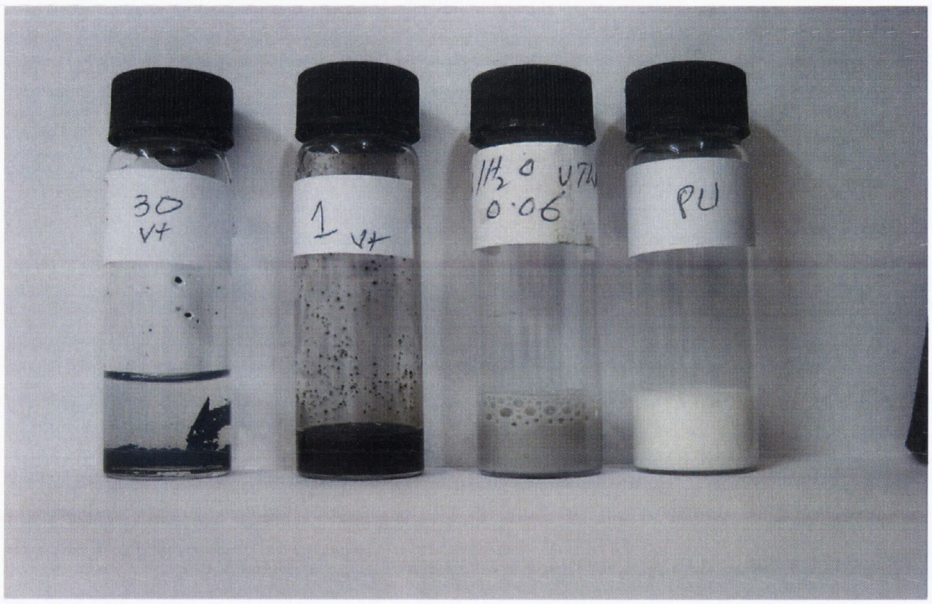


Fig 6.8 From right, first sample is TPU/water, 2nd is 0.039 vol% ,3rd is 0.0078 vol% and 4th is 18.7 vol% VthinMWCT composite solutions. The figure reveals the complete encapsulation of polymer particles by VthinMWCNTs.

The fact that small diameters SWCNT and VthinMWCNT have relatively low maximum loading limits compare to the ThickMWCNT. This can be explained in terms of

1) Small diameters of the SWCNT and VthinMWCNT

2) Bad dispersion of the relatively small diameter CNTs compared with ThickMWCNTs.

3) Because of the large diameter at a given volume fraction, there should be larger diameter pores (uncovered surface of the polymer) in the network formed by MWCNTs than for SWCNTs. Therefore, polymer particles encapsulated with MWCNTs should have greater uncovered surface area to touch each and fuse together to form the composite film compare SWCNTs.

4) The poor dispersions associated with both types of the small diameter CNTs (compare to the large diameter ThickMWCNTs) can be a major factor in limiting the maximum loading. Poor dispersion of the CNTs in the polymer matrix creates aggregates which in turn are responsible for weak sites and inhomogeneous composites. More importantly, as has been mentioned earlier, at high volume fractions the properties of theses composites are dominated by the CNT-CNT interaction hence any factor that affects the CNT-CNT network must influence the overall composite properties. Therefore a poor dispersion also gives rise to a weaker CNTs network and hence a weaker composite. This is because mechanical properties of a CNT-CNT network are proportional to the junction density of CNTs*[46]* . The junction density can be increased by enhancement of the CNTs dispersion. This strongly suggests that the maximum loading limit can be increased by enhancement of the CNTs dispersion.

**Effect of CNT diameter on various properties**

The (highest) relative increase in Young's modulus and $dY/dV_f$ values scale with CNT diameters. (Fig 6.9). This further supports the argument that at a given mass fraction small diameter CNTs form larger thicker networks due to high number densities compared to the large diameter CNTs. This same network formation phenomenon is consistent with maximum loading limit (Fig 6.9). The maximum CNT loading limit for all the three types of CNTs is in the order of the CNT diameter i.e SWCNT<VthinMWCNT<ThickMWCNT (5.9). Further the maximum $V_f$ for a particular CNT which follows Guth's rules also scales with CNT diameters. This again suggests intensified CNT network formation from the smaller diameter CNTs compare with the large diameter CNTs.

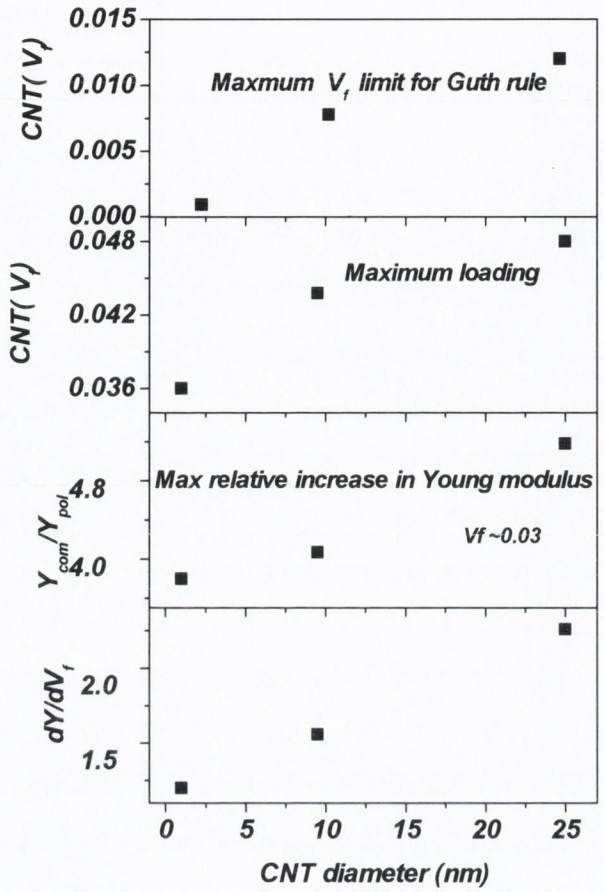


Fig. 6.9. The effect of CNT diameter on various properties of composites.

**Role of functionalised CNTs in the preparation of high volume fraction composites**

As stated previously, in all the pristine nanotube composites, it was not possible to fabricate higher volume fraction composites than 4.8 vol% (10 wt%). One of the reasons for this, can be their poor dispersion, as well as the CNT network formation around the polymer particles. Surfactants are usually used to enhance CNTs dispersion in aqueous media *[47-49]* and thus good composites at high volume fractions could be prepared. Surfactants are molecules having hydrophobic and hydrophilic parts in the one species. The hydrophobic part adheres itself to the CNTs and its hydrophilic part allows it to be suspended/dispersed in the water *[47]*. Surfactants can also impart unwanted properties to a composite*[50, 51]*. For example, surfactants can form a coating around the CNTs which can prevent CNT-polymer interfacial bonding hence stress transfer. Also, trapped surfactant

may act like a plasticiser and adversely effect a composite's mechanical properties. In many cases the CNTs are incorporated into the polymer to enhance its thermal and electrical conductivity. But owing to the insulating nature of surfactants, the resultant composite may have reduced conductivity. To avoid surfactants in this work, another novel approach was tried to facilitate CNTs dispersion, and fabricate higher volume fraction CNT composites. The functionalised SWCNTs were used as a dispersing agent. The commercially available PEG-SWCNTs have demonstrated very good dispersion in water at high concentrations *[52]*. These water dispersible, commercially available PEG-SWCNTs *[22]* resemble a surfactant, having both hydrophilic and hydrophilic parts (Fig. 6.1). The hydrophobic part is the CNT itself and the alkyl group of PEG, while the alcohol group of PEG (OH) plays the role of the hydrophilic part, which allows the CNTs to disperse in water. By mixing the functionalised CNTs with pristine CNTs, the pristine CNTs may attach to the functionalised CNTs. This results in the exfoliation of pristine CNTs from larger bundles to smaller bundles and this way can improve the pristine CNTs dispersion (Fig 6.10). Even though bundles formation is not desirable but CNT smaller bundles are more acceptable than larger bubdles. There are two driving forces for pristine CNT adhesion to the functionalised CNTs: 1) a surfactant type of interaction of CNTs to functionalised-CNTs, 2) at the nano scale particles tend to adhere to each other. Therefore higher volume fractions composites could be fabricated with CNT mixtures (see figure 6.10 for illustration).

For the above proposed approach, the two best CNTs, the very thin MWCNTs and the thick MWCNTs, were selected from the choice of pristine CNTs on the basis of their mechanical performance and maximum loading ability (these mechanical results will be discussed in detail in the coming sections). Theses two types of CNTs were mixed with PEG-SWCNTs. With this approach it was possible to fabricate higher volume fraction composites. In this work, composites of up to 6.7 vol% (~14 wt%) composites was demonstrated. Preparation of volume fractions above 6.7 vol% were not tried because the mechanical properties deteriorated sharply.

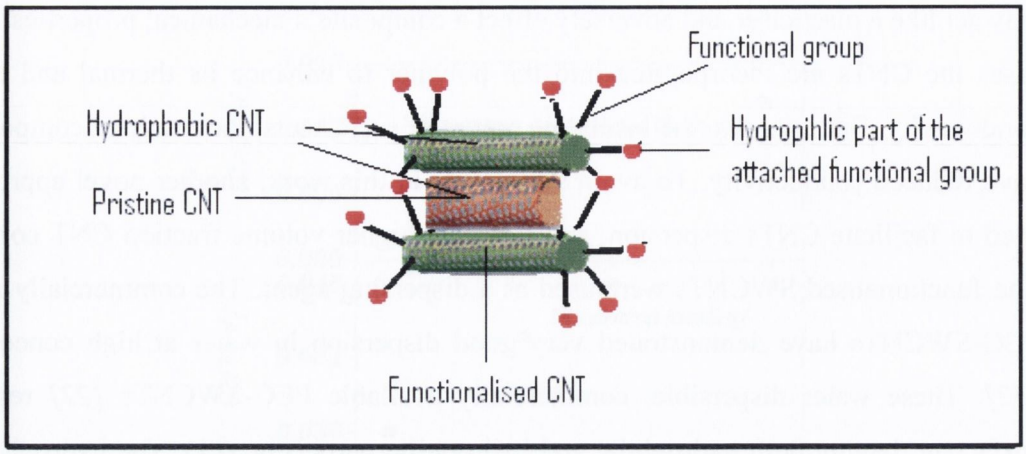


Fig. 6.10 Proposed diagram of functionalised CNTs assisted dispersion of pristine CNTs. The head of the functional groups are hydrophilic and responsible for suspending them in water, while the CNTs it self and alkyl group of PEG is hydrophobic. Possibly the hydrophobic pristine CNTs adhere to the hydrophobic part CNT part of the functionalised nanotube.

**Young's modulus of mixed nanotubes composites.**

For all the mechanical data at least five samples were tested and the value for each Vf is presented as an average of all the five samples. The error bar in each case is the standard deviation. Such relatively large error bars are typical for such type of elastomeric materials.

The water dispersible functionalised SWCNTs were mixed with the VthinMWCNTs and the ThickMWCNTs to prepare composites. With this mix of CNTs (mix-CNTs), it was possible to fabricate composites with higher volume fractions. At 3.4 vol% (7 wt%) CNT loading the Young's modulus was increased 7.4 times compared to the polymer only sample (Fig 6.5 and 5.20). This is the highest relative increase in Young's modulus among all the composites prepared in this work. The increase in Young's modulus with the incorporation of CNTs was not completely linear. The best fit to the data gave the $dY/dV_f$ value as 2.2 GPa, which is similar to the ThickMWCNT composites value( and higher than the SWCNTs and VthinMWCNTs). No work could be found in literature reporting this kind of mixed nanotubes composite preparation for comparison. Comparisons of the Young's modulus of all the composites prepared in this work are summarized in figure 6.5.

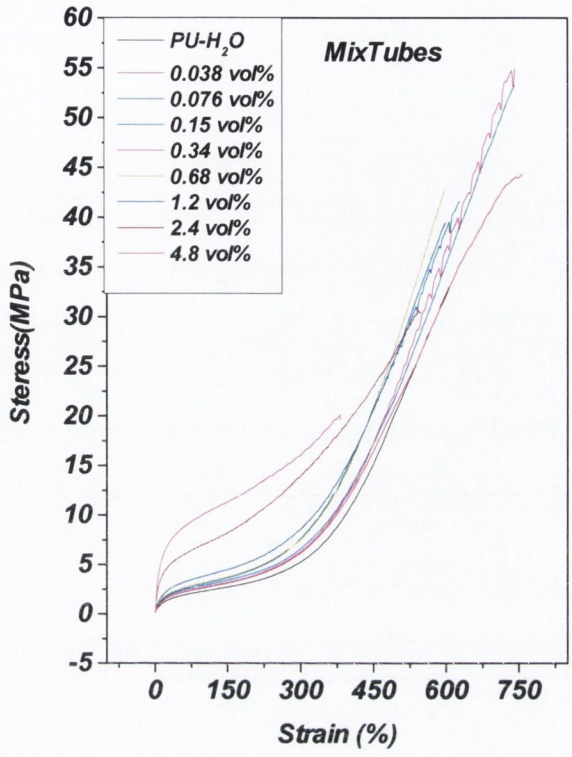


Fig. 6.11. Representative stress-strain graph of composites fabricated with mix-CNTs

**Ultimate tensile strength**

At very low CNTs loading vol% < 1 the UTS increased from ~ 42 to a maximum of ~58 MPa (Fig. 6.12). This strongly suggests that at low volume fractions the CNTs are engulfed by the fusion of the polymer particles and remain embedded in the polymer, therefore imparting strength to the overall composite. Thus, at low concentrations the CNT-polymer interaction is dominant. At low volume fractions, the mix-CNT composites exhibit higher strength than the pristine CNT composites. This infers that the mix-CNTs are better dispersed than the pristine CNTs. Owing to the solid/viscous nature of the polymer particles dispersed in water, it is unlikely that the nanotubes can penetrate into the polymer particles in solution. However, during drying these CNTs are engulfed by polymer particles, but due to the solid/viscous nature of the polymer they may not distribute/disperse themselves within the polymer and rather arrested in polymer. Thus the pre-drying dispersion of the CNTs plays a vital role in determining the mechanical strength. That is the

reason that the well dispersed mix-CNTs display high strengths at low volume fractions. The high strength in the mix-CNT composites may be due to the good dispersion because of the functionalised CNTs.

However at high volume fractions, >0.5 vol%, the UTS drops in all the samples. This reduction in UTS may be due to the aggregation of the CNTs at high concentration and, more pronouncedly, due to the CNTs network formation within the TPU. This suggests that at high volume fractions the composite properties are dominated by the CNT-CNT interactions.

Another factor should also be taken into consideration in the preparation of high volume fraction composites with mix-CNTs, is the strength of CNTs network formed. Blighe *et al.*'s work on PEG-SWCNT reveals that the network formed by PEG-SWCNTs is much stronger than pristine CNT networks *[53]*. Thus, PEG-SWCNTs may impart extra strength to the overall CNT network and hence, at a given volume fraction, the mixed CNTs composite should have greater structural integrity than the pristine CNT composites. This factor seems less effective and is not well supported by the mechanical data. If this was the case, then at high volume fractions the mix-CNTs composites should have higher strengths than those of the pristine CNTs, which is not the case. This, again should be due to the overall good dispersion of mix-CNTs.

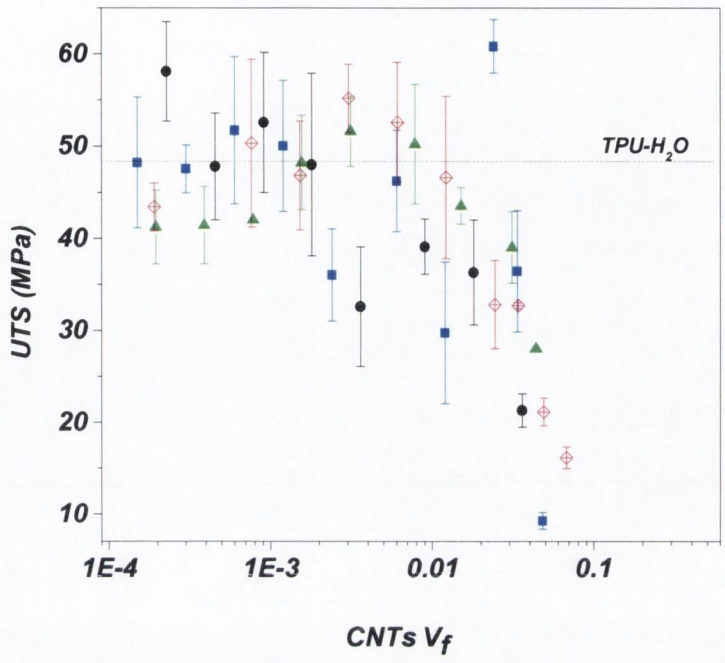


Fig. 6.12. Ultimate tensile strength of composites as a function of CNT volume fraction.

**Strain at break**

In general, up to 1.2 vol % CNT loading, all the samples were very ductile and the strains at break ($\varepsilon_b$) values were almost identical (>500 %) (Fig 6.13). This is because at low volume fractions the CNTs remain embedded within the polymer. Therefore at low volume fractions the mechanical properties are dominated by the CNT-polymer and polymer-polymer interactions. At high volume fractions, the CNT-CNT interactions are dominant due to the CNT network formation *[44]*. In general, compared to the pristine nanotubes, the mix-CNT samples exhibited higher ductility. Again this can be associated to the good dispersion of the mix-CNTs due to the presence of PEG-SWCNTs. It is also possible that, at a given volume fraction, a higher number of mix-CNTs may be embedded within the polymer than for the pristine CNTs. This means there is less CNT-CNT interaction and more polymer-CNT interaction, compared to the pristine CNT composites, and hence higher ductility. Further, as the mechanical properties are mainly affected by the nature of the CNT network, then presence of polyethyleneglycol (PEG) in the network

must be taken into consideration as well. Blighe *et al.*'s work revealed that the PEG-SWCNT network is much less ductile than the pristine CNTs network *[46]* Thus the presence of PEG should decrease the over all ductility in the mix-CNT composites. Therefore, the high ductility in observed in the sample prepared with mix-CNTs may only be ascribed to the good dispersion of the mix-CNTs facilitated by the presence of the water dispersible PEG-SWCNTs.

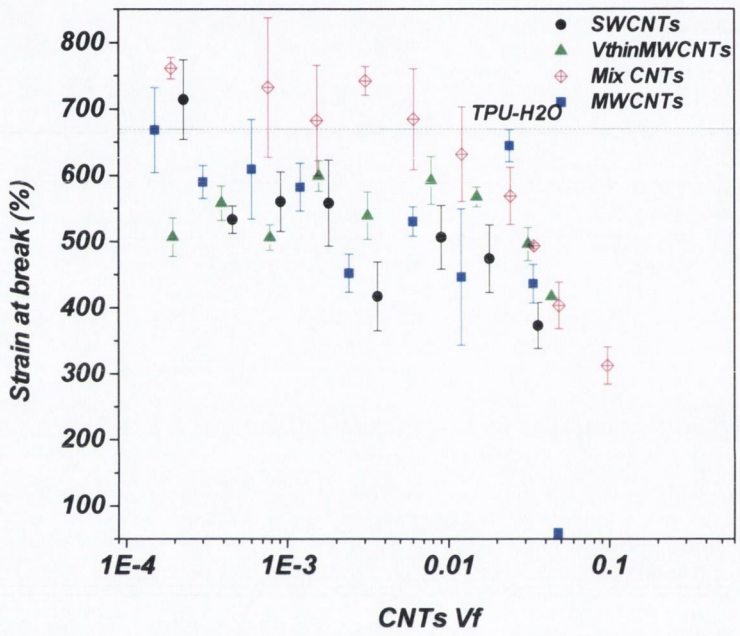


Fig. 6.13 Strain at break values of various composites.

**Toughness**

Shown in figure 6.14 are the toughness values for different CNT-TPU composites at different volume fractions. In all the samples, the toughness of the low volume fraction composites were slightly increased compared to the polymer only samples. The toughness dropped at relatively high volume fractions (>1.2 vol%). TPUs usually have high toughness, mainly due their very high ductility. Thus, the toughness follows the same trend as the strain at break and the same reasons can account for the reduction as has been described for the strain at break values.

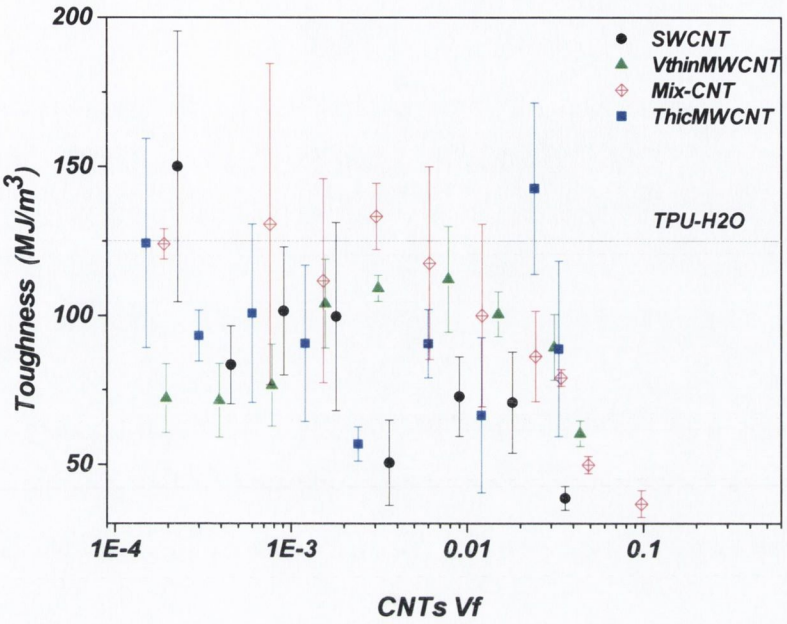


Fig 6.14 Toughness of the various CNT-TPU composites as a function of volume fraction.

**Yield Stress**

Stress at 50% strain is considered as the yield stress for consistency and comparison. It must be noted that the volume fraction presented here for the pristine CNTs are the highest which were achievable. Stress at 50% strain for the SWCNT composites increased by a factor of 2, from 2.7 MPa to 5.4 MPa at 3.6 vol% (5 wt%). Again, the MWCNT composites show a high increase in the stress at the yield point compared to the SWCNT composites (Fig 6.15). For the VthinMWCNTs, the stress was increased to 7.1 MPa at 4.3 vol% (7 wt%) loading and this corresponds to an increase by a factor of 2.6. However, for the ThickMWCNT composites the stress was enhanced by a factor of 3 compared to the polymer only sample at 4.8 vol% (10 wt%). The mix-CNTs composites at 4.8 vol% (10 wt%) had their yield stress increased to 8.3 MPa, (from 2.1 MPa) over the polymer only sample. This corresponds to a 4 times increase. Within the elastic limit, all the components of a composite should strain together under an applied force, i.e. no phase separation or detachment will take place. A departure from the elastic linearity indicates the

separation/detachment of some components, which occurs at the yield stress. Various interactions amongst the components of the TPU matrix can influence the linear elastic behavior. These include HS-HS, SS-HS and SS-SS physical interactions. Within the elastic limit the HS-HS interaction is contributes less because the HS domain is unlikely to deform due to its rigid nature *[27]*. Thus, the SS-SS and SS-HS physical interactions determine the yield stress. Pristine nanotubes are highly hydrophobic and preferentially should interact with the hydrophobic soft segment *[54]* of TPU, hence enhancing the yield stress. Therefore, the reason that the mix-CNTs exhibit significantly larger increases in yield stress may be because the functionalised CNTs have polar hydroxyl groups which can form hydrogen bonds with the HS of the TPU*[38, 55]* . Hydrogen bonding can impart extra reinforcement to the mix-CNT composites, compared to the pristine CNTs. Improved dispersion of the mix-CNTs could be another reason for the relatively high yield point of the mix-CNT composites.

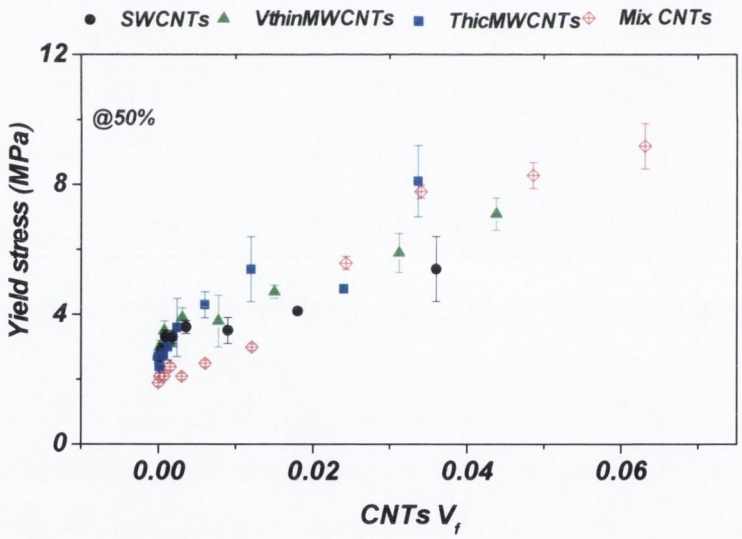


Fig. 6.15. Yield stress of the various CNT composites as volume fraction of CNTs

**Plateau part of the stress-strain curve**

TPU elastomer has quite a good strength, in the range of rigid plastics like PVC and PVA *[56]*, a high ductility >400% and hence a high toughness ~100MJ/m$^3$, in the range of spider silk and Kevlar (>50 MJ/m$^3$ )*[3]* . The big difference is, that both the spider silk and

and kevlar have high toughnesses at low strain values. The main problem with TPU which makes it less favorable for structural purposes is its low stiffness and low yield stress, i.e plastic deformation takes place at very low stresses. One way to increase the stiffness and yield stress of polyurethane is to increase the hard segment content, but an increase in the HS is associated with a loss in ductility because of the rigid nature of the HS *[8, 9]*. To avoid HS increase, and hence low ductility, another approach to increase the yield stress, and the flat region stress. is to incorporate nano fillers in the elastomer. Therefore the aim is to prepare materials which do not only have a high yield stress but at the same time phase separation occurs at a higher yield and hence the material has a high ductility. This essentially means we need to enhance, 1) stiffness 2) yield stress and 3) flat region.

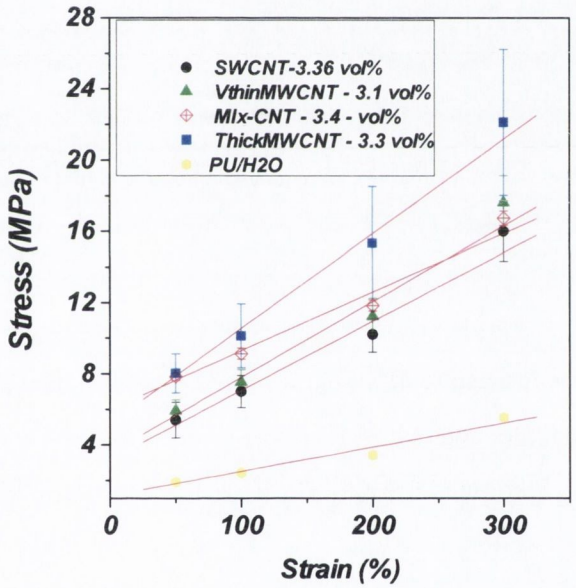


Fig.6.16. The figure shows the significant enhancement in the plateau part of stress-strain curve with incorporation of CNTs.

A very high level of reinforcement in the first two, the stiffness and yield stress, has been reported previously by the incorporation of nano fillers into the elastomer *[44, 55]* . The reinforcement of the plateau part is usually not reported in the literature because a high increase in stiffness and yield stress is usually associated with the loss of ductility *[44][55]* In this work we not only showed significant increases in the stiffness and yield stress, but

more importantly we were able to prepare composites which showed continuous increases in stress in the so called plateau part with each incremental increase of CNT volume fraction. The increases in stresses are shown in figure 6.17. In the case of the pristine SWCNT composites (3.6 vol% or 5 wt%), the stress was doubled from 3.4 MPa to 7 MPa at 100 % strain. For the VerythinMWCNT composites (4.3 vol% or 7 wt %), the stress at 100 % strain was increased by 2.65 times over the 3.4 MPa for the polymer only sample. For the ThickMWCNTs composites (3.3 vol% or 7 wt%), an increase of 3.4 times in stress at 100% strain was observed compared to the polymer only sample. At the same CNT loading levels, the mix-CNT composites exhibited an increase of 3.8 times compared to the polymer only sample .Compare to the polymer only sample stress 5.3 MPa at 200 %, the maximum stress increases for SWCNT= 10.2 MP at $V_f$ 3.6 % (X 1.9) , VthinMWCNT= 12.8 at $V_f$ 4.3% (X 2.4), and ThickMWCNT= 15.3 at $V_f$ 3.36% (X 2.9) figure 6.17. In case of mixed CNT (at 200% strain) stress was increased from the polymer only 3.4 MPa to 9.1 at $V_f$ 3.4 ( X 2.7). At the same stated respective $V_f$ at 300% strain stress for polymer only sample =9.4 MPa, SWCNT= 16MPa, (X 1.7), VthinMWCNT=18.7 MPa (X 2), ThickMWCNT= 22.1 MPa (X 2.3). In case of mixed CNT composites the stress at 300% strain was increased to X 3 at $V_f$ 3.4 % compare to polymer only. Shown in figure 6.17 are the plateau part stresses of all the four types of composites as a function of $V_f$. The figure infers that even though high $V_f$ composite preparation is achievable with mixed-CNTs this gives no improvement in the plateau region (stress) at low volume fraction. However at high $V_f$ mixed CNTs composites exhibits almost the same increase in stresses at 200 and 300 % strain as was exhibited by the best ThickMWCNT composite. Overall these results reveal significant improvements in the plateau part of the stress-strain curve. Again, in analogy to the stiffness and yield stress data, these results also suggest that with pristine nanotubes the reinforcement increases with increasing diameter of the CNTs. The data also reveals that at low $V_f$ the mixed-CNT composites exhibit very low reinforcement in the plateau region compared to the pristine CNTs. The reasons for this are not known. It must be noted that these results are a step forward toward the fabrication of stiff but yet tough materials by filling elastomers with CNTs. These results also infer that, like the other mechanical reinforcement parameters, the stress in the plateau part was higher for the higher diameter CNTs (Fig.6.17).

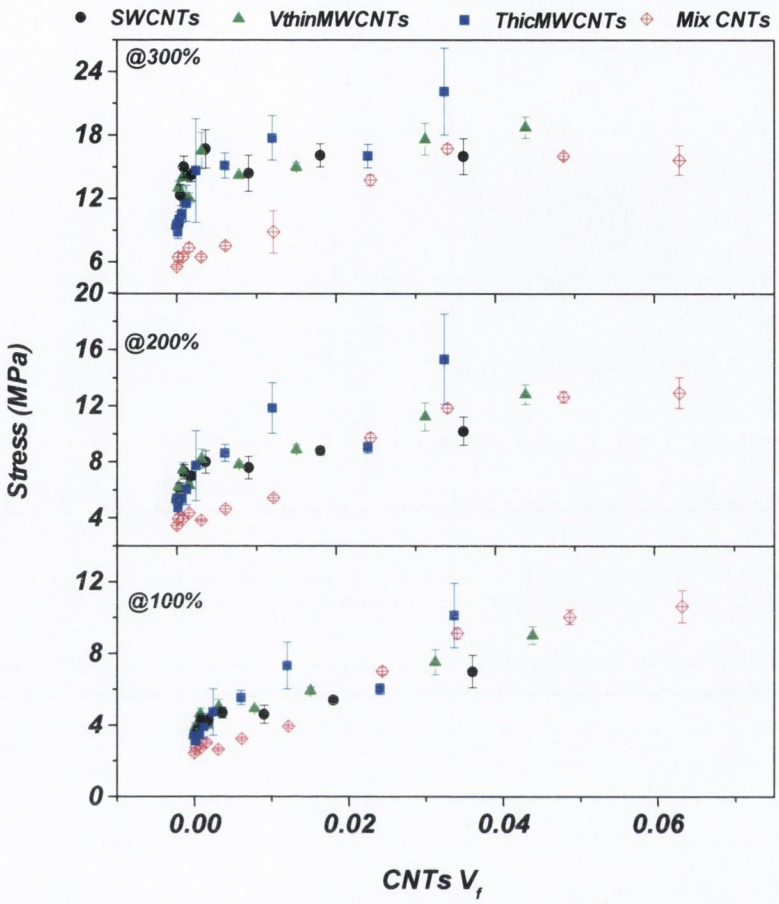


Fig. 6.17. The continuous increase in stress at various strain values as a function of polymer fraction of CNTs.

**Strain induced crystallisation/strain hardening (SIC/SH)**

The plateau part of the stress-strain curve is followed by the steep part, usually called the strain induced crystallisation/strain hardening (SIC/SH) part. The enhancement in this part of the curve was measured in terms of the slope ($d\sigma/d\varepsilon$) at 450 % strain. In general, no real differences in the SIC/SH of composites and polymers were observed. Among the pristine nanotube composites, SWCNTs demonstrated slightly higher strain induced crystallisation/strain hardening compared to other CNTs (Fig. 6.18). Finnigan *et al.*'s work on the silicates-TPU composites reveals that the small silicate particles can enhance the SIC/SH more than the larger particles *[57]*. They propose that this may be due to the

physical entanglement of these particles with the SS or due to the enhanced nucleation effect of the smaller silicate..

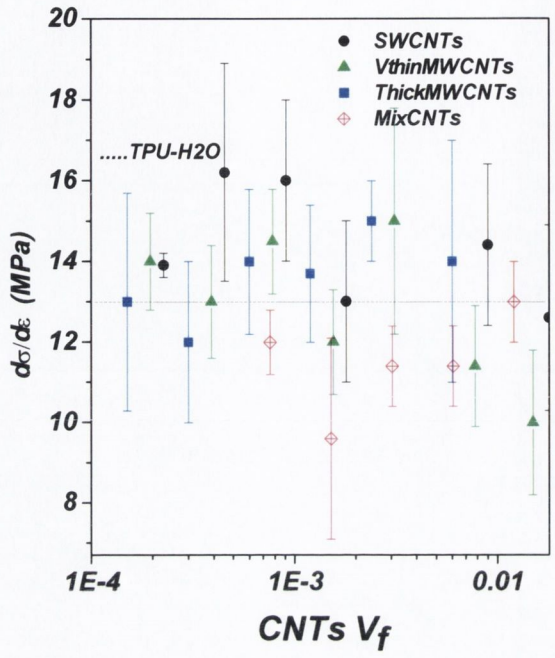


Fig. 6.18 The figure shows the strain induced crystallisation/strain hardening slope for the various CNT composites. The figure indicates the highest SIC/SH in the case of SWCNTs.

As has been discussed, the important goal in TPU reinforcement is to keep the ductility intact while increasing the stress of the plateau part. Remarkably, in the ThickMWCNT composites, at a volume fraction of 1.2 vol% (2.5 wt%) and above, the plateau part of the stress-strain curve has virtually disappeared, as can be observed in figure 6.4 and 6.19. At the yield stress, the plateau part becomes linear and the slope was ~10 MPa. This is slightly higher than the slope of the SIC/SH of the polymer only sample (see figure 6.16). This is a significant achievement. The data shows that by incorporation of CNTs into TPU, the stiffness of the plateau part of the stress-strain curve can be enhanced to the level of the SIC/HS stiffness of the TPU polymer, but at the same time the ductility can also remain largely intact.

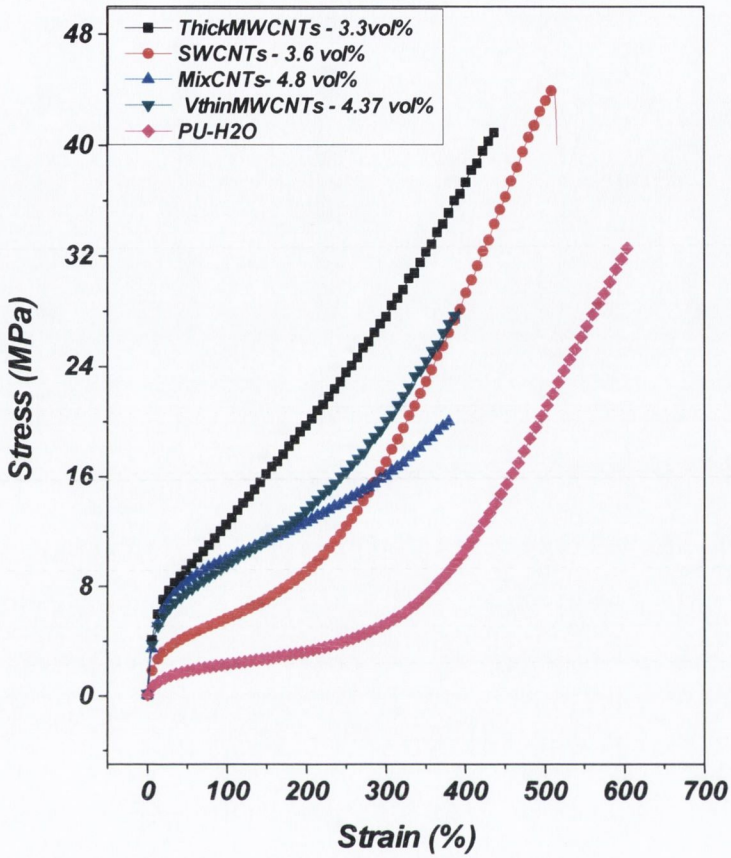


Fig. 6.19. Representative stress-strain curves of relatively high volume fraction composites fabricated with various pristine CNTs and the mixture of pristine + functionalised-CNTs. The figure not only indicates a significant enhancement in the yield/plateau part stress but more importantly the incredible increase in the stiffness of the plateau part which becomes equal to the stiffness of the SIC/SH part of the polymer only sample without any loss in ductility.

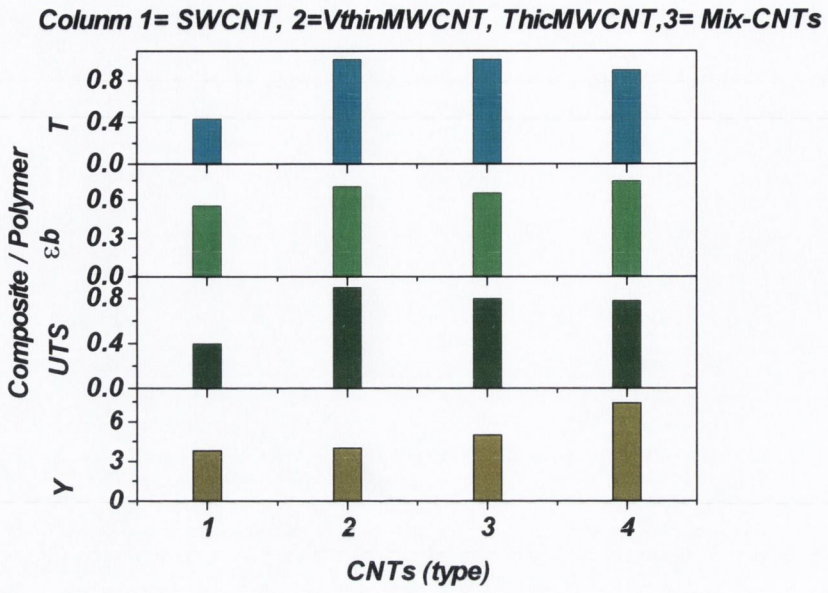


Fig. 6.20 Summary of the mechanical properties of samples exhibited maximum relative increase in Young's modulus i.e 3.6 vol% (5 wt%) SWCNT and 5 wt% (3.1 vol%) VthinMWCNT composites and also the 3.3 vol% (7 wt%) composite of the ThickMWCNTs.

## 6.4 Conclusions

The pristine CNTs show that the mechanical properties generally increase with increasing CNT diameter. The low mechanical properties for the small diameter SWCNT and VthinMWCNT may be due to the bundle formation. This study also reveals that for the pristine CNTs, the maximum CNT loading limits were directly proportional to the CNTs diameter (Fig.6.9). This is because the polymer used in the study was in the form of micron sized particles dispersed in water which cannot fuse together during drying to form a film if they become completely coated with CNTs in solution. During the energetic mixing process the hydrophobic CNTs tends to adhere around the polymer particles (than remained disperse in the water) creating a coating around CNTs. At lower volume fractions than this maximum limit, the CNTs only partially cover the polymer particles and are engulfed by the polymer particles on drying and become imbedded within the polymer. Again, the CNT diameter plays a vital role in this maximum CNT loading limit determination, because at a

given volume fraction, the network formed with larger diameter CNTs should have larger pores and also the number of small diameter CNTs will be greater and hence cover a greater surface area. Thus, at the same volume fraction smaller diameter CNTs should cover more surface area of the polymer particles leading to a lower loading required to restrict polymer-polymer fusion.

Remarkably, it was also demonstrated that large diameter CNTs not only increase the yield stress but, very importantly, enhance the stress of the plateau part as well. Even more impressively, the slope of the plateau part of the ThickMWCNT composites' stress-strain curve approaches the slope of the final SIC/SH part without loosing ductility. Therefore, this work is a step forward towards the fabrication of TPU-CNT stiff, strong and yet tough composites.

Another important result of this study was the mixed-CNTs approach to producing composites. The maximum loading limit of CNTs was increased by the novel approach of mixing different types of CNTs and incorporating them into a single matrix. To prepare high volume fraction composites, PEG-SWCNTs were used as a dispersing agent. In general, the composites prepared with the mix-CNTs showed higher reinforcement than the pristine CNT composite samples.

This work reveals the processes of CNT-polymer and CNT-CNT network formation within the polymer matrix. It is suggested that at relatively high volume fractions these composites should exhibit improved electrical properties as well as good mechanical properties. These composites can be used for the fabrication of novel materials for use as highly flexible electrodes, actuators, artificial muscles, sensing skin etc.

## 6.5 References


[1] N. Becker, E. Oroudjev, S. Mutz, P. Cevel, P. Hansma, C. Hayashi, H. Hansma, *Nature materials* **2003**, *2*, 278.

[2] Y. Liu, Z. Shao, F. Vollrath, *Nat Mater* **2005**, *4*, 901.

[3] K. Stefan, *Angewandte Chemie International Edition* **2002**, *41*, 2721.

[4] F. Vollrath, D. P. Knight, *Nature* **2001**, *410*, 541.

[5] Y. Termonia, *Macromolecules* **1994**, *27*, 7378.

[6] N. Becker, E. Oroudjev, S. Mutz, J. P. Cleveland, P. K. Hansma, C. Y. Hayashi, D. E. Makarov, H. G. Hansma, *Nat Mater* **2003**, *2*, 278.

[7] C. Prisacariu, R. H. Olley, A. A. Caraculacu, D. C. Bassett, C. Martin, *Polymer* **2003**, *44*, 5407.

[8] H.-D. Kim, T.-J. Lee, J.-H. Huh, D.-J. Lee, *Journal of Applied Polymer Science* **1999**, *73*, 345.
[9] L. T. J. Korley, B. D. Pate, E. L. Thomas, P. T. Hammond, *Polymer* **2006**, *47*, 3073.
[10] W. Chen, X. Tao, Y. Liu, *Composites Science and Technology* **2006**, *66*, 3029.
[11] J. N. Coleman, M.Cadek, R. B. ., V. N. ., K. P. R. ., C. B. ., A. F. ., J. B. N. ., Y. K. Gun'ko., W. J. . in *Advanced Functional Materials*, Vol. 14, **2004**, 791.
[12] J. N. Coleman, W. J. Blau, A. B. Dalton, E. Munoz, S. Collins, B. G. Kim, J. Razal, M. Selvidge, G. Vieiro, R. H. Baughman, *Applied Physics Letters* **2003**, *82*, 1682.
[13] C. Velasco-Santos, A. L. Martinez-Hernandez, F. Fisher, R. Ruoff, V. M. Castano, *Journal of Physics D-Applied Physics* **2003**, *36*, 1423.
[14] M. Cadek, J. N. Coleman, K. P. Ryan, V. Nicolosi, G. Bister, A. Fonseca, J. B. Nagy, K. Szostak, F. Beguin, W. J. Blau, *Nano Lett.* **2004**, *4*, 353.
[15] H. Xia., M. S. . *Soft Matter* **2005**, *1*, 386
[16] H. J. Yoo, Y. C. Jung, N. G. Sahoo, J. W. Cho, *Journal of Macromolecular Science, Part B* **2006**, *45*, 441
[17] K. Jiyun, K. Hando, *Journal of Polymer Science Part A: Polymer Chemistry* **2005**, *43*, 3973.
[18] http://www.hydrosize.com/.
[19] http://www.carbonsolution.com.
[20] http://www.unidym.com/.
[21] http://www.nanocyl.com/.
[22] B. Zhao, H. Hu, A. Yu, D. Perea, R. C. Haddon, *J. Am. Chem. Soc.* **2005**, *127*, 8197.
[23] M. B. Fiona, J. B. Werner, N. C. Jonathan, *Nanotechnology* **2008**, 415709.
[24] J. N. Coleman, M. Cadek, K. P. Ryan, A. Fonseca, J. B. Nagy, W. J. Blau, M. S. Ferreira, *Polymer* **2006**, *47*, 8556.
[25] K. P. Ryan, M. Cadek, V. Nicolosi, S. Walker, M. Ruether, A. Fonseca, J. B. Nagy, W. J. Blau, J. N. Coleman, *Synthetic Metals* **2006**, *156*, 332.
[26] S. M. Liff, N. Kumar, G. H. McKinley, *Nat Mater* **2007**, *6*, 76.
[27] H. Koerner, W. Liu, M. Alexander, P. Mirau, H. Dowty, R. A. Vaia, *Polymer* **2005**, *46*, 4405.
[28] G. Eugene, *Journal of Applied Physics* **1945**, *16*, 20.
[29] S. Giordani, S. D. Bergin, V. Nicolosi, S. Lebedkin, M. M. Kappes, W. J. Blau, J. N. Coleman, *J. Phys. Chem. B* **2006**, *110*, 15708.
[30] J. Amadou., D. Begin., C. Pham, *Chemistry for sustainable development* **2006**, *14*, 5549.
[31] J. N. Coleman, U. Khan, W. J. Blau, Y. K. Gun'ko, *Corbon* **2006**, *44*, 1624.
[32] D. William, W. Callister., *Fundamentals of materials science and engineering, an introduction*, Wiley, New Yark **2003**.
[33] H. L. Cox, *British Journal of Applied Physics* **1952**, *3*, 72.
[34] H Krenchel, Copenhagan, *Fibre reinforcement:*, Akademisk Forlag, **1964**.
[35] J. P. Salvetat, G. A. D. Briggs, J. M. Bonard, R. R. Bacsa, A. J. Kulik, T. Stockli, N. A. Burnham, L. Forro, *Physical Review Letters* **1999**, *82*, 944.
[36] M.-F. Yu, B. S. Files, S. Arepalli, R. S. Ruoff, *Physical Review Letters* **2000**, *84*, 5552.
[37] W. Chen, X. Tao, *Applied Surface Science* **2006**, *252*, 3547.

[38] B. Fabian, A. Gustavo, B. P. Abraham, D. R. Grady, *Journal of Polymer Science Part B: Polymer Physics* **2007**, *45*, 490.
[39] H. Xia, M. Song, *Journal of Materials Chemistry* **2006**, *16*, 1843.
[40] R. Sen, B. Zhao, D. Perea, M. E. Itkis, H. Hu, J. Love, E. Bekyarova, R. C. Haddon, *Nano Lett.* **2004**, *4*, 459.
[41] S. Jean-Paul, J. K. Andrzej, B. Jean-Marc, D. B. G. Andrew, S. Thomas, M. Karine, B. Sylvie, B. François, A. B. Nancy, F. Lásló, *Advanced Materials* **1999**, *11*, 161.
[42] S.Giordani, S Bergin.., W. J. Blau, J. N Coleman, *physica status solidi (b)* **2006**, *243*, 3058.
[43] K. Jin-Woo, K. Nalinikanth, K. Jeong-Hwan, D. Russell, *Applied Physics Letters* **2006**, *88*, 213110.
[44] F. M. Blighe, B. J. Werner, J. N. and Coleman, *Nanotechnology* **2008**, *accepted.*
[45] L. Yung-Hsin, C. Nai-Kuan, C. Kuan-Fu, i. H. Guan-Hue, C. Chih-Hao, W. Shoei-Shen, C. Shu-Hsun, H. Kuo-Huang, *Polymer International* **2007**, *56*, 1415.
[46] F. M. Blighe, P. E. Lyons, S. De, W. J. Blau, J. N. Coleman, *Carbon* **2008**, *46*, 41.
[47] L. Vaisman, H. Wagner, G. Marom, *Advances in Colloid and Interface Science* **2006**, *128-130*, 37.
[48] Z. Sun, V. Nicolosi, D. Rickard, S. D. Bergin, D. Aherne, J. N. Coleman, *J. Phys. Chem. C* **2008**, *112*, 10692.
[49] C. Carrillo-Carrion, R. Lucena, S. Cardenas, M. Valcarcel, *The Analyst* **2007**, *132*, 551.
[50] N. Wilfrid, M. P. Maryse, A. D. Miaudet, Z. Cécile, P. Philippe, *Macromolecular Rapid Communications* **2006**, *27*, 1035.
[51] M. B. Bryning, D. E. Milkie, M. F. Islam, J. M. Kikkawa, A. G. Yodh, *Applied Physics Letters* **2005**, *87*, 161909.
[52] J. Amiran, V. Nicolosi, S. D. Bergin, U. Khan, P. E. Lyons, J. N. Coleman, *J. Phys. Chem. C* **2008**, *112*, 3519.
[53] F. Blighe, J. Blau, J. Coleman, *Submitted.*
[54] A. Dong, G. Hou, D. Sun, *Journal of Colloid and Interface Science* **2003**, *266*, 276.
[55] G. Nanda, C. Yong, *Macromolecular Chemistry and Physics* **2006**, *207*, 1773.
[56] D. Blond, W. Walsh, K. Young, F. Blighe, U. Khan, A. Dorothée, C. Leslie, M. Joe, J Blau, J Coleman, *Advanced Functional Materials* **2008**, *9999*, NA.
[57] B. Finnigan, K. Jack, K. Campbell, P. Halley, R. Truss, P. Casey, D. Cookson, S. King, D. Martin, *Macromolecules* **2005**, *38*, 7386.

# Chapter 7

## Conclusions and future work

### 7.1 Conclusion

The aim of this work was to enhance the mechanical properties of polymers by incorporating carbon nanotubes. This work successful demonstrated the preparation of CNT reinforced composites by filling a polymer with very low to very high volume/mass fractions of CNTs.

In the first attempt, PVA was used as a matrix for the reinforcement with CNTs. A lot of work has already been done with PVA carbon nanotube composites and good reinforcement had been reported. Also, CNTs demonstrated good dispersion in PVA. Most of the work reported in literature had used water as a solvent. However, due to the hydrophobic nature of the CNTs, they can not be dispersed efficiently in water without the use of a surfactant. On the other hand, a lot of work has also been done on the effective dispersion of CNTs in organic solvents. Scientists were able to achieve very good dispersions of CNTs in high boiling point solvents like DMSO and NMP. These solvents can also dissolve PVA. Therefore, a good reinforced composite was expected with these three compatible components (CNTs-polymer/solvent). It was expected that an NMP composite would have the best mechanical properties due to good dispersion of CNTs in it. However the NMP composite exhibited the lowest mechanical properties. One of the most important outcomes of the study was that, due to the high affinity of NMP towards the CNTs compared to PVA, it accumulated at the CNT-PVA interface and hence no stress could transfer to the CNTs from the matrix. This coating of the NMP around the CNTs not only prevents stress transfer but also negatively affects the mechanical properties due to its

plasticising effect. The work also reveals that a high BP solvent can remain trapped with in the composites and reduce the overall mechanical properties of samples.

Based on the knowledge of the PVA work, it was desirable to avoid a high BP solvent. In another attempt TPU was used, due to its resemblance with spider silk, in an attempt to reinforce with CNTs. Spider silk has excellent mechanical properties. These excellent mechanical properties lie in its HS and SS morphology. TPU is analogous to the spider silk morphology in HS and SS and its toughness, but it has very low stiffness and yield stress. The stiffness and yield can be increased to some extent by increasing HS but this is associated with loss in ductility. In this work we significantly increased the stiffness and yield stress by the incorporation of the CNTs without losing ductility. Very importantly, it was successfully shown that plateau region of the stress-strain curve can be made as stiff as SIC/SH of polymer without sacrificing the ductility of the composites. It was also shown that at high concentration the mechanical properties of the composites are dominated by the CNT network.

Using a TPU matrix there was a limit for the maximum loading level for pristine CNTs due to bad dispersion and CNT network formation within the polymer. Dispersion in an aqueous medium is usually improved by use of the surfactants. In this thesis a novel approach for enhancement of dispersion hence loading was adopted. Functionalised CNTs were successfully used for enhancement of maximum CNT loading. Functionalised CNTs were mixed with pristine CNTs. Compared to the pristine CNTs, high mass fraction composites were fabricated with mix CNTs approach.

The pristine and mix CNTs-TPU composites work reveals that the introduction of functionalised CNTs increases, not only mechanical properties, but also the maximum loading limit. Also high concentration stable dispersions of functionalised CNTs have been reported in the literature. Therefore functionalised CNTs were used as filler for high mass fraction composite fabrication. Another interesting reason for the selection of functionalised CNTs is the very nature of TPU. The HS and SS of the thermoplastic polyurethane have different hydrophlicity/hydrophobicity. Therefore CNTs functionalised with either hydrophobic or hydrophilic functional groups influence the mechanical

properties by interacting either with the SS or HS. Very high loaded composites without losing strength and ductility were fabricated. Significant improvement in stiffness, strength and toughness were achieved with the funtionalised CNTs.

The overall conclusion is that, functionalised or mixed CNTs would be the future filler/s for modifying properties of polymers. This is due to their good, stable and high concentration dispersion in various solvents, the affinity of an attached group towards the polymer, commercial availability and decreasing cost.

## 7.2 Future work

As it has been demonstrated in the TPU composites, a particular type of functionalised CNT predominantly interacts with either the hard segment or the soft segment domain. Thus, for future work we propose the filling of the TPU with a mix of two or more types of functionalised/CNTs with different functional groups and with different hydrophlicity/hydrophobicity to reinforce both the hard and soft domain. It would therefore be possible to reinforce both the HS and SS simultaneously.

For mechanical reinforcement, in future work, it would also be highly desirable to chemically graft functionalised CNTs into the TPU polymer chain. Hence these CNTs would act like the HS of spider silk. It can be done using commercially available funtionalised carbon nanotubes. For example carbon nanotubes functionalised with PEG can be chemically grafted or crosslinked to the PEG matrix using diisocyanate. One of the important parameters in mechanical reinforcement of polymer with filler is the interfacial bonding between filler and polymer. A chemical bond is stronger than a physical bond and requires more energy to break it. Therefore chemical grafting of CNT into a polymer backbone will result in strong interfacial bonded CNT-polymer; hence mechanically reinforced composites.

The polymer molecules must possess a certain length to entangle with each other; the entanglement length. Therefore if the functional groups of functionalised carbon nanotubes were larger than the entanglement length the resultant composite should have enhanced mechanical properties. This is because the chemically attached functional group

to the CNTs would entangle with polymer matrix and stress would be transferred to the CNTs from matrix. Thus a systematic study is needed to analyse the dependence of mechanical properties on the length of the attached functional group.

For many uses the conductivity of the composite is also desirable but the functionalisation of CNTs makes them less conductive. However, the work with pristine and functionalised mixed CNTs reveals a significant improvement in the dispersion of CNTs and hence the CNT network. Having said that, unlike traditional surfactants which are insulator, these functionalised CNTs are still very conductive. Therefore, their presence in pristine CNT networks would not negatively influence the conductivity of a composite prepared with the mix-CNTs approach. Theses composites should have very high conductivity due to the presence of the proposed CNTs network in the polymer. It is proposed to do electrical experiments on the mix-CNTs composites. These composites could be used for high technological applications, for example artificial sensing skin, muscle/actuators, highly flexible electrode and other sensors.

For all applications good CNTs dispersion is vital. A good dispersion is traditionally achieved either by the use of surfactants or by the dilution of the CNTs in a very large amount of solvent. Both of these methods have their disadvantages. Therefore it would also be very interesting, and important, to carry out a systematic study of the pristine CNTs dispersion assisted by the presence of functionalised CNTs in the system.

## 7.3 Publications list

[1] **U. Khan**, K. Ryan, W. J. Blau, J. N. Coleman, ***The effect of solvent choice on the mechanical properties of carbon nanotube-polymer composites*** *Composites Science and Technology* 2007, *67*, 3158.

[2] **U. Khan** ,J. N. Coleman, ***Mechanical reinforcement of thermoplastic polyurethane by functionalised SWCNTs*** ( submitted)

[3] **U. Khan** ,J. N. Coleman, ***Novel approach of composites preparation: Enhancement of (mechanical) properties of thermoplastic polyurethane composites by incorporation of mixture of functionalised and pristine carbon nanotubes***.( submitted)

[4] J. N. Coleman, **U. Khan**, W. J. Blau, Y. K. Gun'ko, ***Small but strong: a review of mechanical properties of carbon nanotubes-polymer composites.*** *Carbon* 2006, *44*, 1624

[5] J. N. Coleman, **U. Khan**, Y. K. Gun'ko, ***Mechanical Reinforcement of Polymers Using Carbon Nanotubes*** *Advanced Materials* 2006, *18*, 689.

[6] J.Amiran, V Nicolosi,. S. Bergin, **U Khan**, P. E. Lyons, J. N.Coleman, ***High Quality Dispersions of Functionalized Single Walled Nanotubes at High Concentration,*** *J. Phys. Chem. C,* ***2008, 112, 3519-3524.***

[7] D. Blond, W. Walshe, K. Young, F. M. Blighe, **U. Khan**. D. Almecija, L. Carpenter, J. McCauley, W. J. Blau, J. N. Coleman, Strong, ***Tough, Electrospun Polymer-Nanotube Composite Membranes with Extremely Low Density*** *Advanced Functional Materials* 2008, ***9999.***